



5-2023

Nuclear Thermal Rocket Engine Instrumentation Addressing Environmental Limitations on Temperature Measurements

Dan C Floyd
dfloyd7@vols.utk.edu

Follow this and additional works at: https://trace.tennessee.edu/utk_graddiss

 Part of the [Nuclear Engineering Commons](#)

Recommended Citation

Floyd, Dan C, "Nuclear Thermal Rocket Engine Instrumentation Addressing Environmental Limitations on Temperature Measurements. " PhD diss., University of Tennessee, 2023.
https://trace.tennessee.edu/utk_graddiss/8168

This Thesis is brought to you for free and open access by the Graduate School at TRACE: Tennessee Research and Creative Exchange. It has been accepted for inclusion in Doctoral Dissertations by an authorized administrator of TRACE: Tennessee Research and Creative Exchange. For more information, please contact trace@utk.edu.

To the Graduate Council:

I am submitting herewith a thesis written by Dan C Floyd entitled "Nuclear Thermal Rocket Engine Instrumentation Addressing Environmental Limitations on Temperature Measurements." I have examined the final electronic copy of this thesis for form and content and recommend that it be accepted in partial fulfillment of the requirements for the degree of Doctor of Philosophy, with a major in Nuclear Engineering.

Richard T. Wood, Major Professor

We have read this thesis and recommend its acceptance:

Jamie B. Coble, Steven Zinkle, N. Dianne B. Ezell

Accepted for the Council:

Dixie L. Thompson

Vice Provost and Dean of the Graduate School

(Original signatures are on file with official student records.)

**Nuclear Thermal Rocket Engine Instrumentation:
Addressing Environmental Limitations on
Temperature Measurements**

A Dissertation Presented for the
Doctor of Philosophy
Degree
The University of Tennessee, Knoxville

Dan Caleb Floyd
May 2023

© by Dan Caleb Floyd, 2023
All Rights Reserved

Abstract

The development of nuclear thermal rockets has received renewed interest in recent years due to the benefits that can be attained from this method of propulsion. Currently, instrumentation work is focused on the evaluation of current and near-term technology for implementation within a nuclear thermal rocket engine. One aspect of this evaluation is focused on the various instrumentation requirements of the system regarding necessary measurement parameters and environmental conditions for survivability. Historical nuclear rocket programs that have been conducted in the United States provide the basis for this information and indicate a critical need for high temperature measurement technology that can survive extreme environmental conditions. Through a survey of the current state-of-the-art of temperature measurement technology, it is indicated that there are still several gaps between high technology readiness level instruments and their potential application in a nuclear rocket. Due to the need for in-situ re-calibration, Johnson noise thermometry provides the best path forward but requires an extreme temperature resistance temperature detector for operation. Currently, there is no such instrument available for use and requires investigation into the feasibility of such an instrument to be used within a Johnson noise thermometry system. The current work provides a conceptual design for a high temperature resistance temperature detector, an evaluation of the design, and experimental plans.

Table of Contents

Chapter 1: Introduction	1
1.1 Motivation	Error! Bookmark not defined.
1.2 Research Objectives	Error! Bookmark not defined.
1.3 Thesis Organization	Error! Bookmark not defined.
Chapter 2: Historical Experience	4
2.1 Nuclear Thermal Propulsion	4
2.2 Instrumentation of the XE-Prime	4
2.3 Rover/NERVA Trade Study Insight	6
2.4 Historical Investigations of Tungsten Thermocouples	6
2.5 Important Lessons from Historical Investigations	7
Chapter 3: State of Temperature Measurement	8
3.1 Thermocouples	8
3.2 Pyrometry	11
3.3 Ultrasonic Thermometry	13
3.4 Johnson Noise Thermometry	15
3.5 Resistance Temperature Detectors	16
3.6 Instrument Selection	16
Chapter 4: Resistance Thermometry	18
4.1 Material Selection: Sensing Element	21
4.2 Material Selection: Electrical Insulator	21
4.3 Material Selection: Sheath Material	24
4.4 Material Selection: Electrical Insulator	24
Chapter 5: Resistance Temperature Detector Model	25
5.1 Introduction	25
5.2 Thermal Modeling	25
5.3 Chemical Reactions and Kinetics	27
5.4 Electrical Network Model	30
5.5 Neutron Effects	32
5.6 Interconnectivity of Model Components	35
Chapter 6: Modelling Results	36
6.1 Introduction	36
6.2 Mesh Refinement	36
6.3 Heat Transfer and Thermal Stress	38

6.4 Insulator Shunting and Resistance	40
6.5 Chemical Degradation	40
6.6 Neutron Effects.....	43
Chapter 7: Model Verification and Sensitivity.....	45
7.1 Verification of Electrical Shunting Model	45
7.2 Verification of Heat Transfer Model.....	48
7.3 Verification of Chemical Reaction Model.....	49
7.4 Sensitivity Analysis of Electrical Model	50
7.5 Sensitivity Analysis of Heat Transfer Model.....	51
Chapter 8: Experimental Design	57
8.1 Overview of Needs.....	57
8.2 Out-of-Pile Testing.....	57
8.3 In-Pile Testing	59
8.4 Resistor Construction and Test Plan.....	60
8.4.1: Test Element Design	60
8.4.2: Irradiation Basket.....	61
8.3.3: Non-radiation Environment Testing.....	63
Chapter 9: Conclusions	67
9.1 Summary.....	67
9.2 Findings.....	67
9.3 Future Work.....	68
References:.....	71
Appendix A: Funded NSUF RTE Proposal	76
Vita:.....	80

List of Figures

Figure 2.1: Labeled cutaway of the XE-Prime configuration.....	5
Figure 4.1: Coiled element (top) and wire-wound (bottom) RTD design diagrams. Figure adapted from reference [7]......	20
Figure 5.1: Nth electrical subnetwork (left) and circuit diagram of final subnetwork (right)..	33
Figure 5.2: Top-down view of RTD housing.....	33
Figure 5.3: Diagram of the sensing element in the form of a double helix.....	34
Figure 6.1: Response due to a 200K step change with varying time steps.	37
Figure 6.2: Response of the model to a step (left) and ramp (input).....	39
Figure 6.3: Insulator shunting effect on RTD resistance using an impure insulator.....	41
Figure 6.4: "Pure" beryllia sample and effect on measured resistance.	42
Figure 6.5: Impure beryllia sample and effect on measured resistance... ..	42
Figure 6.6: 3-D plot of the mass loss of tungsten during a simulation of a full power ramp.....	44
Figure 7.1: Hysteresis of the niobium RTD produced by ORNL for the SP-100 program (left) and the relationship developed through temperature cycling (right). Recreated from the associated fit provided in reference [98].	46
Figure 7.2: Overall temperature resistance relationship of the ORNL produced niobium RTD. Figure recreated using the associated fit as reported in reference [98].	46
Figure 7.3: Resistance of the proposed equivalent niobium equivalent niobium sensing element with and without the effect of insulator shunting.	53
Figure 7.4: Sensitivity analysis of the wire resistivity for the electrical shunting model.	55
Figure 7.5: Sensitivity analysis of the wire length for the electrical shunting model.	55
Figure 7.6: Sensitivity of the model to changes in the width of the RTD sheath.	56
Figure 7.7: Sensitivity of the model to changes in the width of the RTD mandrel.....	56
Figure 8.1: Visual representation of experimental phases.	58
Figure 8.2: Desired test plan to determine calibration of the resistor.	58
Figure 8.3: Schematic of tungsten resistor test element as well as pertinent dimensions.....	62
Figure 8.4: Example of test element holder implementing large gauge stainless steel wire.....	62
Figure 8.5: Constructed irradiation basket with 16 fl. oz. water bottle for scale.	64
Figure 8.6: View of the physical separator composed of G10 with water bottle for approximate scale. ...	65
Figure 8.7: Cutaway diagram of irradiation basket.....	65
Figure 8.8: 4-wire configuration for test sample resistance measurement.....	67
Figure 8.9: General circuit for measurement of test sample resistance.	67
Figure 9.1: Conceptual design with accommodations made to account for potential challenges due to thermal strain.	70
Figure A.1: Configuration of tungsten resistors for the proposed irradiation experiment.	79

Chapter 1: Introduction

The renewed interest in manned missions to Mars and other extraterrestrial bodies has reinitiated work regarding nuclear thermal propulsion (NTP). Nuclear thermal rocket (NTR) systems implementing this propulsion methodology provide several advantages for manned missions in comparison to conventional chemical rockets. Specifically, NTRs provide an improved specific impulse (efficiency metric relating generated thrust and propellant consumption) and decreased travel time requirements. However, these benefits are paired with extremely harsh environmental conditions that are both internal and external to the system. Environmental conditions limit the applicable materials due to extreme temperatures, presence of a neutron flux, use of pure hydrogen as the propellant, and long-term exposure to space radiation. Furthermore, traditional maintenance techniques are unlikely to be available to correct the performance of system in the event of instrument degradation.

As all instruments experience drift in some form, the inability to conduct maintenance introduces significant concerns regarding the long-term operation of such a system. This is further compounded upon in the event of a single rocket system being implemented in multiple missions that would further degrade the instruments. Since the instruments are necessary to properly operate and control the system, instrument failure can pose significant risk to the success of the mission. Therefore, there is a critical need for a sensing mechanism that is suitable for reliable in-situ recalibration.

1.1 Motivation

The development and deployment of nuclear thermal rocket engines (NTREs) requires specialized instrumentation to allow for safe operation over the course of its use. The in-core temperatures of a NTRE exceeds 2000°C and provide a harsh nuclear and chemical environment. Historically, in-core and nozzle chamber temperatures have been used to provide reactor control in NTREs [1, 2]. Due to the extreme temperature of these systems, tungsten-rhenium alloy thermocouples were employed. To acquire these measurements, the instruments must be in positions that receive appreciable neutron fluence levels over the course of system operation. A trade study completed during Project Rover indicates that these temperature instruments would need to survive a fast neutron fluence ($E > 1 \text{ MeV}$) of $10^{20} \frac{n}{\text{cm}^2}$ for the in-core temperature measurements and $10^{19} \frac{n}{\text{cm}^2}$ for the propellant outlet temperature measurements [3]. Based on several irradiation studies of tungsten-rhenium alloy thermocouples, the expected neutron fluence would cause significant calibration drift that would exceed the accuracy requirements of the system.

The measurement conditions and mission profiles for NTREs greatly limit the temperature instrumentation suitable for these critical measurements. Thermocouples, ultrasonic thermometers, optical or infrared pyrometry, and Johnson noise thermometry (JNT) are the main measuring techniques of interest for these systems. However, only JNT provides a first principles based, in-situ recalibration methodology for a sensor. Because of this, JNT is the strongest candidate for long-term use in nuclear rockets.

The implementation of JNT would provide a methodology for an instrument to perform self-recalibration during the operation of the system. JNT functions by measuring the thermal noise on a resistive element. As temperature is an indicator of the kinetic energy of particles, increasing or decreasing the temperature of a resistor will cause thermal noise to change. While it is possible to use the noise measurement for temperature measurements, it generally requires long periods of time to provide high accuracy results. This is partly due to the minimal magnitude of the thermal noise signal and the susceptibility of the system to external electromagnetic interference. This has led to the desire to use JNT

and a resistance thermometer/resistance temperature detector (RTD) in conjunction. The RTD provides the fast response measurements for a control or monitoring system and JNT provides recalibration of the instrument after some period of time. When looking to implement such a system in a NTRE, there is currently not a RTD capable of withstanding the in-core temperatures of the reactor. As such, a conceptual design for an extreme temperature RTD is proposed and evaluated to meet this need.

Beyond the potential use of an RTD in a JNT self-recalibration system, there are several benefits provided by the use of resistance thermometry in comparison to thermocouples. RTDs can provide measurements with higher accuracy, repeatability, and stability when compared to thermocouples. Most RTDs that are currently available are limited to $\sim 600^{\circ}\text{C}$ with some units capable of operation up to $\sim 1000^{\circ}\text{C}$ [4]. Above these temperatures, thermocouples, pyrometers, or ultrasonic thermometers are implemented. However, being able to provide the benefits of resistance thermometry at these extreme temperatures would be beneficial. It provides a relatively simple measurement technology for these environments and will increase the potential for diversity in measurement.

1.2 Research Objectives

The foremost objective of this work is the advancement of the state-of-the-art (SOA) of temperature measurement technology for NTR systems. This includes the evaluation of the current SOA of temperature measurement technology and its applicability to the environmental and physical constraints that are present. This information is leveraged to support selection of a candidate measurement technology for design and enable an evaluation of its suitability and performance characteristics. Evaluation of the proposed instrument is conducted via modeling the long-term effects of the environmental conditions with currently available information. This evaluation informs the evolution of the conceptual design and provides a pathway to the deployment of high temperature measurement technology for extreme nuclear environments. An additional aspect of the current work is the identification of the various properties of different compounds that require further investigation.

To attain the described objectives, the work progressed in accord with a systematic research approach. The first stage of this work is an in-depth study of the instrumentation implemented during historical development of NTREs. The findings of this investigation provide critical information regarding the environmental conditions as well as programmatic requirements to develop a flight ready system. Subsequently, the SOA of sensing technology for temperature measurement was determined. The information from these investigations serves as the basis for determining applicable temperature measurement technologies that can not only withstand the harsh environmental conditions but have the potential to address the inability for recalibration after mission start. Additionally, reviewing the state of temperature instrumentation allows for potential technological gaps to be determined.

Based on the findings from the literature investigations, a conceptual design of a temperature sensor is established that can withstand very high temperature conditions and is suitable to mitigate issues with long-term fidelity of measurement. The baseline conceptual design of the high temperature RTD is based on the design of currently available industrial platinum resistance thermometers. Essentially, the baseline conceptual design can be described as a wire wound RTD implementing tungsten as the sensing element and beryllium oxide (beryllia or BeO) as the electrical insulation. The initial material selections arise from the historical experience from the NASA NTRE development programs. Both the sensing element and insulation materials have high melting points, with tungsten providing the highest melting point of any pure metal. Additionally, beryllia provides a relatively high electrical resistivity at 2000°C . In theory, the usage of refractory materials in the construction of the RTD should provide a functional instrument; however, the physical constraints and potential interactions of the components require a full evaluation to determine the suitability of the conceptual design.

Following the establishment of the baseline conceptual design for the high temperature resistance thermometer, further refinement of the design involves additional examination of materials and assessment of performance characteristics. This evaluation is completed through the usage of reported material properties as well as the construction of analytical and empirical models. Using the models for material and performance investigations allow for the identification of potential challenges to the conceptual design. Based on findings from these models, prospective modifications of the conceptual design are identified that can resolve performance challenges and improve sensor performance. An experimental test plan is devised to serve as the means by which a sensor prototype can be tested to validate the design. The experimental campaign remains for future work because of access limitations to an irradiation testbed.

1.3 Thesis Organization

The remainder of this dissertation is separated into several chapters covering the pertinent details, basis, and results of the work. In addition, there are several appendices that include in-depth information regarding the historical experience with NTRE in the United States of America, a discussion of the state-of-the-art of temperature measurement technology, and additional topics in support of this work. A short description of the contents of the chapters can be seen as:

- **Chapter 2** provides a historical overview of nuclear thermal propulsion research in the United States. Additionally, the
- **Chapter 3** details a survey of the current state of the art of temperature instrumentation. This provides the basis for the selection of a high temperature RTD as well as some of the challenges associated with various measurement technologies.
- **Chapter 4** provides the foundations of resistance thermometry along with the definition of various performance parameters for an instrument. Additionally, this chapter provides an overview of the desired properties of the sensing element of an RTD as well as the electrical insulator. This is then expanded to provide the justification for the selected materials and a full description of the conceptual design.
- **Chapter 5** discusses the purpose of the model-based evaluation and the various aspects that are needed to model an RTD. This includes various thermal, chemical, nuclear, and electrical components. The equations for each aspect of the model will be provided as well as the assumptions and limitations of the model. The chapter is concluded with a discussion output of the model developed for this work.
- **Chapter 6** provides the results of the model when provided with the expected operational profile of a NTRE. Additionally, a discussion of the methodology implemented in the development of the NTRE operational profile is provided. Finally, the results of the model are interpreted to provide a theoretical estimation of some of the performance parameters of the instrument as well as any needed modifications to the conceptual design.
- **Chapter 7** covers the various experimental programs that are required to verify the estimated performance of the conceptual design. This chapter also includes a discussion of the potential manufacturing process for conceptual design and its construction methodology.
- **Chapter 8** contains the conclusions from this work. This includes a summary of the pertinent results, the potential of the conceptual design, future work, and the recommendations for temperature measurements in the extreme environments produced in NTREs.

Chapter 2: Historical Experience

2.1 Nuclear Thermal Propulsion

Project Rover and the Nuclear Engine for Rocket Vehicle Application (NERVA) Program are the two significant historical investigations into the development of NTP technology in the United States. These investigations occurred between the 1950's to the early 1970's and culminated in a flight-style, close coupled ground test designated as the Experimental Engine-Prime (XE-Prime) [5]. The XE-Prime is the only test of its kind to have occurred within the United States and provides the basis for most of the knowledge regarding the instrumentation requirements of such systems. This information can then be supplemented by the results of instrumentation development and research that occurred with the preceding test reactors developed during the time of the program.

Figure 2.1 provides a simplified diagram of the configuration of the XE-Prime to allow for an overview of the operation of the system. The XE-Prime can be separated into two main sections, the upper and lower modules. The upper module housed the test stand adapter, upper thrust structure, and most of the propellant feed system. Remaining engine components such as the reactor, pressure vessel, external shield, control drum actuators, etc. were in the lower module. Reactor control was provided by several control drums that consisted of a reflector and absorber and were installed on the periphery of the core. Control drum rotation angle influences the power level within the reactor and therefore the temperature of the system. The hydrogen propellant could reach temperatures $\geq 2000^{\circ}\text{C}$ at the outlet of the reactor core and the entry point of the nozzle. While not operating, the hydrogen propellant is in a liquid phase with temperatures that could reach -253°C .

Over the course of an expected mission, the integrated neutron fluence varies depending on the position of the component with regards to the core. For example, the pressure vessel of the NTRE designs of the NERVA era achieve an integrated fast neutron flux of $2.19 * 10^{18} \frac{n}{\text{cm}^2}$ over the course of 10 hours of operation [3]. For a comparison to terrestrial reactors, the integrated fast fluence for the pressure vessel can range from $4 * 10^{18} \frac{n}{\text{cm}^2}$ for a boiling water reactor to $1.1 * 10^{20} \frac{n}{\text{cm}^2}$ for the water-water energetic reactor over the course of 30 to 40 years [6]. While there are several complex structures, the general operation and flow path can be described in simple terms. The propellant is pumped through the reactor core as to reach the desired outlet temperature for thrust. Some propellant is diverted to allow for active cooling systems and warming the fluid before entering the reactor core. The temperature of the outlet fluid and the pressure in the vessel is monitored and implemented in the control of the reactor. As such, these are two critical measurements for the operation of the system.

2.2 Instrumentation of the XE-Prime

The XE-Prime had over 480 measurements to collect the necessary information for model validation, diagnostics, process control, and verification of instrument performance. Platinum resistance temperature detectors (RTDs), copper/constantan (type T), chromel/alumel (type K), and tungsten-rhenium (type C and type G) based thermocouples were implemented in the measurement of the system temperatures [1]. Of these, the tungsten-rhenium based thermocouples were the only instruments implemented for high temperatures due to the melting point of the other instruments being lower than 2000°C . During the test, the instruments are reported to have performed favorably with minimal problems occurring. One of the few comments made regarding the instruments was related to the inability of the thermocouples to provide accurate measurements at the low temperatures that occur when the system is not operating [2]. With this, it was considered that the instruments were adequate for continued ground tests as they further improved the system overall.

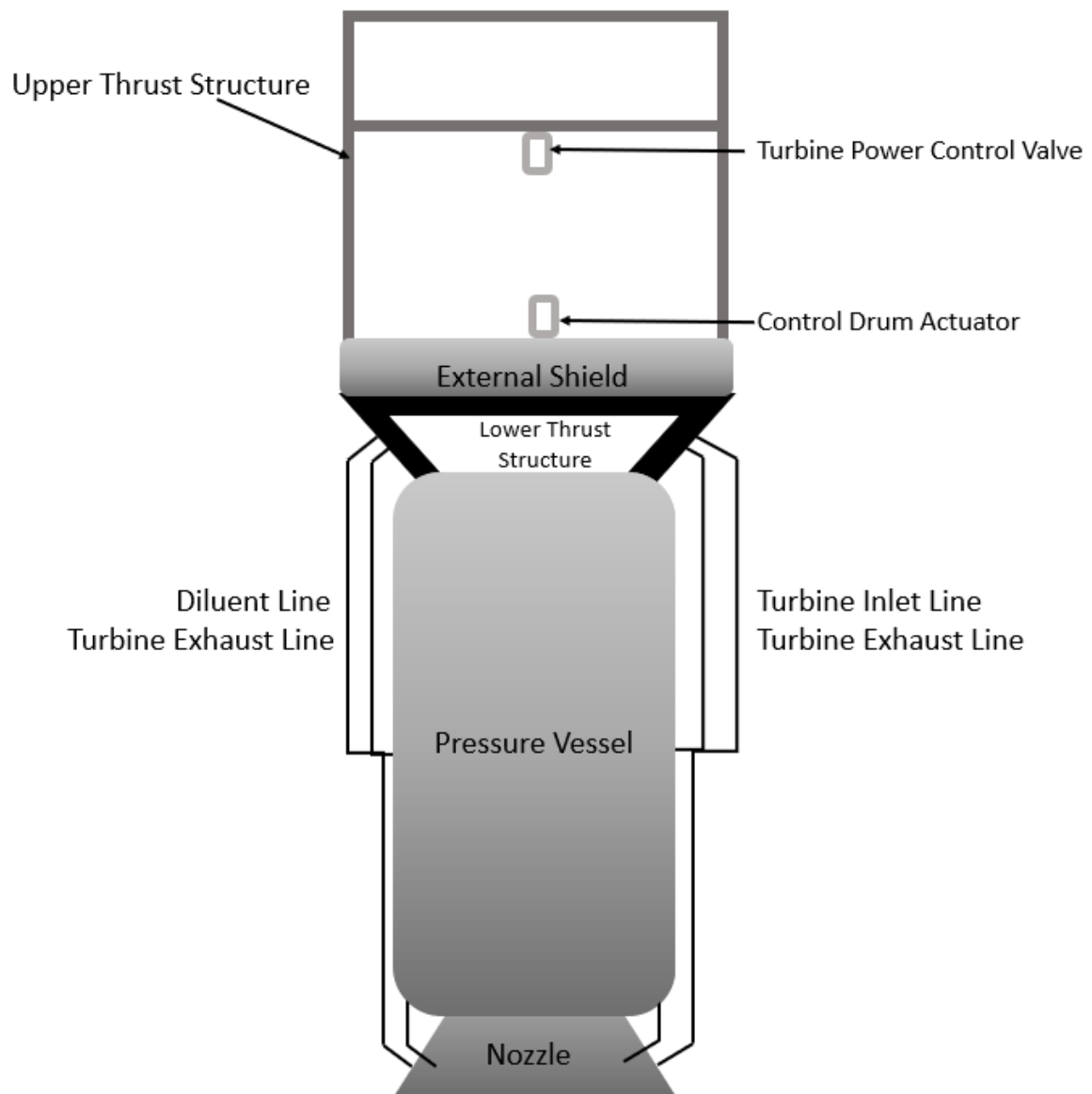


Figure 2.1: Labeled cutaway of the XE-Prime configuration.

2.3 Rover/NERVA Trade Study Insight

A trade study produced near the end of the NERVA program provides programmatic flight requirements for the instrumentation of the core outlet temperature. This study indicated that the core outlet instrumentation needed to be capable of withstanding an integrated fast neutron flux on the order of $10^{20} \frac{n}{cm^2}$ for core fuel element temperatures and $10^{19} \frac{n}{cm^2}$ for the core outlet instruments [3]. The study indicates that both instruments should be composed of tungsten doped with thoria for the sheath material and beryllia for the electrical insulator. The main difference comes in the form of the specific tungsten-rhenium alloys implemented in the thermoelement legs. Type C is indicated for use in the cluster outlet and Type G is indicated for the fuel element temperatures.

2.4 Historical Investigations of Tungsten Thermocouples

The two of the nuclear based factors affecting the performance of the tungsten-rhenium thermocouples are the integrated fast and thermal fluxes experienced by the instrument. The effect of neutron irradiation has been accomplished through theoretical calculations and reactor tests. One early theoretical evaluation indicated negligible changes in the thermocouple drift due thermal neutron exposure [7]. However, the production of rhenium via transmutation of tungsten and the effect of osmium on the EMF-temperature relationship was ignored. It should be noted that the production of osmium from rhenium and depletion of tungsten due to transmutation will alter the calibration of the thermocouple as indicated in reference [8]. A related test evaluating type C and type G thermocouples occurred during this period at the Ground Test Reactor. The type C thermocouple failed within 18.8 hours of the test start and the type G thermocouple experienced a decline in EMF that exceeded computations of the induced error [9]. However, the resultant data was not adequate with respect to determining the exact cause of the failure and drift.

Various irradiation campaigns have been completed during historical investigations of neutron flux effects on tungsten-rhenium thermocouples. During the 1960's, Los Alamos Scientific Laboratories (LASL) conducted a test that exposed type C thermocouples to a thermal fluence of $3.8 * 10^{20} \frac{n}{cm^2}$ over 5,328 hours with an average temperature of 2000°K. Re-calibration of the thermocouples led to calibration changes varying from 60°K at 1200°K and 33°K at 2170°K. These results differed significantly with alloys simulating the transmutation effects of the flux on the EMF-temperature relationship of the instrument. A potential cause of this was the occurrence of phase separation in one of the legs of the irradiated instruments [8]. However, there is significant difficulty in the determination of radiation effects and temperature effects due to the long-term exposure. Irradiating the instrument at such a high temperature can lead to annealing and possible recrystallization of the material.

Additional long-term neutron and temperature exposure tests have provided various results regarding the performance of the instruments. A 5,000-hour test of type D thermocouples in a nuclear environment at 2,000°K compared in-pile and out-of-pile results. Doing so allows the radiation effects to be separated from the temperature effects. The in-pile thermocouples were exposed to an estimated integrated thermal and fast flux of $2 * 10^{21} \frac{n}{cm^2}$ and $4 * 10^{20} \frac{n}{cm^2}$ respectively. The irradiated instruments experienced a larger change in their calibration than those out-of-pile, and the irradiated instruments reading ~190°K lower than the true temperature of 2073°K while the out-of-pile counterparts indicated a change of ~54°K [10]. Further tests have indicated similar deviations in thermocouple output at comparable neutron fluence levels [11, 12].

An additional theoretical evaluation of neutron flux exposure on a type C thermocouple approaches the problem via quantum mechanics. While several simplifying assumptions are made, it is proposed that

thermal flux of $3 * 10^{13} \frac{n}{cm^2-sec}$ with an exposure time of 15 days and temperature of 1800°C could decrease the thermocouple output by 2.7 mV [13]. With the provided flux and exposure time, the integrated thermal flux would be on the order of $3.9 * 10^{19} \frac{n}{cm^2}$.

2.5 Important Lessons from Historical Investigations

Comparing the flight requirements from the NERVA program and the available data regarding neutron flux effects on tungsten-rhenium thermocouples indicates the potential for NTRE operation to alter the performance of the instruments. The irradiation experiments indicate a significant relationship between the thermocouple drift and neutron fluence. While several of the experiments report significant drift at fluence levels an order of magnitude or higher than reported via the NERVA program documentation, the experiments neglect the presence of epithermal or intermediate neutron energies. The three-group approximation used in the NERVA documentation provides a significant intermediate fluence while the experiments indicate only the fast and thermal neutron fluence the instruments experienced. The various isotopes of tungsten, both naturally occurring and produced via neutron capture, have significant neutron capture cross-sections and resonance at epithermal/intermediate neutron energies. Due to the large neutron cross-sections at these energies, the transmutation of tungsten and rhenium will alter the known performance of the thermocouple.

The historical investigations have shown the potential of thermocouple failure and drift during long-term operation in nuclear environments. The flight requirements previously described for NTRs have the potential to significantly alter the performance of critical control instrumentation that can place the mission and the lives of the astronauts on board at risk. As such, it is necessary to ensure that any deviations in performance induced by nuclear and other effects are capable of being corrected to some extent. In terrestrial nuclear power plants, this is completed through scheduled maintenance occurring approximately every 2 years during plant outage and refueling.

The mission time for NTP based systems ranges from 2.5 years to 5 years of operation. The general operational profile for the reactor system consists of 600 minutes at full power, consisting of several short fires over the mission, and long periods of the reactor being turned off [3]. As the thermocouples are critical for reactor control going from startup to full power operation, they will need to be operational continuously to properly monitor the condition of the system even when the reactor is not operating during the mission. Additionally, the thermocouples implemented in startup control are installed within specific locations in the core. It is unlikely that these instruments are capable of being replaced or handled safely when considering the potential radioactivity of the instruments and the complications by being in a zero-gravity environment.

Chapter 3: State of Temperature Measurement

3.1 Thermocouples

Thermocouples take advantage of the electrical phenomena that occurs when dissimilar metals are electrically connected at two junctions which are at different temperatures. One junction is considered the reference and is at a known temperature. The other junction is exposed to the process whose temperature is of interest for measurement. The difference in temperature at the junctions produces an electromotive force (emf) whose overall relationship with the temperature is known as the Seebeck effect. Each material has a Seebeck coefficient relating the magnitude of the generated emf with temperature and with units given in V/K. There are additional thermoelectric effects such as the Thomson effect and the Peltier effect, but these effects are negligible in a properly constructed thermocouple measurement circuit [14].

The response time dynamics of thermocouples, as well as several other temperature measurement technologies, is based solely on the heat transfer between the process and the instrument. This is due to the fact that the generation of the emf in a thermocouple or the resistance change in a resistance temperature detector occurs in a significantly smaller time scale than the time lag due to heat transfer. Thermocouples can be produced to have very small thermal masses, which provides the instrument a fast response time to changes in the process temperature. This is desirable for control applications that require fast responses to process changes. However, there are several drawbacks to the technology in comparison to resistance temperature detectors (RTDs).

Thermocouple emf is in the millivolt range which allows noise to have a higher impact on the measured signal. When comparing the instrument to an RTD, this shows a smaller signal to noise ratio than can be gained from a resistance-based temperature measurement. Additionally, thermocouples are more susceptible to drift and are generally considered to have lower values of certainty associated with their measurement. In contrast to the notable disadvantages of thermocouples, these instruments have the capability to measure significantly higher temperatures than RTDs. Platinum RTDs are generally limited to 600°C with some models capable of measuring 1000°C with desirable values of instrument stability. Type K, N, R, S, B, and tungsten-rhenium alloy thermocouples are capable of measuring temperatures in excess of 1000°C with tungsten-rhenium alloy thermocouples capable of exceeding 2000°C. As such, these are the only commercially available electricity-based temperature measurements capable of measuring the in-core temperature of a nuclear rocket. Furthermore, tungsten-rhenium alloy thermocouples were developed and implemented in historical nuclear rocket programs because of the high temperature requirements.

Currently, there are several commercial options available for equivalent thermocouples that were implemented in historical nuclear rocket programs. From a survey of several vendors, the greatest challenge may be encountered through the process of attaining the appropriate electrical insulator. Beryllium oxide, thorium dioxide, magnesium oxide, hafnium dioxide, and zirconium dioxide appear to be the only insulators capable of use in a system exceeding 2000°C. To recreate historical thermocouples, beryllium oxide would be required; however, beryllium oxide is a highly toxic compound that has special requirements to ensure its safe use. For the desired application of these instruments and to minimize electrical shunting in the insulator, this compound provides the best option for electrical insulation due to its comparatively high electrical resistivity at extreme temperatures.

In addition to the need for beryllium oxide to minimize insulator shunting, tungsten-rhenium thermocouples experience calibration changes when exposed to a neutron flux. This comes from the transmutation of the elements present in the thermocouple wires as well as crystallographic defects and damage induced by neutron collisions. Some potential transmutation products include rhenium, tantalum,

and osmium from exposure to a thermal or epithermal flux. Neutron capture reactions occurring with stable rhenium and tungsten isotopes leads to unstable isotopes that produce the above products. An interesting point of note is the potential for the unstable isotopes to regain stability due to the continued exposure of the neutron flux. For example, ^{185}W (produced via neutron capture of ^{184}W) decays to ^{185}Re through beta decay with a half-life 75. It can also produce the stable isotope ^{186}W if a subsequent neutron capture reaction occurs before decay. However, ^{186}W can also produce the unstable isotope ^{187}W which decays to ^{187}Re through beta decay with a half-life of ~ 24 hours. As the operation of a nuclear rocket includes 6 periods of full power operation at maximum of 10 minutes, the various daughter isotopes produced by irradiation that are allowed to decay due to long periods of the reactor being turned off will alter the composition instrument.

While fast neutron exposure will not significantly alter the composition of the wire due to the thermal and epithermal neutron cross-sections being larger for neutron capture reactions, defects generated in the crystallographic structure of the wire can notably alter the electrical properties of the instrument. Defects such as voids, dislocations, and interstitials effect the electrical transport properties of the material. As the temperature measurement of a thermocouple is based on the measured emf, the known calibration curve of the instrument will no longer be valid. The extent of this drift is dependent on the neutron fluence the material is exposed to, and historical investigations have indicated errors of several hundred Kelvin shifts from the true temperature of several hundred Kelvin with neutron fluences of $10^{20} \frac{\text{neutrons}}{\text{cm}^2}$ [15-17]. The three-group approximation for neutron flux at probable installation points of a thermocouple in historical nuclear rocket designs is on the order of $1.30 * 10^{19} \frac{\text{neutrons}}{\text{cm}^2}$ to $1.71 * 10^{20} \frac{\text{neutrons}}{\text{cm}^2}$ [18]. Additionally, a trade study produced near the end of Project Rover states that the high temperature thermocouples are required to survive a fast neutron fluence ($E > 1 \text{ MeV}$) of $10^{20} \frac{n}{\text{cm}^2}$ for core fuel element temperatures and $10^{19} \frac{n}{\text{cm}^2}$ for the core outlet instruments. Additionally, the desired accuracy the required accuracy of the instruments is $\pm 30^\circ\text{R}$ and $\pm 50^\circ\text{R}$ depending on installation location [3]. These accuracy values are equivalent to $\pm 16.7^\circ\text{K}$ and $\pm 27.8^\circ\text{K}$.

An important note to make regarding the provided fluence values is related to the use of two-group and three-group approximations of the neutron flux and fluence. The documented fluence values for nuclear thermal rocket designs come from three-group approximations that separate the neutron energies into thermal ($E < 0.4 \text{ eV}$), intermediate ($0.4 \text{ eV} \leq E \leq 1 \text{ MeV}$), and fast ($E > 1 \text{ MeV}$) [18]. The thermal energy cut-off is generally placed as 0.025 eV and with epithermal neutrons being defined on the range of $0.025 < E < 0.4 \text{ eV}$. The documentation found describing various tests of tungsten-rhenium thermocouples provide information only on the thermal and fast neutron fluence levels the thermocouple experienced. To improve the comparisons of the provided limits with the documented irradiation experiments, it is necessary to estimate the two-group approximation from the provided three-group approximation value. This can be accomplished by combining the intermediate and fast neutron fluence values provided by the Project Rover documentation. This provides a reasonable estimate due to how a two-group approximation places all neutrons with energies above the thermal cut-off to the fast neutron group. Doing this provides fast fluence estimates of $5.84 * 10^{19} \frac{\text{neutrons}}{\text{cm}^2}$ and $1.024 * 10^{21} \frac{\text{neutrons}}{\text{cm}^2}$.

Irradiation effects on tungsten-rhenium thermocouples have been investigated due to the potential of the instruments to be used in extreme temperature nuclear applications other than nuclear rocket technology. Los Alamos Scientific Laboratory (LASL) irradiated thermocouples whose thermoelements were composed of tungsten and tungsten-25%rhenium alloy. These instruments experienced an integrated thermal neutron flux of $3.8 * 10^{20} \frac{\text{neutrons}}{\text{cm}^2}$. This exposure caused the irradiated thermocouples to require

a temperature 60°K greater than unirradiated thermocouples at 1200°K and 33°K at 2170°K. Additionally, the tungsten-25%rhenium thermoelement underwent phase separation with one portion containing a higher concentration of osmium [8]. While these instruments do not correlate to a known thermocouple type, current tungsten-rhenium alloy thermocouples implement tungsten-26%rhenium or tungsten-25%rhenium. As such, this provides some insight to the potential effects and negatives of using these instruments in a high thermal flux environment.

Investigations of type D (tungsten-3%rhenium/tungsten-25%rhenium) for application in nuclear propulsion technology provide similar insight into the degradation of the instrument. One such investigation exposed several instruments to temperatures ranging between 1900°K to 2100°K for 5000 hours. This test implemented both in-pile and out-of-pile instruments to validate performance and ensure accurate statements could be made regarding the drift. During this test, the thermal and fast neutron fluence was estimated as $2 * 10^{21} \frac{\text{neutrons}}{\text{cm}^2}$ and $0.4 * 10^{21} \frac{\text{neutrons}}{\text{cm}^2}$ respectively. Additionally, the fast neutron energy group was defined as any neutron with $E > 0.18 \text{ MeV}$. The emf decrease of the irradiated thermocouples corresponds to a -190°K error at 2073°K. In contrast, the out-of-pile instruments drifted by -54°K at the same temperature. The maximum deviation of this error for each group of thermocouples was reported as $<\pm 10^\circ\text{K}$ [10]. The relatively small spread in results can be attributed to the fact that the majority of the instruments are from the same batches of wire. However, this allows for the degradation effects to be expected for thermocouples of similar composition and purity.

For information related directly to thermocouples implemented during Project Rover, there are reports related to instrument tests conducted by Aerojet. However, these reports are focused on a test at the ground test reactor (GTR-13) and its applicability to the NRX-A2 reactor design. This reactor design is a precursor to the engine tests that were completed during Project Rover; however, similar thermocouples were used throughout the program. One such report indicated no meaningful effect would be encountered during the NRX-A2 test with regards to the thermocouple performance [7]. The estimation of expected error took into the production of rhenium due to transmutation and its effect on emf and the performance of a similar instrument from a previous test. However, these estimations do account for the effect of osmium or the creation of defects in the wire. Another estimation of the performance of the instrument produced around the same time indicates a calibration shift of 2% [19]. A shift of this magnitude appears minor but would produce a delta of $\sim 47^\circ\text{K}$ at an operating temperature of 2360°K. While this exceeds the accuracy values provided in the previously mentioned trade study, the accuracy requirements for the NRX-A2 were lesser than the described flight requirements.

During the test of the instruments at the GTR-13, the temperature was provided via electric heaters that were given a constant power, excluding some deviations, at intervals through the 100-hour test period. However, the heaters were also irradiated and are a potential source of error. Due to the power variation in the heater, the temperature data was normalized to the pre-irradiation power inputs. Although some reports indicated no notable changes would be affect the instruments, the thermocouple reading varied from 1399°C pre-irradiation to 1306°C after 120-hours of irradiation [9]. This shows a change of 93°C, which exceeds even the less strict requirements for accuracy for the NRX-A2 reactor test. This error exceeds the expected problems from other historical tests. As such, there is likely an additional factor altering the instruments performance. However, this continues to show the potential issues with the use of tungsten-rhenium thermocouples in nuclear rocket environments.

Since the end of Project Rover, there have been several investigations into developing high temperature-irradiation resistant thermocouples. For radiation resistant thermocouples, a specialized instrument has recently been developed by Idaho National Laboratories (INL). The instrument is termed

the high temperature irradiation resistant thermocouple (HTIR-TC). Several tests have been completed regarding the long-term high temperature exposure of the instrument with variable results over standard type N and type K thermocouples. Additionally, they are indicated to be less susceptible to radiation induced drift from long term exposure to a neutron flux [20, 21]. The HTIR-TC has the potential to withstand temperatures up to $\sim 1800^{\circ}\text{C}$ with standardization tests indicating a maximum temperature of 1600°C for the current instruments [22]. However, the temperature limits of the instrument are several hundred degrees lower than the necessary requirements for NTRE systems.

Due to the de-calibration that will occur with tungsten-rhenium thermocouples in a nuclear rocket environment, their use would require software methodologies to correct for the degradation. Due to the lack of high-quality data, there are a limited number of pathways to provide a recalibration functionality. One such method is the use of a soft sensor or software-based sensor. Soft sensors implement high fidelity models of the process of interest to provide what the temperature at the point of interest should be. The input to the model-based sensor would be the various other instruments present in the system. This would allow for a thermocouple to operate as it would normally, as well as having an additional software component that can aid in the validation of the temperature measurement. However, this requires the other instruments to be highly stable and experience minimal changes during the operation of the reactor system. The failure of a critical measurement necessary for the input of the soft sensor would prevent the software-based solution from providing the desired use. Another potential corrective procedure can be implemented by using a highly correlated temperature instrument in a less extreme portion of the system. Implementing an instrument such as the HTIR-TC in such a position would allow for the recalibration of the instrument during operation. However, these are software-based solutions. A temperature measurement technology that is capable of in-situ self-recalibration inherently is more desirable.

3.2 Pyrometry

Standard thermocouples, resistance temperature detectors (RTDs), and ultrasonic thermometers require to be exposed directly to the process to allow for the temperature to be measured. Due to the limitations of materials at extreme temperatures, direct exposure to the process can present a significant design challenge. However, optical and thermal radiation pyrometers do not have to be exposed to the process to provide a measurement. Instead, a line of sight to the measurement point of interest is required. Methods such as this appear to be desirable for application in nuclear rockets and will be discussed in depth.

Optical pyrometry has been used to measure furnace temperatures for numerous years and the technology has evolved significantly since its inception. Initially, the technology was termed as the disappearing-filament optical pyrometer and required a technician operate the instrument. The instrument operated on the principle of thermal incandescence and that at a given wavelength, the electromagnetic radiation emitted by a hot body is temperature dependent. The most basic design implements a tungsten filament that is provided a variable current by the operator; subsequently, the filament must be calibrated to ensure the temperature and electromagnetic emission at a given current is known. An image of the target is superimposed on the filament using an objective lens when the operator looks through the eyepiece of the device. Once the tungsten filament appears to disappear into the superimposed target image, the known temperature and “brightness” of the filament at the provided current can be used to calculate the temperature of the target. This can be seen in Equation 3.1, which states the radiant intensity of the target and the filament are equal.

$$\frac{\epsilon \lambda_e C_1}{\lambda_e^5 \left(e^{\frac{C_2}{\lambda_e T_t}} - 1 \right)} = \frac{C_1}{\lambda_e^5 \left(e^{\frac{C_2}{\lambda_e T_f}} - 1 \right)} \quad 3.1$$

This equation implements ϵ as the emittance of the target, λ_e as the wavelength of any optical filter included in the instrument, T_t as the temperature of the target, T_f as the temperature of the filament, and the constants C_1 and C_2 . The above equation can be simplified for temperatures less than 4000°C, but the provided information is sufficient for understanding the operation of the instrument [14]. While this design is not applicable for industrial process or system operation, there are similar devices that do not require manual operation.

Modern pyrometers make use of the infrared radiation that is emitted by the heated body of interest. Infrared pyrometers implement a detector and an optical system that focuses incoming infrared radiation on the detector. Blackened tip thermopiles are one possible detector that can be implemented and are composed of various thermocouples connected in series or parallel. Placing the thermocouples in a series configuration allows for the sensitivity of the instrument to be increased, and the sensitivity increase is proportional to the number of thermocouples used in the construction of the thermopile [14]. The blackened tip of the thermopile allows for improved radiation absorption and the temperature of the instrument will increase until equilibrium is reached. This allows for an electric signal to be generated based on the amount of incoming radiation. However, these instruments can also implement photon detectors. While there are various types of photon detectors, their operation can be described simply as the freeing of electrons due to incident infrared radiation. This allows for the detector to be calibrated, with the electrical signal generated by the detector being related to temperature.

Temperature measurements that do not require direct contact with the process provide a favorable methodology for extreme temperature measurements in nuclear environments. The use of a standpipe to provide the required line of sight allows for the pyrometer to be installed in positions that receive minimal neutron and gamma radiation. This prevents excessive damage to the instrument and the various electronics that are required to ensure the instrument operates as desired. However, the materials that allow for the instrument to maintain a line of sight will be exposed to harsh environmental conditions.

Standpipe designs to provide optical access in sodium fast reactors (SFRs) have been investigated due to the benefits of this measurement technology. The main components of the standpipe can be simplified to a viewport, mirrors, the pipe itself, and the mount for the pyrometer. Of these components, the viewport is the only material that will be in contact or proximity to the process. Active cooling can be implemented during full power operation of the reactor to combat the high temperatures the material will be exposed to. However, the material will also be exposed to cryogenic temperatures and matching the coefficient of thermal expansion may provide additional difficulties. Referring back to work on optical measurements in SFRs, none of the optical materials were considered to be at a high level of readiness for implementation near-core. Materials such as chemical vapor deposition diamond were considered to be at a medium level of readiness for near-core application with further research required [23]. As environmental conditions present in an SFR are not as severe as those present in a NTRE, it can be reasonably assumed that material readiness for near-core application is significantly lower.

The waveguide could also be constructed of a fiber optic cable with specialized manufacturing techniques. Implementing additive manufacturing for the construction of the external shield that is located above the reactor core would allow for a pathway for a fiber optic cable. However, a viewport or passthrough is still needed to access the reactor pressure vessel. This introduces similar problems as with

the standpipe design as well as potential complications arising from the fiber optic cable being exposed to a neutron fluence and reactor temperatures.

Beyond their potential use as waveguides, fiber optic cables can also be used as temperature measurement devices. Work at the Ohio State University Research Reactor (OSURR) has investigated the effects of radiation and temperature the degradation of the cable [24-26]. However, these tests reached a maximum of 1000°C and lower fast fluences than expected in a NTRE. Additionally, the usage of fiber optic cables at 2000°C or greater is not viable. At the operating temperatures expected in an NTRE, the fibers would experience significant structural damage and melting.

Overall, the benefits provided non-contact optical measurements are impinged by the limits of the materials necessary for their use. This is especially apparent for in-core measurement of the NTREs where attaining a line of sight is complicated by the system configuration. The technology appears to be best suited for measurements of the core outlet temperatures but would require significant engineering to properly sight the point of interest for measurement.

3.3 Ultrasonic Thermometry

The speed of sound in a material is a temperature dependent quality and ultrasonic thermometry (UT) takes advantage of this property to measure temperature. Essentially, the measurement is based on the time-of-flight of an ultrasonic signal or acoustic pulse in a waveguide/sensing element. The signal is generated at one end of the waveguide using a piezoelectric or magnetostrictive material and then travels the length of the waveguide. At the end point of the waveguide, the difference in acoustic impedance between the waveguide and environment causes the signal to be reflected to its point of origin. The time required to return to the point of origin can then be used to calculate the current average speed of sound in the material. Temperature is then determined via a calibration curve like those used in resistance temperature detectors and thermocouples.

A notable benefit of this measurement technology is the capability to provide a measurement of the temperature gradient of the process. As reflecting the ultrasonic signal requires alterations in acoustic impedance, discontinuities such as notches can be added to increase the number of reflection points in the waveguide. With the position of these notches known, the reflected signals between the discontinuities can be related to provide temperature measurements of specific segments of the waveguide [27]. However, additional signal processing is required to properly measure and attain the temperature gradient.

Signal processing is an important aspect of ultrasonic thermometry to properly compute the speed of sound from the reflected ultrasonic signals. Multiple reflections or echoes can be produced by a single acoustic pulse from the signal generator. This can cause the reflected signals to overlap and hinder the computation of the speed of sound in the material. Another problem of note is related to the occurrence of undesirable echoes occurring. These can originate from discontinuities not intentionally included in the waveguide. One such cause of these unintentional echoes comes from the endpoint of the sensing element coming in contact with its sheathing material. This causes the echo to become distorted and prevents the measurement from providing the correct value [28].

Properly designed ultrasonic thermometers are capable of measuring temperatures greater than 2000°C. In theory, the melting point of the sensing element is the only limit on the maximum measurement temperature [27]. Using a tungsten sensing element, this would provide a measurement approaching 3400°C. This is likely why such instruments have been investigated for liquid metal fast breeder reactors, reactor safety experiments, centerline fuel measurements, and nuclear thermal rockets

[27, 29-33]. Because of the historical investigations, the effect of nuclear environments on the instrument can be postulated through the evaluation of existing documentation.

Investigation of an ultrasonic thermometer using a rhenium sensing element for nuclear rocket application occurred during the time of Project Rover. During this investigation, rhenium wires received a thermal neutron fluence of $8.7 * 10^{19} \text{ nvt}$ and a fast neutron fluence of $2.6 * 10^{19} \text{ nvt}$. The irradiated samples were then annealed and then tested in a vacuum with control wires to provide a comparison. From this, no significant change was noted between the annealed and irradiated wires and the control wires [34]. While the conductors of the previous investigation indicated that this result was viable to show limited radiation damage, annealing the irradiated wires likely removed any fast neutron damage that occurred during irradiation. A study at Oak Ridge National Laboratory implemented the same instruments in the High Flux Isotope Reactor (HFIR) with a total thermal and fast neutron fluence of $1.55 * 10^{22} \text{ nvt}$ and $4.6 * 10^{21} \text{ nvt}$ respectively. After irradiation, the instruments showed a shift of -1070°C at 1000°C due to the transmutation of rhenium to osmium. Furthermore, the volume of the sensing element did not decrease as expected and this was attributed to void deformation and intergranular volume increases. [31]. While both of these experiments do not replicate the expected fluence of a nuclear rocket, they provide some insight regarding the use of rhenium as the sensing element. From these experiments, it is likely that the calibration of such an instrument would drift due to neutron exposure. Especially when taking into account the cyclical nature of nuclear rocket operation and the limited time for high temperature annealing to occur.

The usage of other refractory metals in ultrasonic thermometers has also been investigated in nuclear environments. Some of these metals include tungsten, tungsten-25%rhenium, and thoriated tungsten. Tests of ultrasonic thermometers using thoriated tungsten in nuclear environments have indicated minimal drift due to irradiation. A 2000-hour test at 2273K produced an estimated drift of $\pm 30\text{K}$ with a thermal and fast neutron fluence of $1 * 10^{21} \text{ nvt}$ and $1.5 * 10^{21} \text{ nvt}$ respectively [35]. Additionally, the use of thoriated tungsten as the sensing element has been tested up to 2700°C and has been indicates to work satisfactorily. However, it is noted that the material is sensitive to contamination from vapor deposition of the sheathing material to the wire [36].

A significant concern is the possibility of sticking, which is a contact weld between the sheath and waveguide. The contact causes acoustic discontinuities that negatively effects the accuracy of the temperature measurement. One study produced 300°C calibration errors at 2000°C over 6 days [32]. Another study tested two UTs for fuel temperature measurement with one instrument failing after 14 hours due to sticking problems. The other instrument experienced sticking, but power cycling the reactor corrected the problem when it occurred [37].

A potential solution to sticking is the implementation of standoffs at point along the sensing wire [38]. This can localize the reflections due to contact with the sheath at known points to allow for signal correction. However, a study of a 10mm length thoriated tungsten sensing element by Carlson et. al indicated the reflections from the standoffs were too excessive for their application. Instead, a thorium dioxide (thoria) sheath was implemented as it would not cause sticking as it is an oxide ceramic [27]. For NTRE application, the use of an oxide ceramic in a high temperature hydrogen environment is a potential concern that requires further investigation into the compatibility of the material.

Overall, ultrasonic thermometry provides a viable path to allow for in-core temperature measurements in a nuclear rocket system. Depending on the sensing element, the instrument can be considered relatively irradiation resistant. However, the various concerns related to their use are a notable hindrance to their deployment and long-term use. As these systems are unable to go maintenance for 5 years at a time, there

is not an opportunity to correct sticking if it occurs. If it is used in conjunction with other temperature instruments, such as thermocouples, it provides additional diversity to the system, but does not fully replace the instrument. Additionally, the configuration of the reactor system can increase the complexity of the necessary path for the ultrasonic thermometer. Any bends or curves in the wire can induce changes to the acoustic impedance and therefore interfere with the measurement.

3.4 Johnson Noise Thermometry

Due to its nature as a first principles temperature measurement technology, JNT has been heavily investigated for application in nuclear reactor environments [31, 39-43]. The common drawbacks to measurement technology are the susceptibility of the instrument to EMI, the small magnitude of the signal, complexity of the signal processing, long measurement time requirements for high accuracy, and the cost of the system. Historically, the issues regarding the signal have been handled by comparing the noise voltage of two resistors, one at a known temperature and one at the temperature of interest. Switches were then used to place the signal onto a single pre-amplifier channel. However, switching can cause noise spikes that can be blocked via the use of an additional switch depending on the amplifier circuit [41]. Furthermore, there is noise inherent to critical components such as the amplifier required to increase the magnitude of the noise signal.

Since the advent of JNT, there have been significant advancements in technology that have lowered the cost of signal processing components. Additionally, there have been advances in signal processing algorithms for noise removal in JNT applications. Issues such as amplifier noise can be removed via cross-correlation techniques. By sending the noise signal through two amplifiers, cross-correlation will remove the uncorrelated noise of the amplifiers [39, 41]. For the removal of EMI on the Johnson noise signal, Oak Ridge National Laboratory (ORNL) has developed a rejection method and a subtraction method. The rejection method applies time domain and frequency signal processing techniques to detect and “reject” transient and periodic noise from the collected signal. The subtraction applies a hardware modification with advanced signal processing to remove EMI from the signal. Essentially, an antenna runs the length of the lead cable from the sensor to the amplifier electronics to provide a measurement of the environmental EMI. The CPSD of the EMI signal from the antenna can then be subtracted from the output of the amplifiers. The implementation of the subtraction method has shown promising results in both laboratory conditions and in harsh EMI environments such as the Kingston Fossil Plant located in Harriman, Tennessee [42, 43]. While this is a simplistic and abbreviated description of the methodology, it is sufficient for the purpose of discussing signal processing improvements for JNT. Detailed information regarding both methods and tests can be found in reference [42] and [43].

Additional complications with JNT thermometry for NTRE application exist with the resistor or RTD implemented in the system. As relatively long time periods are necessary to improve the accuracy of JNT, the use as a recalibration methodology for an RTD would be preferable for control system applications. However, there is currently not an RTD capable of withstanding the challenging environmental conditions of an NTRE. There is also the potential for issues due to the magnitude of resistance change over range of temperature exposure. NTRE requirements for high temperature measurement indicate minimum temperatures of 278°K and 556°K with a maximum temperature of 2500°K [3]. The electrical resistivity of a resistor will alter significantly among this range. There is an indication that the signal processing electronics of JNT limits resistance changes to a factor of 3 around the operational resistance due to amplifier electronics [44]. While this may limit the range of resistance change, a potential solution could implement a switch-based circuit that allows for modified circuitry to be implemented at specific points of resistance change.

3.5 Resistance Temperature Detectors

Commercially available RTDs are not capable of measuring temperatures up to or in excess of 2000°C. The measurement of such a temperature via an RTD would require the implementation of a refractory material capable of surviving the environmental conditions of the system. A prime candidate would be a tungsten-based instrument, due to its high melting point and resistance temperature relationship. Historical investigations of such an instrument appear to be limited but have been completed with the intent of nuclear applications. Reports indicate the capability of a tungsten RTD to attain stabilities equivalent to platinum RTDs with the potential to provide an improved value [45]. A constructed tungsten RTD provided a 63% response time of 0.4 seconds in water flowing at a rate of ~9 m/s. Performance in an nuclear environment provided minimal change to the instrument but were at fluence levels several orders of magnitude less than expected in an NTR [46, 47]. However, the favorable performance of the historical instrument provides a potential pathway for the construction of a tungsten RTD capable of measuring high temperature extremes.

3.6 Instrument Selection

The potential for instrument degradation that cannot be corrected with maintenance activities is a critical issue in the deployment of an NTR. Unavoidable drift that can occur from long term operation, exposure to extremely high and low temperatures, and high neutron fluence levels will degrade the capability of the control system to properly operate the system. As such, in-situ recalibration is required to correct for potentially devastating alterations in instrument behavior. Based on the current SOA of temperature measurement technology, it appears that JNT provides the best pathway forward for the deployment of a measurement system capable of in-situ recalibration. However, there are several factors that impede the implementation of this technology's deployment in a nuclear rocket.

The main needs for JNT implementation in a NTR are: 1) a strong understanding of the noise environment due to the reactor and space, 2) an RTD capable of withstanding the operating conditions of the rocket, and 3) an appropriate electronics system. Each of these needs for JNT are significantly complex and require extensive work to ensure proper application for a flight ready NTR. Due to advancements in signal processing for JNT, the development of an RTD that is capable of measuring temperatures $\geq 2000^\circ\text{C}$ can be considered one the greatest challenge to deployment of a JNT measurement system. Additionally, without a functioning resistance-based sensing element the implementation of JNT would not be possible.

Not only does the development of an extreme temperature RTD provide a critical need for JNT, but it also provides an additional methodology for temperature measurement in extreme environments. This includes additional diversity in temperature measurement as well as the potential for in-core temperature measurements for other reactor designs. The common benefits of RTDs in comparison to thermocouples can be summarized as: higher measurement stability, higher accuracy, and the linearity of the relationship between the measured parameter (resistance) and the desired parameter (temperature). While there are several disadvantages to the use of an RTD, such as lower response times and monetary cost, the improved stability and higher accuracy provided by the measurement technology are desirable for application in NTR application. For a reference of RTD accuracy, there are commercially available platinum RTDs listing an accuracy of $\pm 0.05^\circ\text{C}$ up to 962°C . A thermocouple with a comparable measurement range, the type E model, provides a standard accuracy of $\pm 1.7^\circ\text{C}$ or $\pm 0.5\%$ of the measurement above 0°C and $\pm 1.7^\circ\text{C}$ or $\pm 1.0\%$ of the measurement below 0°C with the value being determined by whichever value is greater. As a brief example, consider two processes at temperatures of 900°C and -1000°C . The mentioned platinum RTD provides an accuracy of $\pm 0.05^\circ\text{C}$ for at both

temperatures, while the type E thermocouple provides an accuracy of $\pm 4.5^{\circ}\text{C}$ at 900°C and $\pm 1^{\circ}\text{C}$ and -100°C .

Another factor informing the selection of RTD development and evaluation is the use of a temperature measurement device located in the fuel for startup and general reactor control. The previously noted trade study from the NERVA program indicates a desired measurement range of 4.5°C to 2225°C [3]. While tungsten-rhenium thermocouples are capable of measuring temperatures down to 0°C , the accuracy of this measurement suffers significantly. During tests of the XE-Prime, the uncertainty of the measurements at 4.5°C were estimated to be $\pm 72.2^{\circ}\text{C}$ or greater [2]. Additionally, there is the potential for the even lower temperature measurements to be necessary for startup control and approaching a desired idle point of operation that can be transitioned to full power. While commercially available type C thermocouples indicate better uncertainties at this temperature, there is no listing for temperatures below 0°C . Thermocouples also suffer from issues related to decreased sensitivity at extremely temperatures in comparison to RTDs. As such, the development of a resistance-based measurement with improved sensitivity in the startup temperature range of a NTR system is desirable.

Beyond comparison of the selected measurement device to thermocouples, there are several advantages to the use of an RTD in comparison to optical pyrometry and ultrasonic thermometry. In comparison to these measurement technologies, RTDs are incredibly simple devices that require minimal signal processing electronics. A temperature measurement for an RTD requires a voltage source, a Wheatstone bridge, and knowledge of the relationship between the measured resistance and temperature. In contrast, both ultrasonic thermometry and optical pyrometry require specialized electronics to collect and process signals to provide a temperature measurement. This along with the necessary materials needed for the construction of the instrument and waveguides complicate the design of the instrument especially upon considering limited space available within a NTR system for instrumentation.

Chapter 4: Resistance Thermometry

Resistance thermometry has been used for several decades in various industrial processes as well as the development of the temperature scale provide by the National Institute of Standards and Technology. The basis of this measurement is the inherent relationship between the electrical resistivity of a material and its temperature. Depending on the specific type of instrument, the resistor used in the instrument can be composed of a ceramic, polymer, or a metallic conductor. RTDs commonly make use of wire composed of a metallic conductor that is coiled to provide a nominal resistance 50 Ω , 100 Ω , 500 Ω , or 1000 Ω . In this definition, nominal indicates the resistance of the element at 0°C. However, there has been research into the usage of other materials for the resistive element. For nuclear power plants, platinum RTDs are the most common due to desirable performance provided by the material.

The relationship between the resistance of an RTD and the temperature can be represented via the Callendar-Van Dusen equation. This equation can be expressed as:

$$R(T) = R(0)[1 + A * T + B * T^2 + (T - 100) * C * T^3] \quad 4.1$$

Equation 4.1 provides R(T) as the resistance at temperature T, R(0) as the resistance at the freezing point of water, the coefficients A through C, and is valid to ~660°C. However, the equation can be simplified to use a single coefficient to provide a linear relationship between resistance and temperature over a specific range. For platinum RTDs, the value of the coefficient is described by the standard IEC 60751: “Industrial platinum resistance thermometers and platinum temperature sensors”. The direct relationship between the resistivity of the material and temperature can be used, but this provides the potential need to include the effects of thermal expansion on the resistance measurement. This can be better represented via the standard resistance equation, which can be seen as:

$$R = \frac{\rho_e L}{A_{xs}} \quad 4.2$$

In Equation 4.2, the resistivity is represented by ρ_e , the length for electron transport is L, and the area for the application of an electric field is A_{xs} . When considering a wire, the area is the cross-sectional area for the wire and the L is the total wire length. Therefore, increasing the length and decreasing the diameter of the wire will increase the resistance when provided a constant electrical resistivity. For platinum RTDs, 0.05 mm to 0.5 mm diameter wire is commonly implemented [48].

The use of fine diameter wire allows for the sensing element to provide the desired resistance without requiring excessive lengths of wire. For example, platinum has an electrical resistivity of 9.81 $\mu\Omega$ -cm at 0°C; therefore, a platinum RTD with a nominal resistance of 100 Ω that implements 0.05 mm diameter wire would require ~2 m of wire [49]. In contrast, a 0.5 mm diameter platinum wire would be 200 m in length to provide a resistance of 100 Ω . The required length to provide the desired resistance prevents the use of a straight wire in practical applications. However, modern RTD designs coil the wire to minimize the space necessary for the sensing element to fit the desired application.

The main RTD designs of pertinence can be considered as the wire-wound design and coiled element design. The commonalities between the designs include mechanical support for the wire, electrical insulation, and coiling to the wire to minimize the space it requires. Beyond this, the most significant difference comes in how the wire is wound and placed inside its protective housing. Wire wound RTDs implement a supportive mandrel made of an electrical insulator. The wire is then coiled around the mandrel in either a single or double helix. Each end of the wire is then welded to the appropriate lead wires and the coils are coated with a glass or ceramic to provide additional protection. The entire structure

is then placed into a thermally conductive sheath to prevent exposure to the process. Coiled element RTDs implement a similar mandrel but includes bores. The coiled wire is then placed into the bores and then loosely packed with a powdered form of an electrical insulator. A simple diagram of each RTD design can be found in Figure 4.1 to provide greater clarity regarding the differences in the wire.

A critical aspect of the design of an RTD is related to limiting the thermal strain and minimizing the potential for mechanical flaws. Both can lead to alterations in the resistance of the measurement. Issues regarding strain come from the differences in the coefficient of thermal expansion of the sensing element material and the electrical insulator. By having mismatched coefficients, tensile or compressive strains can be induced in the wire. These strains can cause significant changes to the diameter and length of the wire. As seen from Equation 4.2, any alterations in the diameter or length will induce some change in resistance. Wire-wound RTDs are more susceptible to issues related to the coefficient of thermal expansion (CTE) due to the wire being wrapped fully around the mandrel and then cemented to its surface. In the coiled element RTDs, the placement of the coils into the boreholes allows for the materials to expand with minimal thermal expansion. While the boreholes are filled with electrical insulation, it is in the form of a powder which is then loosely packed into the holes. Keeping the powder loose allows the wire to thermally expand and contract without the insulator causing significant errors. However, providing materials with similar coefficients of thermal expansion should help minimize the effects of thermal strain.

Beyond the basics of RTD design, the performance of the instrument can be quantified through the implementation of performance parameters. For this work, the main parameters of interest are the response time and the stability. These two parameters were chosen due to the ability to estimate their value based on model simulations.

Instrument response time can be defined as the time required for the measurement to reach 63% of its final value when exposed to a new input. However, the time required for the output of the instrument to reach 50% or 90% of the new value may also be used. Commercially available platinum RTDs can provide response times that range from less than a second to several seconds. This range is largely due to the thermal mass of the instrument and heat transfer rate from the process to the sheath of the RTD. As the temperature induced change in resistance occurs on a much smaller timescale than heat transfer, it can be assumed that heat transfer is the main factor effecting RTD response time. The time required for heat from the process to transfer to the sheath, insulator, and sensing element can be used as the response time. In practical applications of an RTD, this is further complicated by the use of thermowells. Thermowells are fixtures that allow for an instrument to be placed in a flowing process that allow for simple replacements to be completed. While useful, the inclusion of a thermowell can have a negative impact on the response time of the instrument. This can occur due to minor errors during the installation of a new RTD into a thermowell. It can be difficult to properly install the instrument, causing air to be trapped in the thermowell with the RTD. This air pocket negatively impacts the response time due to its thermodynamic properties.

The stability of an RTD is an indication of its ability to maintain its calibrated state over a period of time. It can also be considered the measurement drift that can be expected in the instrument during its operational lifetime. Any drift in an RTD is related to alterations of the known resistance temperature relationship. Mechanical strain, chemical reactions, and neutron exposure are some of the factors that can the instrument to drift during operation. While the exact effect each factor has on the resistance-temperature relationship are difficult to quantify, they can be used to estimate the overall feasibility of a proposed RTD design. With these factors in mind, the following sections will discuss the selection of the materials for the proposed RTD design that is the focus of this work.

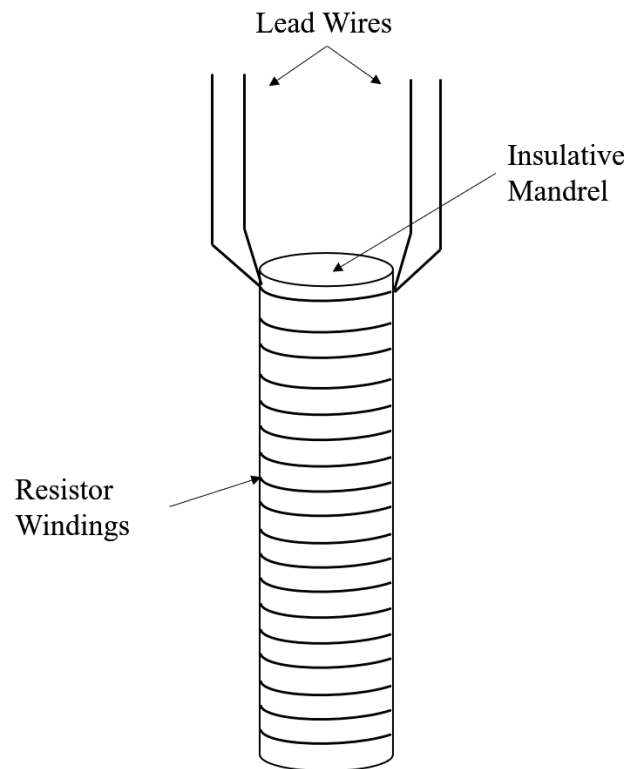
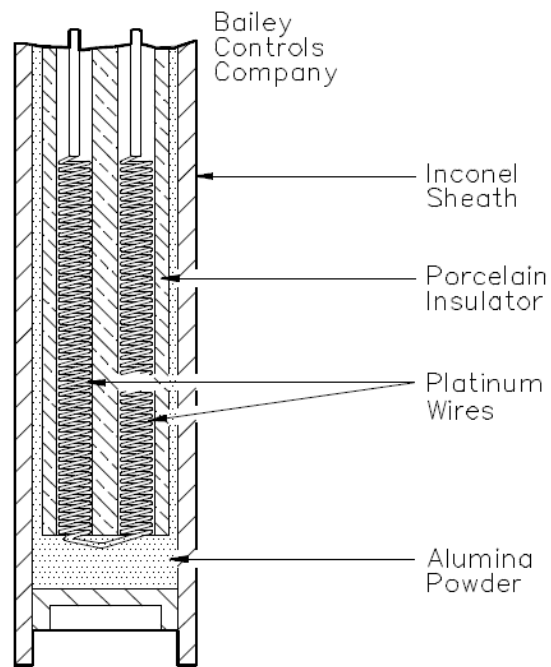


Figure 4.1: Coiled element (top) and wire-wound (bottom) RTD design diagrams. Figure adapted from reference [50].

4.1 Material Selection: Sensing Element

Due to the operating conditions of an NTRE, the sensing element of the RTD is required to have an extremely high melting point to prevent phase transitions. As such, the refractory metals comprise the potential materials for the sensing element of the RTD. This category includes tungsten, rhenium, tantalum, niobium, and molybdenum. Of these metals, tungsten has been used previously in the construction of RTDs for application in nuclear reactors [47]. However, these instruments were designed for much lower temperatures than that expected within a nuclear rocket. From the investigation that led to the construction of these historical tungsten RTDs, it was determined that tungsten resistors were capable of attaining the stability of platinum resistors [45]. Additionally, the tungsten sensing element was capable of withstanding pressure tests over 5,000 psi without failure [47]. The historical experience shows that a tungsten based RTD can be constructed and perform as desired.

Furthermore, tungsten provides desirable properties for its use in a high temperature RTD. The resistance temperature relationship of a sensing element is desired to be as linear as possible. While the electrical resistivity over the range of 40°K to 3600°K is best described by a nonlinear fit, a linear fit of the data over the expected process conditions of 111K to 2700K provides a root mean square error of ± 0.0552 and a coefficient of determination of 0.997. In comparison to rhenium and tantalum, this is noticeably better than the fits that have been generated for those materials. Further supporting the use of tungsten is that it remains chemically inert over a wide range of temperatures. The main reactions that are of concern for tungsten are the adsorption of oxygen and oxidation. Adsorption occurs at room temperature and can lead to outgassing as the temperature increases. Oxidation of tungsten occurs at approximately 300°C and the material readily undergoes this reaction [51]. Tungsten oxides have vastly different properties than the pure metal and could significantly affect its use as a sensing element. However, oxidation is a concern with the other refractory metals as well. Even with oxidation, the chemical properties of tungsten appear to be more favorable for a high temperature sensing element.

The largest drawback to the use of tungsten is the brittleness of the metal. This causes significant concern regarding mechanical strain and any vibration that may cause the sensing element to break. It also causes the material to be extremely difficult to work with, which is part of the reason that it is alloyed with rhenium. Tungsten-rhenium alloys provide improved mechanical characteristics over pure tungsten samples [52]. Increased mechanical strength can also be seen through adding an impurity like thoria to a tungsten sample [3]. However, tungsten still appears to be the best option for a sensing element in a high temperature RTD. While its mechanical strength is a significant drawback, the advantages provided by its other material properties are more than adequate to account for this.

The final benefit of tungsten comes from the large swathe of information that is readily available on the material. As the purpose of this work is the refinement and simulation of a proposed instrument design, the availability of the properties of the selected material is critical. Surveying the available literature, the properties of tungsten have been heavily investigated and documented. Its ability to survive temperatures over 3000°C has led to several evaluations of the material for application in nuclear fusion reactors. Several reports have detailed both empirical relationships and raw data for the various properties of tungsten [51, 53-57]. This also includes several investigations into the changes in tungsten's electrical resistivity due to neutron exposure [58-63]. Currently, a comparable level of detail was not found to exist for the other refractory metals during the literature survey.

4.2 Material Selection: Electrical Insulator

As the process temperature exceeds 2000°C, the list of potential candidates for the electrical insulator is extremely limited. Not only does the insulator need to have a high melting point but it should also

maintain a relatively high electrical resistivity at the operating temperature. The materials capable of withstanding the operating temperature are hafnium dioxide (hafnia), beryllium oxide (beryllia), zirconium dioxide (zirconia), magnesium oxide (magnesia), and thorium dioxide (thoria). Alumina is not considered due its low melting point and low resistivity at high temperatures. Of the high temperature materials, zirconia does not provide a desirable resistivity at the operating temperature of the system. For example, the electrical resistivity of beryllia is three orders of magnitude larger than zirconia at 2000K. Because of this, zirconia is not further considered in the evaluation of insulator materials.

Each material has a melting point higher than the desired operating temperature of the system, but the relationship between the electrical resistivity and temperature differs significantly. For example, beryllia is expected to provide an electrical resistivity that is two orders of magnitude greater than hafnia and thoria at 2000°C [3]. However, this is only one estimation of the electrical resistivity of beryllia. The available data on the material provides vastly different values for electrical resistivity and conductivity. This is due to beryllia being an impurity-controlled ionic conductor. Even small amounts of key impurities can alter the resistivity of a sample by several orders of magnitude [64-68]. One investigation implementing beryllia provides an electrical resistivity several orders of magnitude less than thoria, likely due to the fact that the purity of the material was only 99.95% [69, 70]. Currently, beryllia is commercially available at purity levels of 99.999% and conductivity effects of impurities should be minimal. Further comparing the electrical resistivity of the materials shows that even the impure sample of beryllia provides an electrical resistivity that is at least one order of magnitude larger than magnesia and hafnia.

Another point of evaluation is the CTE for the electrical insulator and the sensing element. A significant mismatch between the materials can induce additional errors as well as potentially damaging the sensing element. For example, consider that the electrical insulator has a CTE that is ten times greater than that of the sensing element. This would indicate that the insulator will expand an order of magnitude more than the sensing element that is coiled around it. This can cause the wire to be stretched and the strain may cause a mechanical deformation that causes a permanent change in the resistance of the system. Therefore, it is preferable to keep the mismatch between the two materials to a minimum. As the sensing element has been chosen as tungsten, the insulator with the closest CTE should provide a viable choice. Table 4.1 contains the information regarding the linear CTE of each material, its difference from tungsten, and the ratio of the two values. Based on the value provided in Table 4.1, it appears that hafnia provides the closest linear CTE to tungsten. Beryllia has a CTE that is almost twice that of tungsten, but it still more favorable than both thoria and magnesia.

Another factor that can impact the selection of the electrical insulator is related to the volatilization of the ceramic oxide. Exposure to high temperatures make it is possible for materials to undergo vaporization which can cause the presence of undesirable elements to occur. For the oxides of interest, it can lead to the production of oxygen within the housing of the RTD. The presence of oxygen will then lead to the tungsten oxides being formed and can impact the known resistance curve of the instrument. As such, it is preferable to use an insulator that will produce the least amount of oxygen within the system. According to historical work regarding the vaporization of oxide systems, hafnia provides has the lowest volatility of the potential materials [71]. In contrast, magnesia has a vaporization rate that is several orders of magnitude higher than the other available materials even in an inert environment [72]. Additionally, beryllia has a marginally more desirable vaporization rate than thoria at ~2000°C [72, 73]. There is also a larger amount of information currently available for beryllia in comparison to hafnia. Even though hafnia is reported to be less volatile than beryllia, the lower vaporization rate than thoria and magnesia along with the availability of information make beryllia the more feasible option.

Table 4.1: Linear Coefficient of Thermal Expansion for Candidate Electrical Insulators and Tungsten

Material	CTE 20°C ($\mu\text{m}/\text{m}\cdot\text{K}$)	Difference ($\mu\text{m}/\text{m}\cdot\text{K}$)	Ratio
Tungsten	4.5	0	1.00
Beryllia	8.0	3.5	1.78
Hafnia	6.0	1.5	1.33
Thoria	11	6.5	2.44
Magnesia	10.8	6.3	2.40

Overall, the best electrical insulator for high temperature applications appears to be beryllia. While it has some disadvantages, the large electrical resistivity at high temperatures more than makes up for these drawbacks. Errors induced in the measurement due to the decreased resistance of the insulator, i.e.: insulator shunting, are one of the largest concerns for an electrically based temperature measurement. Additionally, this material has been implemented in historical investigations of high temperature sensors during the NERVA program and Project Rover. Because of this, the material with the highest resistance at elevated temperatures is required even with some minor drawbacks.

4.3 Material Selection: Sheath Material

Due to the hydrogen propellant used in NTRE systems, the sheath material must be chemically compatible at extreme temperatures. Hydriding of the sheath material is a notable concern regarding the survivability of the instrument over its lifetime. Because of this, tungsten provides a viable option as it has both a high melting point and is unreactive with hydrogen [51]. This fact was noted during the Rover/NERVA era of NTRE research but indicated there were some concerns regarding the materials integrity at high temperatures. This led to the identification of tungsten, tungsten-2% thoria, and tungsten-26% rhenium as the prime candidates for instrument sheaths [3].

There are several metrics that can be used to evaluate the suitability of a material for use as the sheathing material of the instrument. These include the yield strength, creep-rupture strength, and effect of recrystallization. From these values, both pure tungsten and the noted tungsten-rhenium alloy are outperformed by thoriated tungsten. The inclusion of dispersed thoria in the tungsten retards the effects of recrystallization and improve the strength of the metal. The benefits provided by the use of thoriated tungsten show that it is the best option for an instrument's sheath. However, the available information detailing the thermophysical properties of thoriated tungsten and their temperature dependence appears limited. Some papers have been found detailing the change in heat capacity of thoriated tungsten between the temperatures of 1400K to 3600K. Comparing this data with that of pure tungsten provides a similar relationship with the maximum deviation from pure tungsten being 7.3537 J/kg-K over the stated temperature range.

Due to the limited information regarding the temperature dependence of the material properties of thoriated tungsten, the proposed instrument makes use of a tungsten sheath. While this is not the best sheathing material available, it provides the best path forward regarding the modeling of the instrument. However, the use of tungsten instead of thoriated tungsten will have minimal impact regarding the results of the model. For the model, the sheathing material is necessary to estimate the response time of the instrument due to heat transfer. The properties of this material beyond its purpose in heat transfer are not of significance for this work.

4.4 Material Selection: Electrical Insulator

This chapter has provided the basic knowledge necessary for RTDs as well as the justification behind the various materials that have been selected for the conceptual design. As the most feasible materials have been selected for the initial design, the dimensions and configuration of the RTD must be finalized. This is completed through the implementation of the RTD model. The model allows for various geometries to be investigated to allow for design to be improved by modification of the dimensions. However, the equations describing the behavior of the model require presentation before providing results.

Chapter 5: Resistance Temperature Detector Model

5.1 Introduction

Modeling an RTD requires several factors to be taken into consideration to estimate the capabilities of the conceptual design. Heat transfer, thermal strain, oxygen production, oxidation of the sensing element, and the electrical network of the RTD are all aspects that are important to modeling the instrument regardless of application. As the tungsten RTD is being designed for use in NTREs, a critical aspect is how the instrument's performance/calibration will change due to neutron exposure. As such, the proceeding sections will deal with each of these in turn and then provide how these factors are interconnected.

The overall purpose of the models is to provide verification of the materials selected in the construction of the conceptual RTD model. Due to the cost of irradiation experiments and high purity materials, the analytical investigation of the materials is necessary to ensure that desirable materials have been selected. Viewing the available data, it appears that the best materials have been selected for high temperature; however, this does mean the actual materials will perform as expected. There are several parameters that may cause undesirable interactions or results. Because of this, each model focuses on a different aspect that can be used to indicate the performance of the conceptual design and the choice of materials.

The purpose of each model is to indicate a specific performance parameter for the conceptual design and indicate potential challenges that may arise. Thermal modeling provides insight into the response time of the RTD configuration as well as a conservative estimation of the thermal strain. The chemical and irradiation models provide insight into the expected change in the resistance of the sensing element due to fast neutron induced defects, thermal neutron induced transmutation, and the loss of tungsten due to oxidation. This provides a rough approximation of the damage that the instrument will receive over the course of its operation. Finally, the electrical shunting model provides a conservative estimation of shunting due to the decrease of the electrical resistivity of the insulator. These models provide an indication of the performance of the chosen materials for the conceptual design and potential challenges that may occur.

5.2 Thermal Modeling

The most critical facet of thermal modeling for the conceptual RTD is the estimation of the response time of the instrument due to heat transfer. However, the current system does not take into account the time constant associated with the heat transfer from surrounding environment to the instrument. As such, response time estimates are used as a figure of merit to evaluate the instrument. The temperature of a material exposed to some heat source can be computed via a partial differential equation, which can be seen as:

$$\rho c_p \frac{dT}{dt} - \nabla^2 kT = \dot{q}. \quad 5.1$$

In Equation 5.1, the variables represent: density (ρ), specific heat capacity (c_p), thermal conductivity (k), temperature (T), and a spatially independent heat source (\dot{q}). The heat equation can be solved analytically and numerically when provided the appropriate initial and boundary conditions. For example, the current work replaces the heat source term with a time dependent boundary condition. This work focuses on the usage of a central space, forward time finite difference scheme to solve the temperatures in the system.

Using a time dependent boundary condition, allows for a specific temperature to be applied to the boundary of the RTD that can then be propagated through the system. Solving the heat equation for the defined system requires several additional assumptions and conditions. As it is desired to replicate the operation of a NTRE, the initial condition for all points of the RTD system should be at some standard low point. The assumption that all points of the RTD are the same temperature comes from the fact that an NTRE has long periods with no reactor operation. An additional condition occurs at the interface of the different materials that comprise the system. The change in materials at the interface can cause significant shifts in the properties used to solve the heat equation which can lead to various problems with the solution. As such, defining the spatial derivative of temperature at the interface as:

$$k_1 \left. \frac{dT}{dt} \right|_{x_{interface}} = k_2 \left. \frac{dT}{dt} \right|_{x_{interface}} \quad 5.2$$

allows for these terms to be removed from the difference scheme without causing additional complications. This also aids in the removal of potential instabilities and discontinuities that occur due to the spatial dependence of the material properties being piecewise in nature.

Generally, the material properties are maintained at some known temperature and are not updated during simulation. This is only valid for small perturbations from the initial temperature and the wide temperature expected in the simulation of the conceptual RTD will violate this. Therefore, the temperature dependence of the material properties is consistently updated during simulation. When solving the temperature at some time $T(t_n)$, the model implements the temperature of the previous time step to provide a thermal conductivity of $k(t_{n-1})$. This allows for the system to accurately update the material properties over wide temperature ranges as a suitable time step is implemented.

With the temperature known through the system, additional thermal effects can be calculated. Specifically, the potential for non-elastic damage to the wire from the expansion or contraction of the electrical insulator and the creep strain that may occur. Investigating these effects through modeling allows for potential design iterations, aid in improving recommendations of future work, and the eventual construction of the instrument.

Thermal expansion is the ability of a material to experience changes in its physical dimensions as its temperature increases or decreases. Linear expansion can be computed via the usage of a linear CTE. For an isotropic material, the CTE for area and volume are two and three times the linear CTE respectively. However, only linear thermal expansion is necessary to determine the changes in the dimensions of the electrical insulator and sensing element. The linear CTE of a material (α_L) and the change in length (L) with temperature are related via:

$$\alpha_L = \frac{1}{L} \frac{dL}{dT}. \quad 5.3$$

If the event that α_L does not vary excessively with temperature and that the change in length is relatively small, the equation can be simplified to the form:

$$\alpha_L \Delta T = \frac{\Delta L}{L_{initial}}. \quad 5.4$$

In Equation 5.4, ΔT and ΔL are used to signify the difference between the initial and final values of their respective parameter. Due to the large temperature range of the desired application, Equation 3.3 could be considered more suitable for use. However, the temperature of the RTD is being computed through a

discrete time method. As such, the simplified equation can be applied at each time step to allow for the initial and final conditions as well as the CTE to be updated at each time step. Calculating the overall expansion of the sensing element and the insulator, strain induced on the sensing element by the insulator can be computed.

Thermal creep has been investigated extensively to improve the performance of structural materials and system components. Research in this area has provided an empirical equation to estimate the creep strain of various materials. One such equation requires knowledge of the diffusion coefficients for dislocations. Additionally, the initial dislocation density of the material is needed for computation [57]. The implementation of this equation requires extensive knowledge of the material and can be difficult to implement. As such, a simpler empirical equation requiring less parameters can be seen as:

$$\dot{\epsilon}_{creep}(T) = K_c \sigma^n e^{-\frac{Q}{RT}} \quad 5.5$$

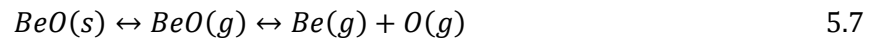
where $\dot{\epsilon}_{creep}$ is the creep strain rate, K_c and n are material constants, Q is the activation energy of creep, and σ is the stress on the component [74, 75]. For this application, the stress on the component comes from the thermal strain that is induced by the expansion of the wire and electrical insulator. This can then be compared to estimates of the yield strength of the wire to determine if it will experience a mechanical failure due to thermal effects. Specifying the equation for tungsten when the stress is less than 20 MPa within a temperature range of 1500K to 2900K can be seen as:

$$\dot{\epsilon}_{creep}(T) = 1.3 * 10^3 \sigma^{3.53} e^{-\frac{53370}{T}} \quad 5.6$$

with this equation providing values that are relatively close in agreement with various sources of experimental data [76]. While this equation has some error, it can provide an estimate of the thermal creep strain for conceptual design.

5.3 Chemical Reactions and Kinetics

Due to the significant concerns regarding the oxidation of tungsten, it is necessary to determine the amount of oxygen that may be produced by the volatilization of the insulator. Exposure to high temperatures has been shown to cause the production of gaseous BeO before it reaches its melting point, but this is dependent on the environment in which this occurs. For example, beryllia is considered to be volatile above 1300°C when it is in the presence of water and water vapor [72]. There are several studies regarding the vaporization of beryllia at temperatures approaching and exceeding 2000°C. These investigations have worked to determine the vapor pressure of BeO and the composition of the vaporized ceramic. The evaporation of beryllia and its dissociation can be written as:



where “s” and “g” represent the phase of the element or compound. The dissociation reaction has an average activation energy of ~104.4 kcal/mole. This value can then be used with the Arrhenius equation as:

$$k(T) = A e^{-\frac{E_a}{RT}} \quad 5.8$$

where k is the rate constant, A is a pre-exponential factor, E_a is the activation energy of the reaction, R is the universal gas constant, and T is the absolute temperature of the system [77]. While this equation provides adequate results, there are additional equations that are like the Arrhenius equation that are based on collision theory and transition state theory. The Eyring rate equation is based on the development of

transition state theory where there is a short-lived transitional state between the reactants and the products. This allows the rate constant to be calculated as:

$$k(T) = \frac{k_B T}{h} e^{-\frac{\Delta G^\ddagger}{RT}} = \frac{k_B T}{h} e^{\frac{\Delta S^\ddagger}{R}} e^{-\frac{\Delta H^\ddagger}{RT}} \quad 5.9$$

where k_B is the Boltzmann constant, h is Planck's constant, ΔG^\ddagger is the change in Gibbs free energy from the reaction, ΔS^\ddagger is the change in entropy, and ΔH^\ddagger is the change in enthalpy [78]. Collision theory bases the determination of the reaction rate and the rate constant in terms related to the chance of the reactants interacting with each other. The rate constant can be calculated via:

$$k(T) = P \sigma_c \left(\frac{8k_B T}{\pi \mu} \right)^{\frac{1}{2}} e^{-\frac{E_a}{RT}} \quad 5.10$$

where P is a steric factor to correct the predicted value, σ_c is the collision cross-section, and μ is the reduced mass of the system from the atomic mass of the reactants. The use of the steric factor is needed as the theoretical prediction can be several orders of magnitude larger than the real value [79]. For a conservative estimate, the steric factor can be assigned a value of 1 to overestimate the reaction rate.

The various rate constant equations can be related to provide a calculation of the pre-exponential factor that can be applied with the standard Arrhenius equation. Relating Equations 5.8, 5.9 and 5.10 provides:

$$A = \frac{e^1 k_B T}{h} e^{\frac{\Delta S^\ddagger}{R}} \quad 5.11$$

where all the variables have been previously described [80]. Using this representation, the only unknown factor is the change in entropy from the reactants to the transition state. There are two ways to determine this value. The first is a simple assumption that there is no change in entropy ($\Delta S^\ddagger = 0$) due to the reactants being in the same phase of matter. The second method is more accurate and requires the implementation of molecular quantum mechanics, also known as quantum chemistry. This can allow for various parameters of materials to be estimated analytically and can provide improved data.

With the appropriate rate constant provided, the system of equations describing the chemical reaction can be constructed through the implementation of differential equations. The general ordinary differential equation (ODE) for the reaction between two reactants that results in a single product can be represented as:

$$\frac{dA}{dt} + \frac{dB}{dt} = \frac{dC}{dt} \quad 5.12$$

where A , B , and C are the time dependent concentrations of the compounds of interest. The differential equations describing the reactions of interest are simple and generally take the form of the general equation.

The main reactions of interest for this research are the evaporation of beryllia, the dissociation of beryllia to its base elements, and the production of tungsten trioxide. The production of tungsten trioxide can be represented via:



which represents the stoichiometric process of this reaction. While tungsten trioxide is the focus, there are several other oxide forms that can be formed during this process. However, they are produced in a much smaller volume than WO_3 . Additionally, it should be noted that the oxide of tungsten is in a gaseous form instead of maintaining the solid phase of the tungsten reactant. This is due to the boiling point of WO_3 being a several hundred Celsius lower than the BeO vaporization point. As such, the assumption that $\Delta S^\ddagger = 0$ does not hold as strongly as it does for the dissociation of gaseous beryllia. In spite of this, the assumption is still implemented as it is expected to provide a reasonable estimate of the amount of oxide formed.

As the RTD is expected to be constructed within a helium or vacuum environment, any oxygen is assumed to come from the vaporization of the electrical insulator. The majority of information regarding a change from a solid to a gaseous form of BeO has been conducted using Knudsen cells with a vacuum [71, 81]. Within a vacuum, BeO is stable until it reaches a temperature of ~ 2000 K. In contrast, BeO is considered stable up to 2300 K when it is in a helium environment [71]. Using the information regarding vaporization of the insulator in a vacuum will provide the calculation of a worst-case scenario.

As the vaporization of BeO has been studied extensively, there is a large amount of data available regarding its loss of mass at high temperatures. The available data provides a larger view of the mass loss that the ceramic will undergo in a vacuum environment at extreme temperatures [72, 82-84]. Furthermore, the currently available information covers the temperature range expected to occur within a nuclear thermal rocket system. The tabulated data from these experiments can be fit to a curve to provide a specific mass loss rate or loss of mass after being at a known temperature. The general equation relating mass loss of BeO to temperature can be written as:

$$y = (2.62 * 10^{-13})x^3 - (1.68 * 10^{-9})x^2 + (3.59 * 10^{-6})x - 0.0026. \quad 5.14$$

The fit to this equation is provided using the curve fitting toolbox in Matlab. The fit has a root mean square error of $1.14 * 10^{-5}$, a sum square error of $9.07 * 10^{-10}$, and an R^2 of 0.996. The error associated with the fit is relatively large but provides a reasonable estimate of the mass loss at each temperature. Issues with the fit appear to come from the dispersion of the data points as the temperature increases. While the data appears to be somewhat linear, there are specific points that appear to harm the quality of the fit. However, the amount of data available is too limited to remove problematic points without further calling into question the quality of the fit.

With the estimated amount of gaseous beryllia present in the system handled, a differential equation describing the production of the gas of interest and its dissociation into its constituent elements can be written in the form:

$$\frac{dC_{BeO(g)}}{dt} = G(T) * t - k_d(T)C_{BeO} \quad 5.15$$

where $C_{BeO(g)}$ is the current concentration of gaseous BeO, $G(T)$ is the rate of mass loss, $k_d(T)$ is the reaction rate constant at temperature T, and t is the amount of time the system is at the specified temperature. The equations for the rate laws of the dissociation of sublimed beryllia and subsequent consumption of tungsten can then be written as:

$$R_d = k_d(T)C_{BeO} \quad 5.16$$

$$R_{oxidation} = k_o(T)C_w(C_o)^3 \quad 5.17$$

where $k(T)$ is the temperature dependent reaction rate, R indicates a chemical rate law, and C is indicative concentration. Applying these rate laws provide the following system equations:

$$\frac{dC_{Be}}{dt} = k_d(T)C_{BeO} \quad 5.18$$

$$\frac{dC_O}{dt} = k_d(T)C_{BeO} - k_o(T)C_W(C_O)^3 \quad 5.19$$

$$\frac{dC_{WO_3}}{dt} = k_o(T)C_W(C_O)^3 \quad 5.20$$

where each equation details the change in concentration of a specific element or compound with respect to time.

Tungsten trioxide is a semiconductor and has a boiling point that is 100 K to 300 K below the vaporization point of BeO. The presence of the material on the tungsten sensing element will alter the electrical resistance of the material and decrease the mass of the resistor. However, it appears that the literature regarding the effect of tungsten trioxide on the resistance of tungsten is not available. Additionally, it is unknown how the existence of the oxide at temperatures greater than its boiling point will alter the resistance of the sensing element. As such, the mass of the tungsten is decreased based on the amount of the material that has been consumed by oxidation. It is then assumed that the mass is lost equally through the sensing element with the volume and dimensions being adjusted appropriately. The dimensions of the sensing element after oxidation are then used to compute the change in resistance that is due to the consumption of tungsten.

5.4 Electrical Network Model

A significant concern regarding electrical measurements in extremely high temperature environments is the electrical resistivity of the insulator. As the resistivity of the material decreases, it will impact the capability of the measurement to be taken accurately. This is commonly referred to as insulator shunting and can cause unwanted electrical transmission between the various conductors in the instrument. Because of this, it is an extremely important aspect to aid in the evaluation of the proposed high temperature RTD.

Insulator shunting can occur between the lead wires, between the coils of the double helix (axially and radially), and between the wires and the sheath. However, the shunting from the wires to the sheath has been indicated to be a minimal factor in the overall shunting of the insulator in thermocouple models. As such, the other three aspects of shunting are the focus of the electrical network. The physical dimensions of the wire and insulator are discretized to some length, ΔL , and into n subnetworks. Additionally, the line is assumed to be terminated with some resistance of the wire. Figure 5.1 provides a view of the n -th network as well as the termination of the system.

Viewing the subnetworks in Figure 5.1 shows a relatively simple circuit consisting of various conductors. The value $G_w(n)$ indicates the conductance of the sensing element in the n th subnetwork. The values $G_1(n)$, $G_2(n)$, and $G_w(End)$ indicates the insulator shunting between the wires axially, the shunting between the coiled insulator across the diameter of the insulator, and a final conductive element to terminate the lines of the sensing element. $G_2(n)$ and $G_3(n)$ represent the same value and but connect different components.

The first aspect of the electrical evaluation requires the determination of the various equations that can be used to provide a value for the various shunt resistances. Historical investigations of electrical

shunting were focused on its application in transmission line theory and thermocouples. This can be applied to the proposed RTD by separating the lead wires and the resistive coil portion into different regions. Focusing solely on the lead wires, a top-down view provides Figure 5.2. The geometry provided here has been implemented in various analytical models regarding insulator shunting within thermocouples [69, 70, 85-87]. The model can be seen as a shielded pair transmission line and the conductance between the lead wires can be calculated via:

$$G_1 = \frac{2\pi\sigma_{ins}\Delta L}{k_0} \quad 5.21$$

$$k_0 = 2 \ln \left(\frac{2D(S^2 - D^2)}{a_1(S^2 + D^2)} \right) \quad 5.22$$

where G_1 is the conductance between the wires, ΔL is the length of the material discretized to be evaluated at some point z , σ is the electrical conductivity of the insulator, and k_0 is a constant determined based on the geometry of the shielded pair. Further expanding on this, the resistance between a single wire and the sheath can be determined by viewing the wire as an eccentric conductor encased within another conductor. The conductance between the wire and the sheath can be calculated via:

$$G_{w2s} = \frac{2\pi\sigma_{ins}\Delta L}{\cosh^{-1} \left(\frac{S^2 + a_1^2 - D^2}{2a_1S} \right)} \quad 5.23$$

where G_{w2s} is the resistance from a single lead wire to the sheath. Transmission line theory provides the necessary basis which is used to get the provided equations [88]. As the conductance is simply the inverse of resistance, the desired resistance R_1 can be determined by inverting the appropriate conductance value.

The resistance of the insulator in the helical portion of the sensing element is more complicated than the relatively simple configuration of the lead wires. Computing the resistance of the insulator between the lead wires relies on the usage of a 2-D representation using z -dimension for the length of the wire and the x -dimension for the length between the cables. This is possible due to the fact that the lead wires, and the wires in the two-wire insulated transmission line model, are straight. The position of the wire can be easily described in terms of x and z . The configuration of a helix is more complicated and requires the usage of trigonometric functions to accurately describe its geometry and position. Additionally, the coiling of the wire around an insulator provides additional pathways for shunting to occur. While both of these effects can be handled simultaneously, the following proposes a simplified set of assumptions that should be sufficient for approximating the insulator shunting.

Shunting between the coils of the sensing element is proposed to be approximated as a two-wire, unshielded transmission line. While this is not exact, using:

$$R_{c2ca} = \frac{\rho_{ins} \ln \left(\frac{b}{a} \right)}{\pi \Delta L} \quad 5.24$$

is based on the proposed configuration of the sensing element as a double helix as well as separating the radial shunting through the insulator. For the shunting between the coils to be represented by Equation 5.24, several assumptions must be applied. Additionally, Figure 5.3 provides a diagram of the double helix to improve clarity. The shunting across the diameter of the insulator temporarily ignored. This allows for the axial direction to be the only one considered. Viewing Figure 5.3, this corresponds to the vertical distances between the positive and negative wires, red and grey respectively. Additionally, the

insulator shunt of interest is between a set of positive and negative coils and not between coils. Essentially, this ignores the effects that the different sets of coils may have on each other and the differences in the charge density that would occur at these points. With the above stipulations, the system becomes roughly equivalent with a two-wire transmission line. The only significant difference that exists is the length of the wire being described by sinusoidal equations, instead of a line.

The shunting that occurs across the cylindrical insulator to the wires is critical and can show potential needs to alter the radius of the insulator. The insulator shunting of across the diameter of the insulator can be computed similarly to that of a resistive disk with a given thickness. Based on Gauss' law, the electrical conductance of a resistive disk with a given height of H and diameter of D_c when provided an electrical potential from a wire with a radius of r_w :

$$G_{2,3} = \frac{\pi H \sigma}{2 \ln \left(\frac{D_c + r_w}{r_w} \right)} . \quad 5.25$$

This equation defines the conductance of the disk when the electrical contacts are placed at the same height [89]. To account for a difference in the height placement of the contacts given the symbol η , Equation 5.25 can be modified to provide:

$$G_{2,3} = \frac{\pi H \sigma}{2 \ln \left(\frac{\sqrt{(D_c + r_w)^2 + \eta^2}}{r_w} \right)} . \quad 5.26$$

This allows for the electrical conductance of the insulator of the calculated to aid in evaluating insulator shunting of the conceptual RTD design.

The electrical conductance of the insulator shunts and of the sensing element can be combined to provide a single equivalent conductor. If the insulator was perfect and provided an electrical conductance that approached zero, equivalent to an infinite electrical resistance, the equivalent conductance would be the value provided by the sensing element. As the insulator is not perfect, it creates several parallel connections in the electrical network. To calculate the effect of the insulator shunting, Equations 5.21, 5.24, and 5.26 are implemented to compute the equivalent conductance of the circuit. Due to the configuration of the system, each conductance due to insulator shunting is in parallel. This is also in parallel with the overall conductance of the wire. As there are a large number of subnetworks, the equivalent conductance requires the usage of a simple script to be computed. The equivalent resistance can then be found by inverting the conductance and it can then be compared to the design resistance of the RTD.

5.5 Neutron Effects

The properties of various materials have been investigated extensively for several years. As tungsten is a desirable material for various extreme temperature nuclear systems, there have been several investigations into the effect of neutron irradiation on the physical and electrical properties of tungsten. Furthermore, several of these studies have investigated the recovery of the electrical resistivity after neutron flux exposure [58-63, 90-93]. The available data regarding these experiments provide a foundation for understanding the neutron induced resistivity alterations and the development of empirical models that can be used to predict the residual resistivity of tungsten based on neutron fluence.

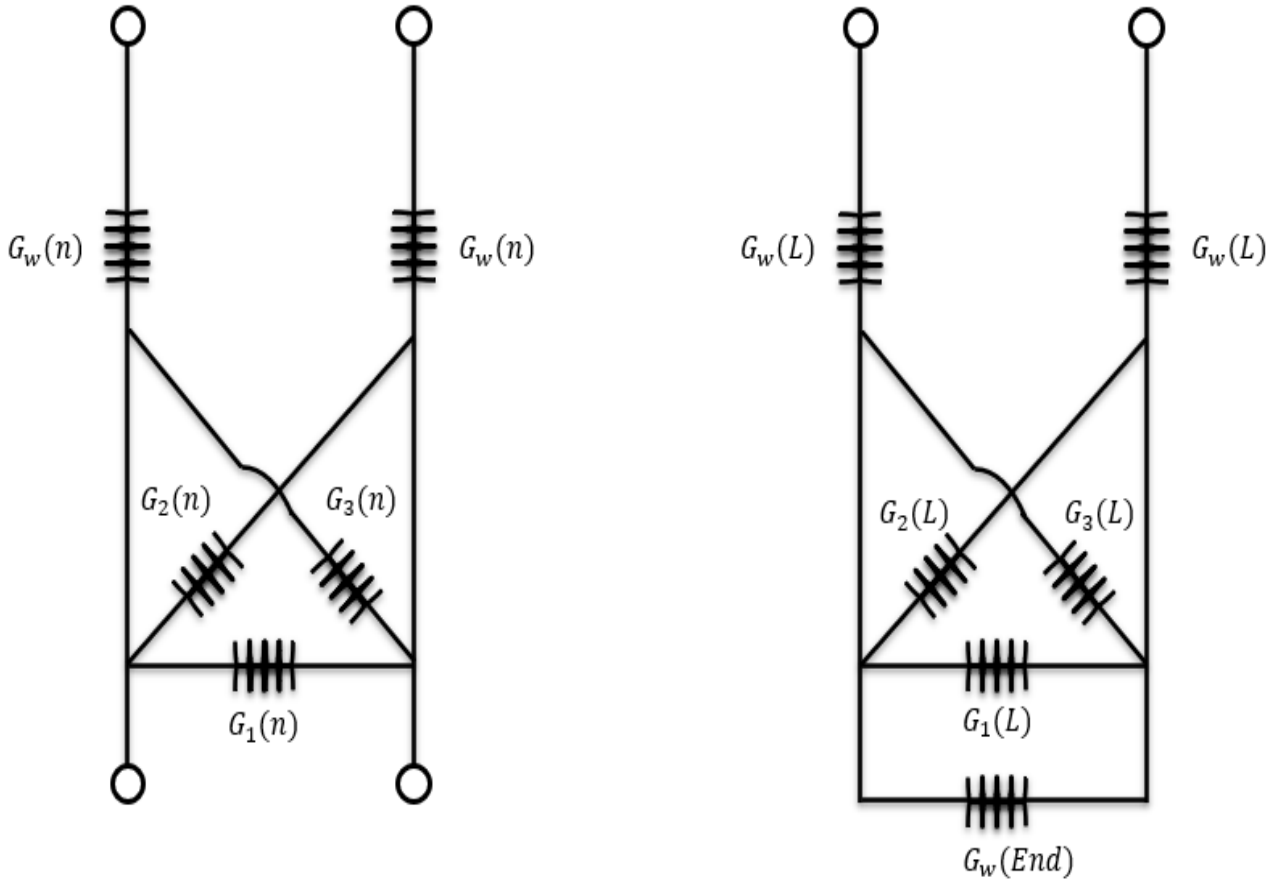


Figure 5.1: Nth electrical subnetwork (left) and circuit diagram of final subnetwork (right).

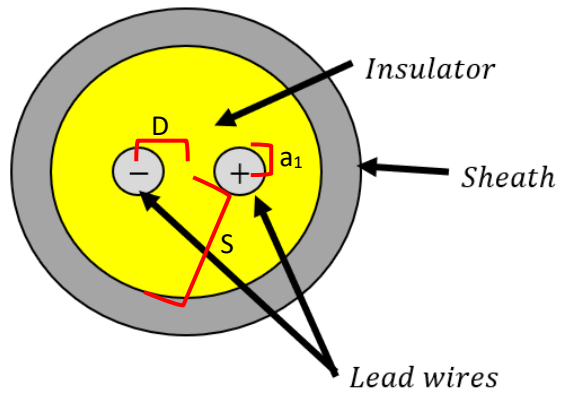


Figure 5.2: Top-down view of RTD housing.

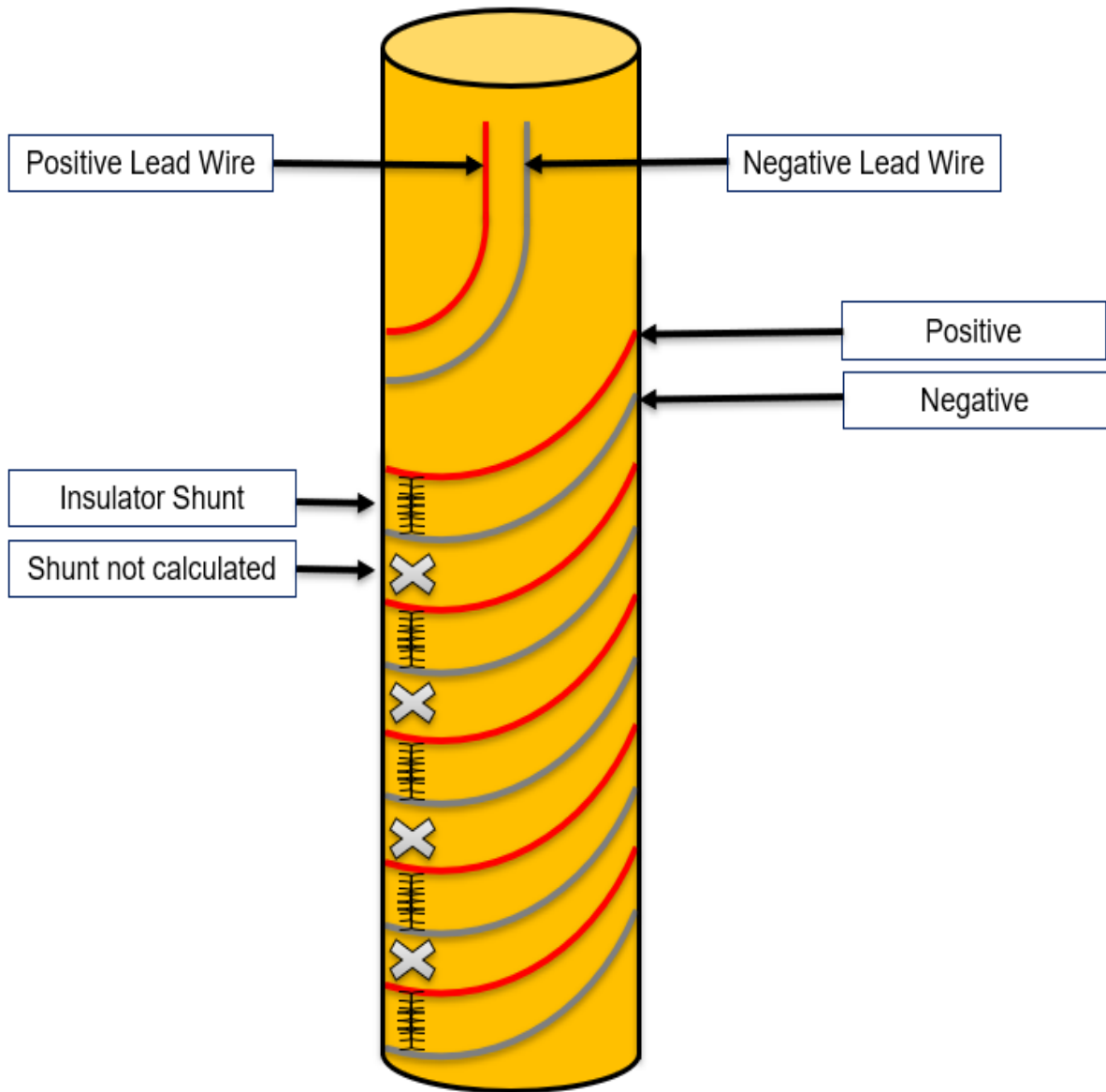


Figure 5.3: Diagram of the sensing element in the form of a double helix.

The construction of a predictive model for neutron induced changes in the resistivity of tungsten is complicated due to the limited data available. To provide the highest level of accuracy, it is desired to minimize the influence of factors such as the irradiation temperature of the tungsten sample. For example, several reports investigating the property changes of tungsten due to neutron irradiation for fusion reactor application indicate irradiation temperatures of 500°C to 600°C [92-94]. This temperature corresponds to the Stage III Recovery region of the material leading to the full extent of the damage not being captured [60, 62]. As such, it is preferable to use a data set generated using constant conditions for a large number of samples. The available data set is limited to 20 samples which prevents the implementation of complex empirical models and limits the current problem to relatively simple fits of the data. However, this is viable for the current usage of the of the data and evaluation of the conceptual design.

The relationship between the electrical resistivity of tungsten and the fast neutron fluence can be modeled via a function relating the original resistivity, the fast fluence resistivity delta, and the fast fluence. This equation can be written in the form of:

$$\frac{\Delta\rho_F}{\rho_0} \approx 2.08(1 - e^{-1.06*10^{-19}\Phi_F}) + 8.1(1 - e^{-6.51^{-21}\Phi_F}) \quad 5.27$$

where $\frac{\Delta\rho_F}{\rho_0}$ is the fast fluence induced resistivity divided by the unirradiated resistivity and Φ_F is the fast neutron fluence [60]. Implementing this equation with the associated tungsten data provides a root mean square error (RMSE) of 0.2735 Ω -cm. Notably, the RMSE of the reported fit is larger than the smallest recorded fast fluence induced resistivity change. Furthermore, the provided fit only accounts for the fast neutron fluence and the fast neutron induced resistivity change as computed after annealing the sample to remove defects from radiation exposure. However, the transmutation of tungsten from thermal and epithermal neutrons is a significant factor that cannot be ignored.

Additionally, there are some problems regarding the precision of the computer and the magnitude of the coefficient in the exponential of Equation 5.27. Normalizing the data to have a mean of 0 and a standard deviation of 1 continues to provide results with a high associated error. To improve upon the performance of the fit and to include the effect of thermal neutrons, more advanced regression algorithms have been applied. The Regression Learner application in Matlab has been used to apply 24 different regression algorithms with and without cross-validation. Initially, it was believed that a neural network would provide the highest accuracy; however, a Gaussian Process Regression (GPR) provided the lowest RMSE of all the available models. GPR is a non-parametric technique that employs kernels and Bayesian statistics. Using an exponential kernel function, the GPR provides a fit with a RMSE of $\pm 0.0047 \mu\Omega - cm$ when validation is not implemented and an RMSE of $\pm 0.2682 \mu\Omega - cm$ when cross-validation is implemented. While the GPR without using cross-fold is likely over-fit, it is used as it represents a physical relationship.

5.6 Interconnectivity of Model Components

The main interconnections of the model components are related to the temperature effects and effects of the irradiation on the electrical resistance of tungsten. Computing the temperature of the RTD system at each time step provides the component necessary for computing the oxidation of the tungsten and the properties of the material at each time step. Similarly, the total neutron fluence is used to determine the change in the electrical resistivity of the tungsten. Combining these effects, provides an estimate of some basic characteristics of the instrument and an evaluation of its feasibility/performance.

Chapter 6: Modelling Results

6.1 Introduction

The initial modeling has been conducted through the use of a geometry that attempts to maintain the dimensions of tungsten-rhenium thermocouples that were proposed for Project Rover and the NERVA Program. Table 6.1 provides the initial dimensions of a nominal 100 Ω RTD that is composed of a tungsten sensing element. In Table 6.1, pitch is related to the distance between the center of the wires and the height of the helix in the distance the coiled wires will reach when wrapped around the cylindrical insulator. These values are loose approximations to recommendations for in-core thermocouples during the NERVA program [3]. The results of simulating the geometry provided in Table 6.1 will be provided with additional sections providing a discussion of alterations in the dimensions to improve performance.

6.2 Mesh Refinement

The use of a finite difference approximation requires the mesh to be refined to ensure accuracy, stability, and a reasonable computation time. During preliminary simulations, both implicit and explicit methods were investigated to determine the preferable difference scheme. Explicit difference schemes are not inherently stable but generally do not require as much computer time as implicit methods. However, the stability requirement can take longer when requiring a large number of time steps to provide stability. As the dimensions of the geometry are on the order of 10^{-5} , the discretization in the time domain becomes exceedingly fine to provide stability. For example, a time step of 10^{-10} seconds is required to provide stability to the explicit solution with the geometry provided in Table 6.1 while any time step may be used with the implicit solution. Having a time step this fine causes significant issues with hardware and computer slowdown. Assuming a simulation time of 30 seconds and a total of 700 spatial nodes, an array containing 21 trillion elements. The memory requirements for such an array are not provided exactly, but an array containing 350 million elements from the implicit method requires 1.73 GB. As this data is stored in the computer's random-access memory (RAM), this can cause the processing speed of the computer to decrease significantly and potentially crash. Because of this, the implicit solution to the heat equation is implemented. While this solution requires a matrix inversion at every time step, the coarser requirements for the discretization of time is preferable regarding computational resources.

Due to the inherent stability of the implicit method, the time step requires empirical search. The necessary time step is considered to be found when the difference between the solutions using varying time step becomes negligible in the time domain. Time steps ranging from 10^{-2} seconds to 10^{-5} seconds were simulated with an arbitrary number of spatial nodes provided with an initial system temperature of 300K with a step increase to 500K. Figure 6.1 provides a graphical view of the temperature response of the simulation. From Figure 6.1, it can be seen that refining the mesh to 10^{-3} seconds provides a significant change in the temperature solution of the system. However, further refining the time step by up to two orders of magnitude provide increasingly miniscule improvements. The most significant change occurs early in the temperature response of the system. After a few milliseconds, the finer discretization of the time domain matches coarser meshes. Additionally, the difference between a time step of 10^{-4} seconds and 10^{-5} seconds is insignificant with the only difference of note being the increased computational time required to use a finer mesh. As such, the two potential time steps are 10^{-3} seconds and 10^{-4} seconds. Final selection of the time domain discretization requires using both of these potential time steps in the refinement of the spatial mesh.

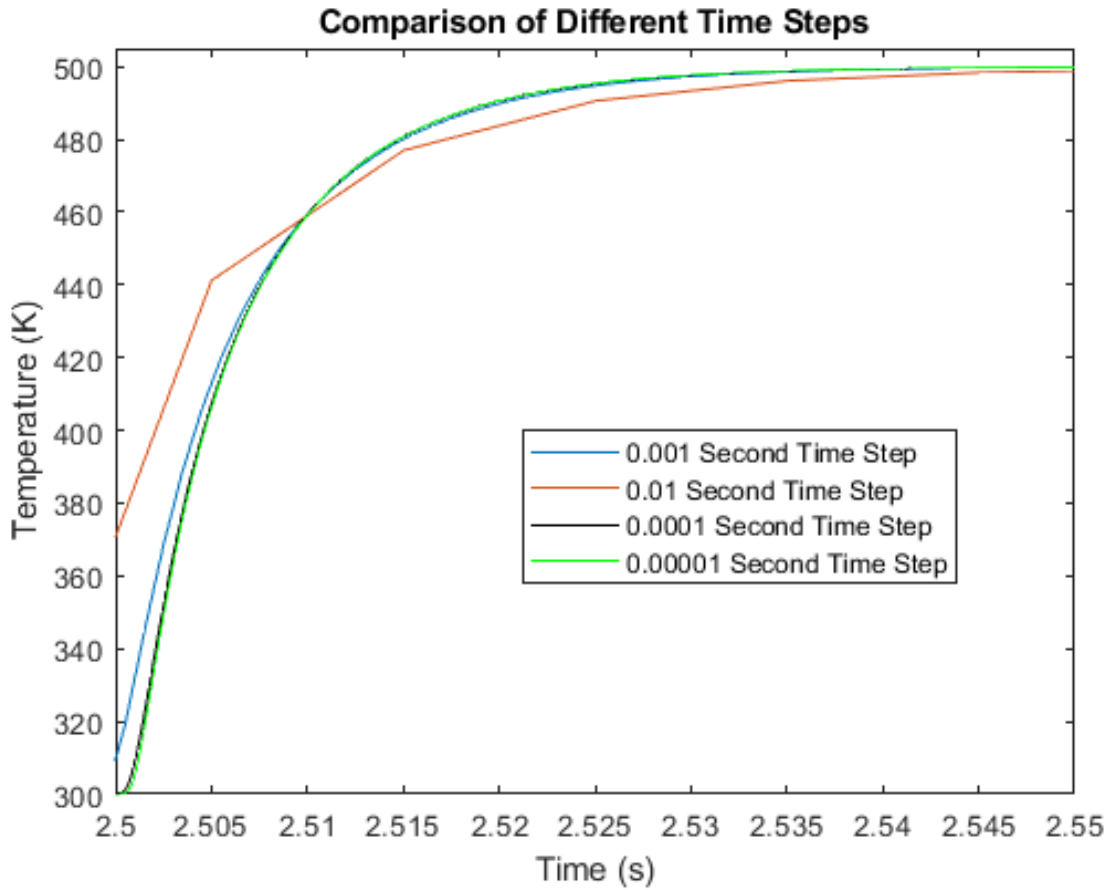


Figure 6.1: Response due to a 200K step change with varying time steps.

Table 6.1: Dimension of Nominal 100Ω Tungsten RTD with a 20μm Diameter Wire

Wire Length (cm)	65.2
Wire Diameter (μm)	20
Pitch (cm)	0.01
Helix radius (cm)	0.0711
Helix Height (cm)	1.46
Sheath Thickness (cm)	0.0254

In one dimension, the conceptual design can be represented by four regions to account for the cylindrical insulator, the sensing element, the insulation between the sensing element and the sheath, and the sheath material. By varying the step size in each of these regions and then comparing to a figure of merit and computational time, the optimal step size for each region can be determined. The figure of merit implemented in this analysis is the 100% response time of mean temperature of the discretized sensing element. This value is determined by providing a step increase from 300K to 2400K and determining the earliest time in which the mean sensing element temperature reaches 2400K. The results of this analysis can be seen in Table 6.2 and Table 6.3.

From this data, it can be seen that the number of nodes implemented in the sensing element region does not have an appreciable effect when increased beyond 10 nodes. The largest factors effecting the response time figure of merit are the materials surrounding the sensing element. Additionally, it can be seen that the order of magnitude difference in time steps causes a mean difference of 2.25 milliseconds with the coarser time step causing the response time estimate to be larger. The smaller time step also allows for a significant decrease in the necessary computational time by an order of magnitude.

From this point forward, simulations of the system's temperature response implement a time step of 10^{-3} seconds and a total of 1,250 nodes discretizing the spatial dimension. The spatial discretization makes use of 50 nodes in the sensing element and 400 nodes in each of the other regions. Using the larger time step causes the accuracy to be lower by 1 millisecond but provides an order of magnitude decrease in necessary computational time. Additionally, the spatial discretization provides the necessary accuracy for the current system. While there is no noticeable impact when increasing the number of nodes in the sensing element region beyond 10, using 50 nodes provides a miniscule impact on the necessary computational time.

6.3 Heat Transfer and Thermal Stress

Temperature response of the initial geometry is conducted via simulating a ramp increase in temperature and step changes. Both simulations consider the system to be at an initial temperature of 300K and have a final temperature of 2400K. These values cover a range that encompasses a historically defined low power idle point of 667K to a temperature that is 40K above to the historically defined operating temperature. Figure 6.2 provides the simulation of the mean sensing element temperature when provided with the described step input, ramp input, and initial conditions. This provides ~132 ms and ~476.5 ms as estimated time constant when provided with a ramp and step input respectively. The plot of the ramp input is magnified in Figure 6.2 to provide a visual representation of the time lag between the boundary condition and the sensing element temperature. Due to the potential for underestimation, the 100% response time is used for the step input. Additionally, the largest time constant will be implemented. While this does not account for the effect of heat transfer from the fluid, it provides some indication of the capability of the instrument's response speed. The small-time constant is also due to the small dimensions of the instrument which are more in line with that of a thermocouple.

To simulate the stress and strain effects that will occur during operation in a NTRE, a 20 second ramp from 300K to 2400K is replicated. The thermal stress is calculated by the relationship between stress, strain, and the Young's Modulus. Due to thermal expansion, the diameter of the electrical insulator is expected to increase by 26.2 μm which causes the circumference of the cylinder to be 88.7 μm . The wire increases in length and diameter by ~7.6 mm and 234 nm. Due to the mismatch in CTE between the insulator and the tungsten wire, the wire will experience additional strain. The geometry of the system requires that the sensing element be wrapped around the mandrel ~146 times. This causes the necessary increase in the sensing element's length to be 12.9 mm, which is 5.3 mm greater than thermal expansion.

Table 6.2: Spatial Mesh Refinement with a 10^{-4} Second Time Step

Mandrel Nodes	Sensing Element Nodes	Intermediate Insulator Nodes	Sheath Nodes	Computational Time (Minutes)	Estimated Response Time (ms)
100	100	100	100	17	479.1
200	50	200	200	33	476.1
200	200	200	200	44	476.1
200	100	200	200	36	476.1
300	50	300	300	54	475.1
400	50	400	400	76	474.6
400	100	400	400	78	474.6
500	50	500	500	106	474.3

Table 6.3: Spatial Mesh Refinement with a 10^{-3} Second Time Step

Mandrel Nodes	Sensing Element Nodes	Intermediate Insulator Nodes	Sheath Nodes	Computational Time (Minutes)	Estimated Response Time (ms)
100	100	100	100	1.67	481.5
200	10	200	200	2.86	478.5
200	50	200	200	3.0	478.5
200	200	200	200	4.0	478.5
200	100	200	200	3.4	478.5
300	50	300	300	5.0	477.5
400	50	400	400	7.7	476.5
400	100	400	400	8.0	476.5
500	50	500	500	10.65	476.5

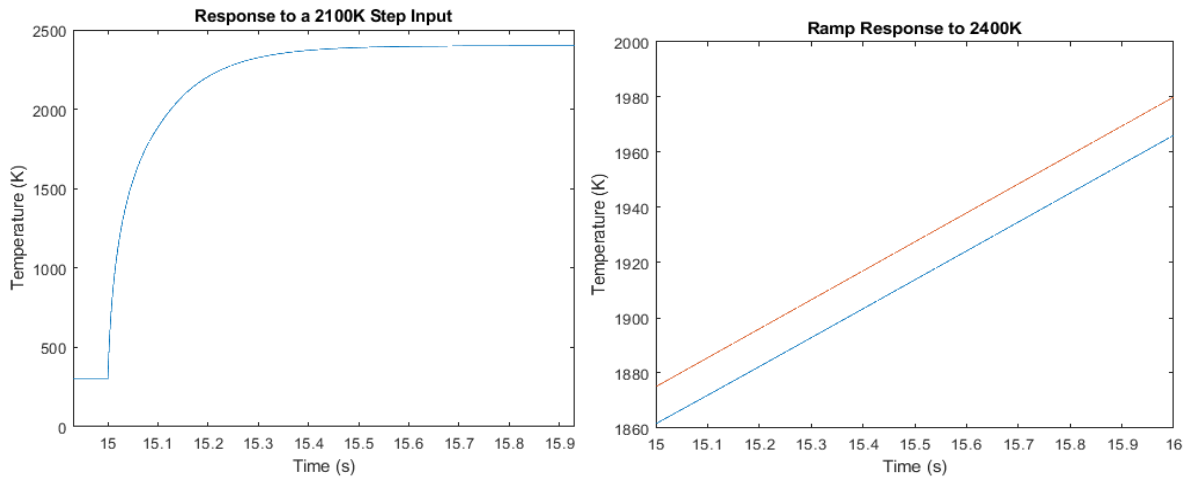


Figure 6.2: Response of the model to a step (left) and ramp (input).

At 2400K, the stress due to thermal expansion is 5.9 GPa when using an empirically derived Young's Modulus of 296 GPa. The yield strength of tungsten at ~2360K, based on historical experience from the Rover Program, is ~45 MPa [3]. The thermal stress exceeds the estimated yield strength by several orders of magnitude. As such, further analysis of the strain rate and potential failure of the wire due to creep is unnecessary and the thermal stress exceeds the boundaries of the known empirical relationship for creep rate. However, this indicates a significant potential challenge to producing a functioning RTD.

6.4 Insulator Shunting and Resistance

The electrical shunting associated with increase in temperature can be approximated by taking the nodes that compose the wire and insulator. The resistance of the wire, the mandrel, and the insulation between the coils of the wire as the temperature changes from 300K to 2400K can be seen in Figure 6.3. For this figure, an important note to make is the relationship used for resistivity of beryllia with temperature. The relationship is based on an impure sample that has a resistivity several orders of magnitude lower than a pure sample. From Figure 6.3, it can be seen that the change in the insulator's resistivity has a minimal effect on the measured resistance until 1500K. Past 1500K the shunt caused by the insulator causes the resistance of the circuit to significantly decrease. Increasing the resistivity of the beryllia by two orders of magnitude provides a closer representation of a pure insulator. However, this simply shifts the turning point in resistance to 2000K. To improve insulator shunting, the geometry of the conceptual design requires reevaluation.

The simplest way to alter the effect of insulator shunting is to change the nominal resistance of the RTD. Due to the insulator shunts occurring in parallel with the wire, decreasing the nominal resistance by a factor of 4 significantly improves the measured resistance at 2400K. Figures 6.4 and 6.5 provide infographics that show the effect of decreasing the nominal resistance by several different factors. This is done for impure beryllia as well as for a "pure" sample that has been corrected by a factor of 100 to match the expected resistivity at 2400K. From the figures, it can be seen that improving the resistivity of the insulator has a significant impact on the total resistance of the system. Additionally, reducing the nominal resistance significantly improves the measured resistance at high temperatures. This can be seen by the 25 Ω nominal resistance providing a relatively linear response until 2200K in Figure 6.4 while the 100 Ω nominal resistance becomes nonlinear at a lower temperature.

6.5 Chemical Degradation

The chemical effects are evaluated from 2123K to a maximum of 2400K with the time taken from the expected maximum operating period of 10 minutes applied. Evaluation period also includes the transitional period from 300K to the maximum temperature as well as the decrease in temperature at the end of 10 minutes. Figure 6.6 shows a 3D-plot of this simulation and the effect of dissociation of the electrical insulator in the system. As expected, the mass of tungsten experiences a notable decrease over an operational period. The total change in the mass of tungsten is approximately 0.105 mg and this would require a total time of 6 hours at 2400K to replace the majority of tungsten with its oxide form. The effect this has on measured resistance is approximated by evaluating the change in the sensing elements mass and the dimensions of the of the sensing element. The change in resistance would be greatest by assuming that the volume change is due only to alterations in the diameter of the wire. For the mass loss of tungsten reported above, the diameter of the wire would change by ~0.267 μm from an initial value of 20 μm to 19.7 μm . Due to the decrease in area, the resistance of the wire can be expected to change by 3.072 Ω (~7 K) when the nominal resistance is 100 Ω .

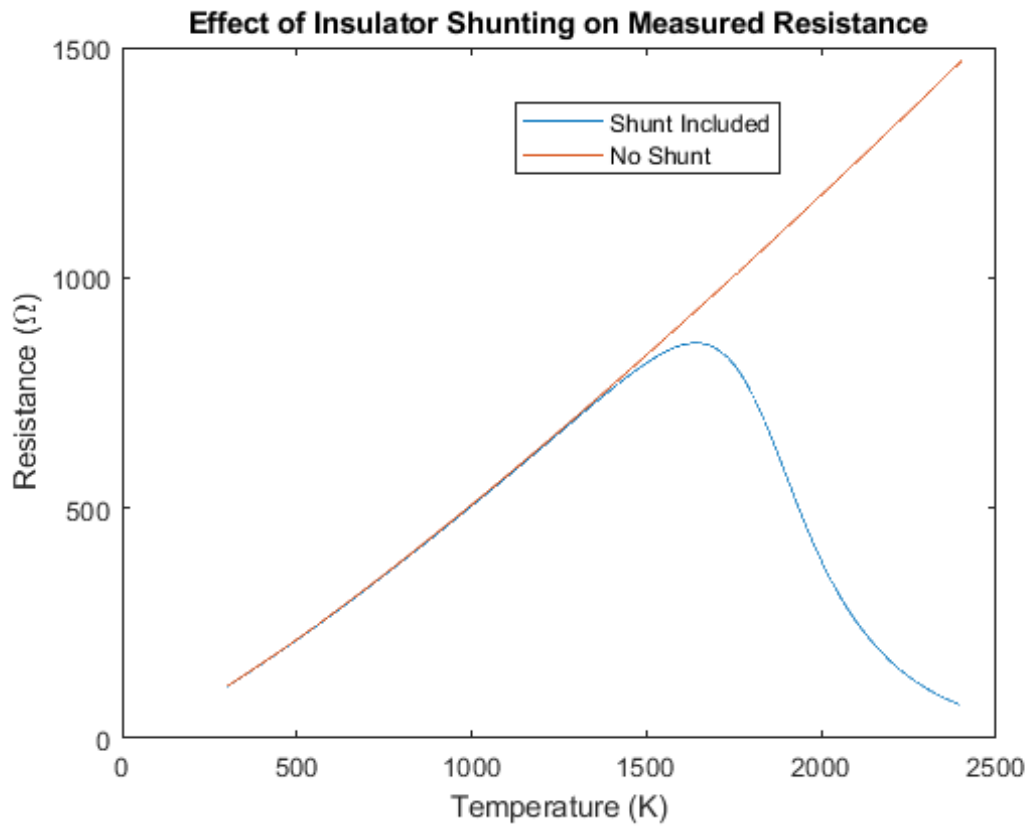


Figure 6.3: Insulator shunting effect on RTD resistance using an impure insulator.

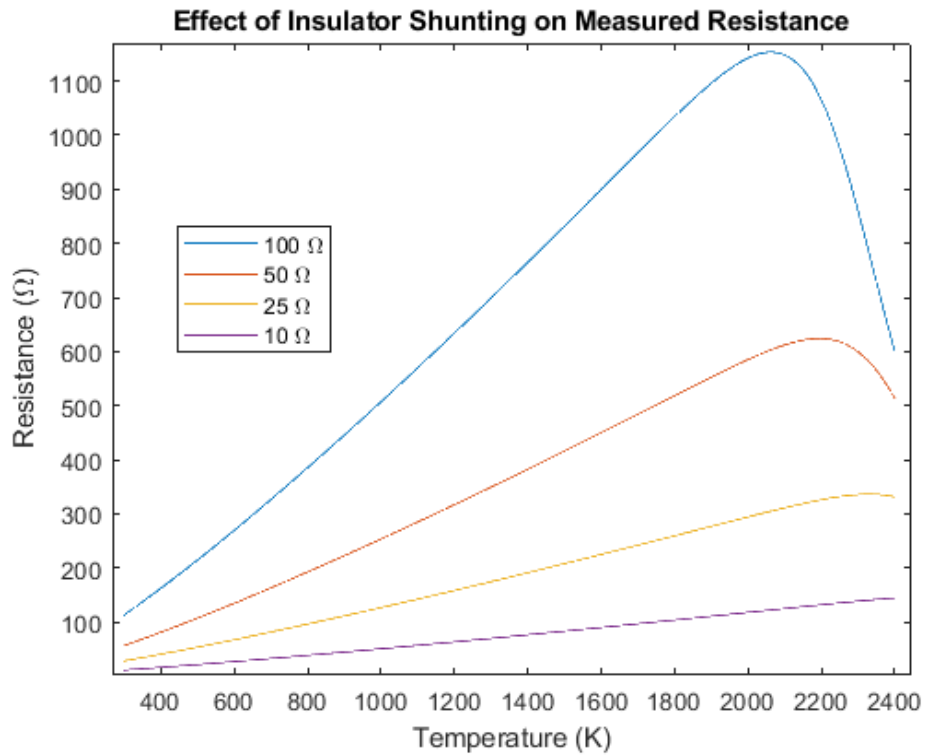


Figure 6.4: "Pure" beryllia sample and effect on measured resistance.

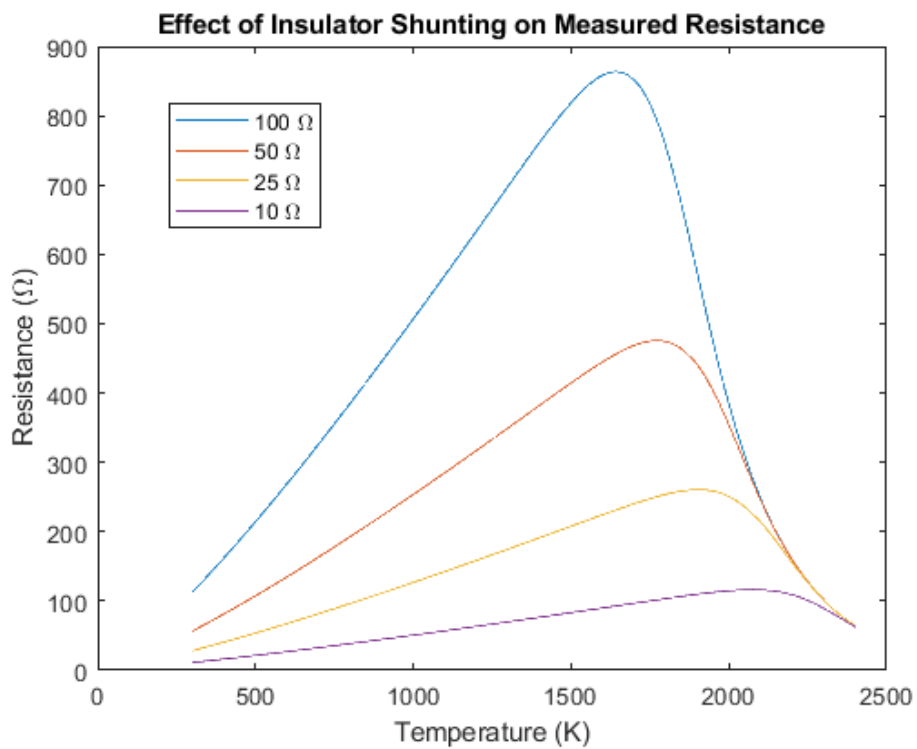


Figure 6.5: Impure beryllia sample and effect on measured resistance.

6.6 Neutron Effects

Using the 10-hour neutron fluence data, $1.62 * 10^{20} \frac{\text{neutrons}}{\text{cm}^2}$ fast and $1.32 * 10^{17} \frac{\text{neutrons}}{\text{cm}^2}$ thermal, the resistivity of the wire changes by $3.74 \mu\Omega\text{-cm}$ at 77 K. Generally speaking, changes in resistivity due to the presence of impurities, dislocations, and crystallographic defects are not temperature dependent. This allows for changes in resistivity to be applied as an offset to the standard resistivity-temperature relationship. As such, the neutron fluence expected in a NTRE will cause the measured resistance of the RTD to be increased by 77.7Ω . The additional resistance causes the measured temperature to have an induced delta of 150 K. However, this increased resistivity is likely larger than what would occur in an actual system. The operating temperature of an NTRE exceeds the recrystallization temperature of tungsten and the annealing of the sensing element will cause a significant reduction in the sensing element's crystallographic defects and therefore the induced resistivity. The true extent of resistance change needs to be validated via irradiation testing.

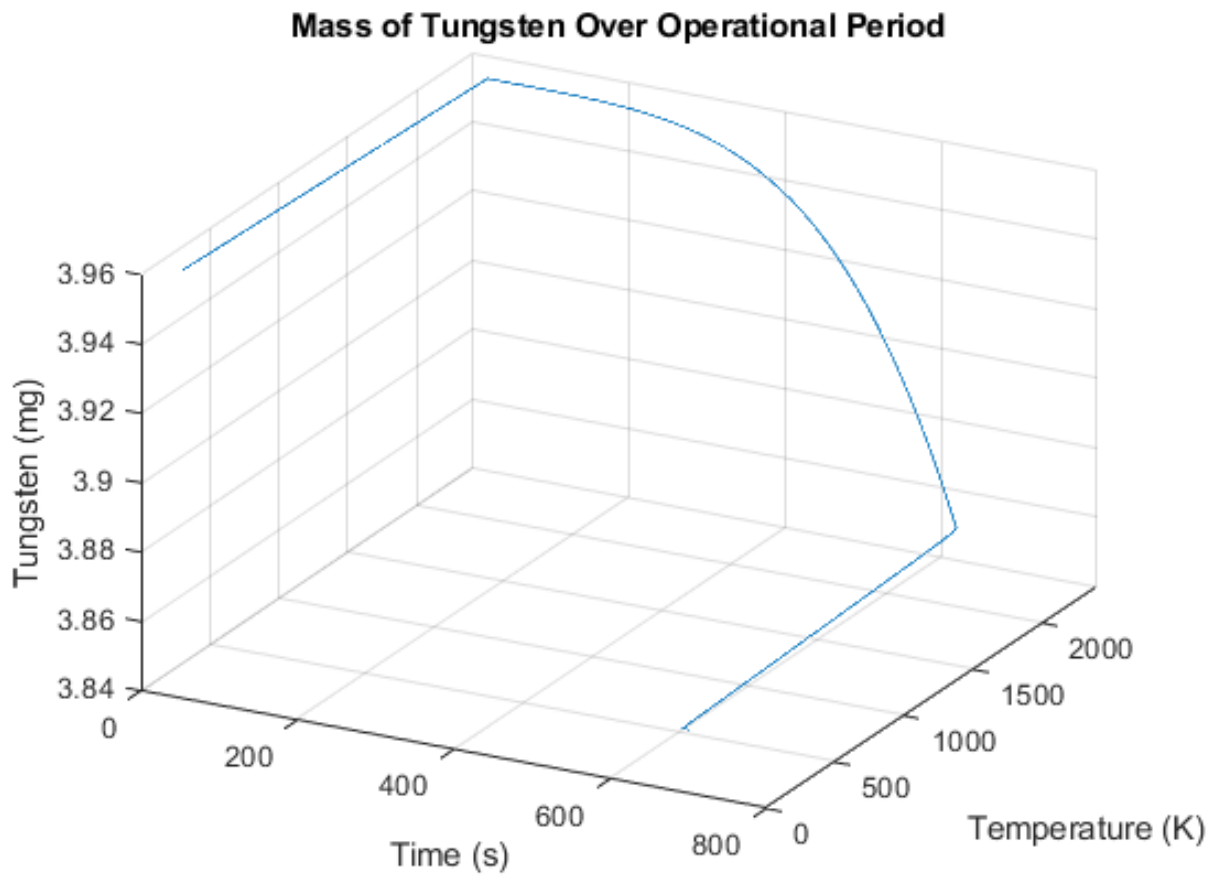


Figure 6.6: Three-dimensional plot of the mass loss of tungsten during a simulation of a full power ramp.

Chapter 7: Model Verification and Sensitivity

7.1 Verification of Electrical Shunting Model

While fully validating the electrical shunting model for the conceptual design requires extensive experimental testing of the materials of interest, the use of historical research can be used to provide an indication of its accuracy. There have been several studies focused on the effect of insulator shunting on standard platinum resistance thermometers (SPRTs); however, these instruments implement insulators such as mica or silica and are incompatible due to their geometric configuration [95, 96]. The most likely candidate for model validation is a special high temperature niobium-1% zirconium resistance thermometer (RT) developed as part of the SP-100 program for use in a Johnson Noise Thermometry (JNT) system [97]. The goal of this work was to develop an RT capable of sustained operation at 1375K to function in tandem with a JNT system to ensure measurement accuracy. Due to the unavailability of the necessary niobium-1% zirconium, unalloyed niobium was used as a substitute to generate a full sized prototype of the instrument. However, a smaller prototype using the desired alloy was constructed but test results are not fully reported.

The prototype niobium RT can be described as a coiled element RTD implementing either high-purity alumina or yttria in a low density crushable preform. The initial desire was to use yttria as it was expected to be less reactive with niobium, but alumina was chosen due to its higher insulation resistance. The sensing element was composed of high-purity niobium wire with a diameter of .127 mm. The total length of the instrument was 3 m with an outer diameter of 5 mm. The sensing portion was contained to a ~100 mm portion at one end of the instrument. A resistance of ~100 Ω was desired at the operating temperature of 1375K, which became ~126 Ω when the prototype was constructed. To attain this resistance, 3 m of niobium wire is needed in the construction of the sensing element. Due to the size constraints and the chosen wire diameter, the sensing element was coiled to form a 0.74 mm diameter helix with a coil spacing of 0.127 mm. The coiled wire was then snaked through a 4-hole insulator to generate a sensing length of ~107 mm. The resistance of the sensing element is measured via the standard 4-wire measurement with 0.76 mm diameter niobium lead wires. Chemical milling was used to reduce the outer diameter of the lower 50.8 mm of two of the lead wires to allow for them to be welded to the sensing coil [97]. Further information regarding the construction of the niobium RT can be found in reference [97].

Termination of the SP-100 program led to the continued investigation of this instrument. However, preliminary studies regarding hysteresis and the effect of short-term repeated exposures to 1375K were completed. The data collected during this period indicated desirable performance characteristics and was empirically fit. The reported fits are for the ascending and descending resistance of the sensing element, the resistance of the sensor with exposure to 1375K, and the overall resistance temperature relationship of the sensor. Figure 7.1 provides the empirical relationships of the ascending, descending, and repeat exposure to 1375K. From this, it can be seen that there are limited hysteresis effects, and the sensor resistance appears relatively stable after high temperature exposure. The final fit is provided in Figure 7.2. This figure is separated due to the uncertainty regarding the accuracy of the fit. The report of this work provides the overall resistance-temperature relationship for the discussed niobium prototype as well as the smaller scale niobium alloy prototype. Based on the other empirical fits and labeling, an error in reporting appears to have occurred at the time of documentation. It appears the labels for the overall temperature relationship were inadvertently flipped at the time of writing. Because of this, the niobium sensor fit used in this report is reported as the relationship for the niobium alloy prototype in the original documentation.

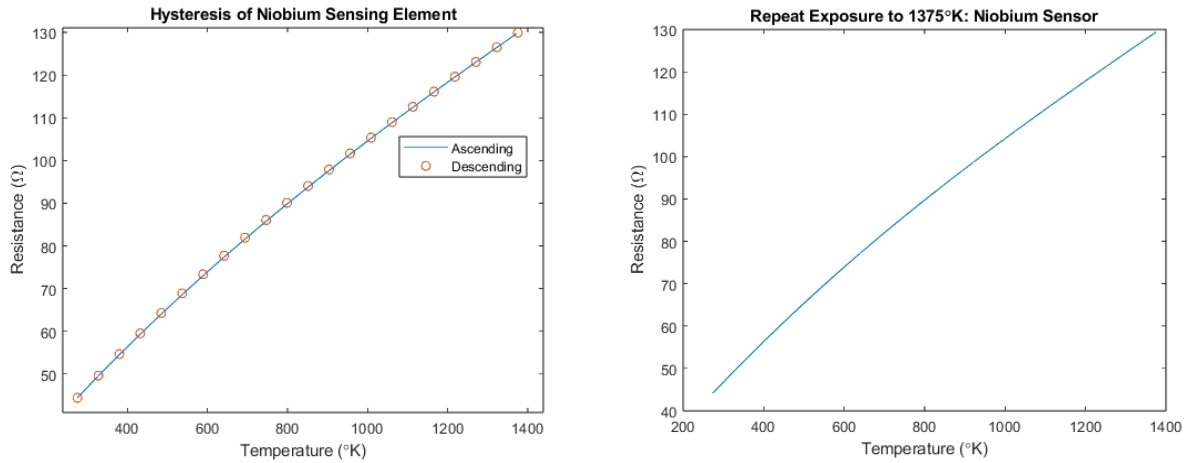


Figure 7.1: Hysteresis of the niobium RTD produced by ORNL for the SP-100 program (left) and the relationship developed through temperature cycling (right). Recreated from the associated fit provided in reference [97].

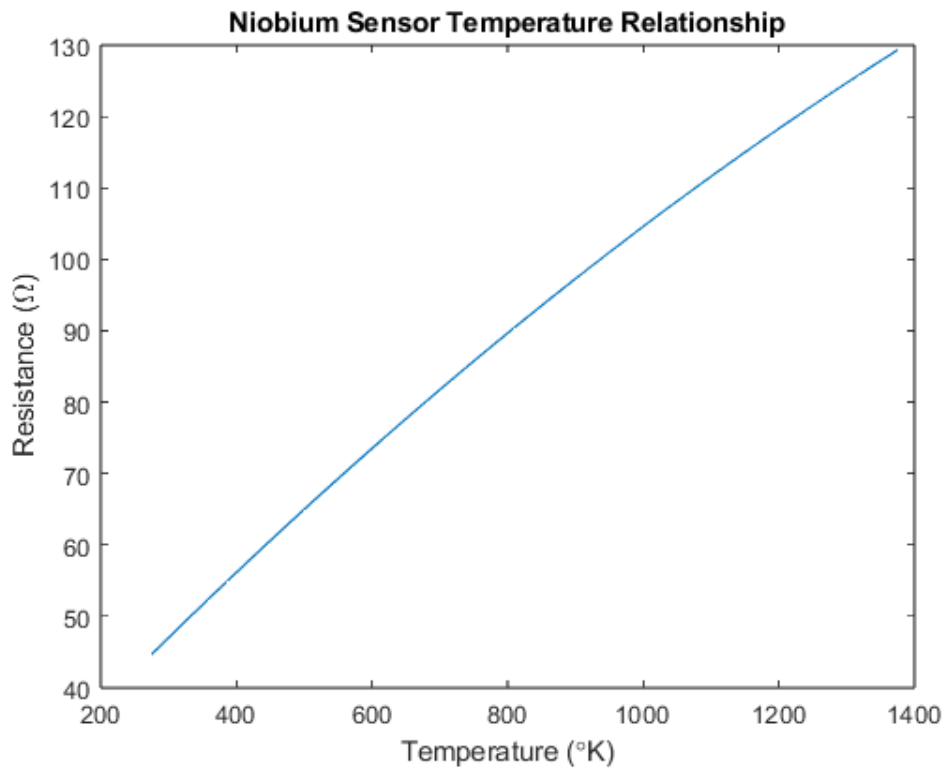


Figure 7.2: Overall temperature resistance relationship of the ORNL produced niobium RTD. Figure recreated using the associated fit as reported in reference [97].

The difference in geometric configuration provides a significant challenge for model verification. As they are not the same, an exact statement regarding validity cannot be made. However, it can be used to provide an order of magnitude estimation. This can be done by producing an equivalent wire wound design of the niobium RT and determining if the model computed resistance change due to shunting is within the bounds of the provided data. The coiled element design of the niobium RT should provide additional avenues for shunting due to the presence of the four coils and closer proximity of the coils in the insulator. This comes in addition to the shunting that occur between the winds of the coil itself. As such, the model computed resistance should be within the bounds of that provided by the reported documentation.

The next challenge comes in the form of interpreting the ambiguity of the labels of the reported empirical relationships. The labels alternate between sensing element and sensor as if to indicate there is a significant difference between these labels. However, based on the provided information it can be taken as roughly equivalent statements. When investigating the empirical fits, it can be seen that the resistance values for the ascending relationship at 1375°K provides a resistance 0.5 Ω greater than the repeated temperature exposure fit and 0.54 Ω greater than the provided relationship between resistance and temperature for the sensor. Similarly, the descending relationship at 1375°K provides resistances that are 0.54 Ω and 0.58 Ω greater than the respective fits. While this may seem to indicate that the ascending and descending fits do not include insulator shunting, the fits do not include uncertainty bounds to indicate if these differences would fall within the expected error of the fit.

This is further compounded by the difficulty in determining the nominal resistance (temperature of 273°K) of the sensing element. The reported length of wire, wire diameter, and the known niobium resistivity-temperature relationship would indicate a nominal resistance of $\sim 33 \Omega$. However, empirical fits provide a nominal resistance value ranging from 44.3 Ω to 44.7 Ω . At 1375°K, the expected resistance would be $\sim 126.8 \Omega$ (without accounting for thermal expansion) and the provided fits give resistances ranging from 129.3 Ω to 129.8 Ω . If it is assumed that the initial length of wire is reported incorrectly, the achieve similar nominal resistance values a length of ~ 4 m would be necessary. However, this would provide a resistance of $\sim 169 \Omega$ at the desired operating temperature. Further literature survey indicates an additional relationship that provides similar results to the already provided fits. Included in this work is an uncertainty range indicates that there is a 0.2% uncertainty at 1375°K, which translates to an approximate uncertainty of 0.26 Ω . Using this information, all of the provided temperature resistance relationships are within the bound at 1375°K except for the overall relationship initially provided. Additionally, this work indicates that errors due to insulation shunting should not exceed 0.8% with a sharply increasing temperature profile. For a more steadily increasing temperature profile, temperature errors range from 0.2% to 6.2% lower than the actual temperature [98]. This model likely only accounts for the shunting that can occur within the lead wires but can be used to indicate potential ranges for insulator shunting. As such, the validity of the current model will be investigated with expectations of being around this range and through the comparison of the empirical fits of the niobium sensor.

The relationships for the niobium sensor indicate that the resistance of the sensor at an operating temperature of 1375K is $\sim 129.9 \Omega$. Assuming the reported wire diameter of the niobium sensing element is accurate, this indicates a $\sim 2.4\%$ increase in the total wire length or put simply a wire length of 3.073 m. If the opposite assumption is made, the calculated wire diameter decreases by $\sim 1.19\%$ from the reported value. Computed a nominal wire resistance using these values provides a resistance of 34.03 Ω and 34.9 Ω . Both of these values are lower than the estimated nominal resistance of the reported relationship of the niobium sensor by 10.25 Ω and 9.42 Ω . If only the provided wire dimensions are used, the initial offset is more noticeable and provides a difference of $\sim 11 \Omega$. However, this difference is not constant and its value decreases as the temperature of the materials increase.

Due to the resistance of the niobium sensor being measured via the 4-wire method, this difference should not be induced by the full length of the lead wires. A potential cause of this difference is the

welding of the lead wires to the sensing element. The wires were joined through using a laser weld to melt the material to form a strong mechanical connection [97]. This connection can alter the electrical transport across the material and cause a significant change in the measured resistance. A prime example of this can be seen in circuits that have low quality solder joints and the added resistance due to that joint. Additionally, it appears that the resistance of the joint has a temperature dependent factor that decreases the added resistance as the temperature increases. However, before this can be further investigated the proposed equivalent sensor must be provided to further indicate potential anomalies for validation. For simplicity, it is assumed that the provided information regarding the wire diameter and length is accurate for the purposes of this work.

The insulator implemented in the design of the niobium sensor was a 4-hole alumina mandrel with a length of 108 mm, a hole size of 0.84 mm, and an outer diameter of 4.2 mm. The spacing between the holes is 0.66 mm, indicating the thickness of alumina separating the sheath from the sensing coil is ~0.62 mm. Using a wire-wound design implementing 0.127 mm diameter wire, one would then implement an alumina insulator with an outer diameter of 2.71 mm to maintain the spacing between the wire and the sheath. Using a wire spacing of one wire diameter, this leads to a wound height of 89.6 mm. This is a difference of ~17 mm from the coiled niobium sensor, but the difference is acceptable as the same spacing between the coils and the distance to the sheath is maintained.

With a roughly equivalent design provided, the calculated insulator shunting can be compared to the experimental results provided earlier. Figure 7.3 provides the expected resistance of the described RTD as well as the calculated effect due to insulator shunting. As noted previously, the nominal resistance of the modeled RTD and the prototype is significantly different. Therefore, comparison can be made regarding the trend of the data and the differences from the available niobium RTD fits provided previously. Comparing Figure 7.2 and 7.3 shows that the computed effect of insulator shunting is significantly larger than the results of the historical investigation. The model indicates a parabolic drop in resistance after 1200°K, while the reported data indicates a more linear change in resistance at high temperatures. In comparison to the theoretical RTD with no shunt, the computed shunt indicates a -6% change in the measured resistance. Comparison to the fits of the ORNL produced niobium RTD provides a difference of -7.4%. While this exceeds the expected error provided earlier, it is within reasonable region for error to occur when taking into account the difference between the historical empirical fits of the niobium sensor and the theoretical niobium RTD.

While the error due to shunting appears reasonable, it indicates that there is a need to further improve the model. The implementation of finite element analysis will allow for a higher fidelity model with a more limited number of assumptions. Additionally, it can better account for different configurations of the RTD than the current model. Another critical aspect that can be investigated in the future is the cause of the significant increase in the nominal resistance of the historical niobium RTD. This unaccounted-for factor significantly impacts the results of the shunt model and cannot be explained the implemented wire being low purity. Generally, impurities do not alter the resistance temperature relationship of a material beyond the inclusion of a bias and are not temperature dependent. To improve the model, effects such as this need to be included to properly define the expected shunting behavior of the system. While the current model is appropriate as a material selection tool, it requires significant development to have effective use beyond this.

7.2 Verification of Heat Transfer Model

The dynamic response of a resistance thermometer is solely dependent on the time constant associated with heat transfer to the system. This is due to the change in resistivity being on such a small-time scale in comparison to the heat transfer that it does not make a notable contribution to its response time. For the conceptual design, the computed response time is closer to that of a thermocouple due to its small dimensions (~2 mm overall diameter). However, resistance thermometers generally have response times that are significantly greater than thermocouples due to their greater mass. Additionally, the low

response time calculation is related to the lack of the model including the effects of heat transfer from the propellant to the instrument. Due to this, it is necessary to ensure the accuracy of the model results via verification of previous studies regarding resistance thermometer response times.

There have been several historical studies regarding heat transfer and its effect on the dynamic response of a resistance thermometer. Similar to this work, these investigations implemented numerical methods to solve for the instrument temperature [99, 100]. However, these investigations implemented different means to determine the sensing element temperature than directly calculating the value from the numerical model. One example of this is done by taking the mean temperature of discretized points of the insulator and sheath material to approximate the measured temperature. This study provides a comparison between the computed response time to the experimentally determined value from a variety of methods. As such, this provides a desirable point of comparison to evaluate the accuracy and validity of the model developed for the conceptual design.

Evaluation of the model requires the usage of the geometry of a general platinum RTD design. The information provided by the historical references provides a general value for some of the critical parameters for the platinum RTDs that are needed for verification. For the purposes of this work, two generalized designs have been implemented with the provided dimensions that can be seen in Table 7.1. While these dimensions are not exact, they are within reason based on the information provided by the historical documents as well as information reported via RTD manufacturers. Along with the geometry, a range of response time values are provided that can be used to determine the accuracy of the model. The response time for the previous models ranges from 170 ms to 10 s [99, 100]. For the purposes of this work, the model can be considered valid if the response time is within this range of values.

The model predicts a response time of ~3.5 seconds for a 10 mm outer diameter RTD with 1.85 mm thick sheath walls. This is in-line with expectations of similarly constructed systems and a similar model produced a response time of ~5 seconds. Further comparisons can be made by using a much smaller geometry that appears to have been implemented by additional researchers. For an RTD composed of similar materials and an outer diameter of 3 mm, the model indicates a response time of ~360 ms. This value is larger than that predicted by the historical model and is larger than the available data for instrument response times. The differences between the results of the historical models, the recorded response time data, and the currently provided model can be attributed to several factors. The main points being the use of a one-dimensional system to represent the heat transfer in the RTD and the current model not including the effect of the flowing process. However, the indicated accuracy of the current model suits its purpose as a verification tool.

There are several ways to improve the results of the model. The first would be to expand the system to a 3-dimensional space. The second would be to include the effects of the process. Finally, the system would need the geometry to be well characterized to ensure the accuracy of the input data.

7.3 Verification of Chemical Reaction Model

The current model for the oxidation of tungsten functions as a method to provide a tentative investigation into the potential oxidation of tungsten as the beryllia insulator volatilizes. This model is developed through the known relationships between the Arrhenius equation and chemical Transition State Theory. However, there are several factors that are not included in the current model and may lead to significantly different results than desired. Because of this, relating the results of the model to previous investigations into the oxidation of tungsten will provide insight into the validity of the oxidation calculations.

Historical investigations into the oxidation of tungsten provide a variety of values relating to the expected oxidation rate of the material. However, it also indicates that pressure has a noticeable effect on the oxidation rate of tungsten. In this report, it indicates that a temperature of 1000°C and a pressure of 76 torr causes an oxidation rate of $10^{17.95} \frac{\text{atoms}}{\text{s}}$ [101]. Attempting to replicate this value using the current model has provided mixed results. While the mass of tungsten is provided, the amount of oxygen is unknown. The report indicates that a constant supply of pure oxygen was provided during heating and therefore complicates this process. If the amount provided would be the stoichiometric value needed for the provided 0.825 g mass of tungsten, the amount of oxygen provided can be estimated as 0.215 g. This allows for the oxidation rate to be determined via a balanced reaction in the system.

Using the values for the mass of tungsten and oxygen provided in the preceding section allows for the model to predict the rate of oxidation for this system. Based on the expected mass of each reactant and the temperature of the system, the model prediction was lower by several orders of magnitude. This indicates that the computed reaction rate constant is underestimated by the model. There are several potential factors that may be the source of this issue. These range from assumptions that may not be adequate for the specific system, geometric factors, and environmental factors that are not accounted for in the model.

The model currently assumes that there is no change in entropy between the reactants and the transition state to the product. This assumption is the most accurate when the reactants are in the same phase of matter. While it can be considered a reasonable initial guess for materials that are not in the same phase, it is not as accurate. To determine a more accurate value, the use of ab initio methods or quantum chemistry would be required to determine a more exact value. This will allow for greater accuracy and an improved prediction of the amount of tungsten consumed by oxidation.

Another pathway for model improvement is through the inclusion of the effects that may be present due to environmental conditions other than temperature and the geometry of the sample. Based on the previously mentioned study, it appears that the pressure within the system can alter the rate of the reaction. While the difference in the oxidation rate is not several orders of magnitude, it is still a significant factor that can alter the predicted results of the model. Additionally, the surface area of the material can affect the rate of the chemical reaction. Determining how this factor affects the rate of the reaction will allow for the improvement of the analytical model.

The current model for the oxidation of tungsten appears to significantly underestimate the rate at which the material oxidizes. The improvements detailed above can allow for the model to better the accuracy of the model. However, the current accuracy of the model is sufficient for providing an approximation of the oxidation rate in its current usage. As the focus is on material selection and survivability, the current performance of the model is acceptable but requires significant development for additional functionalities.

7.4 Sensitivity Analysis of Electrical Model

The current models employ idealized materials and dimensions, but these parameters are unable to be attained in the real world without some form of uncertainty. The expected effect that changes in the parameters may have on the computed results can be evaluated through a sensitivity analysis of the model. This can be completed either empirically or analytically to evaluate the total effect that each parameter will have on the computed result. Regarding the electrical insulator model, an empirical method is employed to conduct a sensitivity analysis of the model.

The electrical properties of the insulator and sensing element as well as the geometric configuration are of interest for the study of the model sensitivity. To determine the effect of each parameter, they are evaluated separately by applying a $\pm 5\%$ and $\pm 10\%$ change in its value over the desired temperature range. Any results that indicate the model is comparatively sensitive to a particular parameter can then be further investigated by expanding the amount the parameter is changed by as well as providing a range of values to indicate the model's behavior.

The sensitivity analysis of the electrical shunting model indicates that only two of the parameters of interest provide notable changes to the computed resistance of the system. The model is extremely sensitive to the electrical resistivity of the wire as well as its length. Figure 7.4 and 7.5 show the results of altering these parameters in comparison to the unaltered value. Upon further investigation of the data, it can be seen that the nominal resistivity changes in accordance with the percent change of the implemented parameter. However, the maximum resistance value does not experience a $\pm 5\%$ or $\pm 10\%$ change when the parameter under investigation is altered. Additionally, the final resistance value is only altered by a maximum of $\sim 5\%$ when implementing a $+10\%$ change in the resistivity of the wire and $\sim 0.08\%$ change when the length is altered by -10% .

While altering these parameters provides a significant change in the computed resistance values, the overall trend of the model is maintained with respect to the temperature relationship. The model's sensitivity to these parameters can be expected due to their effect on the total sensing element resistance. Based on this analysis, the statements regarding changes to the sensing element resistance in Section 6.4 are valid. However, the analysis does not verify statements regarding the electrical insulator because the model is not sensitive to the implemented changes in this study. This is due to the electrical resistivity of the insulator requiring changes that greatly exceed $\pm 10\%$ before effecting the results of the model. Minor variations in the electrical resistivity of the insulator do not make a significant impact, but Figures 6.4 and 6.5 indicate that increasing the electrical resistivity by two orders of magnitude allow for the shunting effect to be altered. As such, this shows that further characterization of the materials can further aid in the certainty of the results of the analysis of the model. While it is shown to not provide a significant change when altered by $\pm 10\%$, the resistivity of the electrical insulator can serve as a notable example for this. As noted previously, beryllia is an impurity controlled ionic conductor and several ppm of select materials can alter its resistivity by several orders of magnitude. Therefore for, further characterization of the materials based on purity level and impurity type will allow for the model to improved.

7.5 Sensitivity Analysis of Heat Transfer Model

There are several parameters of interest with respect to the heat transfer model that can be investigated for a sensitivity analysis. These include the width of each material as long as the thermal conductivity, density, and specific heat capacity of the materials. However, the material properties can be related through the thermal diffusivity of the material and have their effect approximated through changes in this single parameter. The same method implemented in the analysis of the electrical shunting model is implemented to determine the effect each parameter on the model results. The effect is quantified by the change in the computed 100% response time of the RTD system to a step change of 153K from a nominal value of 300K.

The thermal response time of the system is highly dependent on the thermal mass of the material. Therefore, any increase in the dimensions of the system will provide an increased response time and any decreases will provide the opposite effect. For the various components in the system, the width of the sheath provides the greatest effect on the response time of the system. Altering the width of the sheath by $\pm 10\%$ produces a corresponding change in the response time of approximately $\pm 7.2\%$. In comparison, the other component that provides a similar effect is size of the mandrel. For a similar change in its width,

the response time experiences a change of approximately $\pm 6\%$. A visual representation of the data can be seen in Figures 7.6 and 7.7. These two components having the largest effect can be expected due to them providing the largest thermal mass in the system. Because of this, it can be seen that the altering the sheath width of the sheath will provide the simplest path to improving the response time of the RTD without changing the materials.

Regarding the materials, altering the thermal diffusivity alters the response time significantly more than the dimensions of the material. Decreasing the thermal diffusivity increased the response time by $\sim 11\%$ while increasing the thermal diffusivity introduced a decrease of $\sim 9\%$. These changes are marginally larger than the effect that the sheath width has on the response time. Because of this, if a significant change in the thermal response time of the instrument is necessary the best option would be in the materials selected. Altering the sheath material or the electrical insulator to have a better thermal diffusivity value would allow an increased response time. While section 6.3 does not make any suggestions regarding the response time, this provides a strong basis for any changes that may be needed to improve the response of the conceptual design.

Due to the availability of most of these materials, this should not be a constraint to the physical construction of the conceptual design. While these results are significant, the current analysis suffers from being unable to investigate each material individually. This is due to the construction of the model and how the material properties are handled as inputs to the system. To fully investigate the sensitivity to the model to changes in the thermal properties of the materials, the program would require significant modifications to allow for this functionality. For the purposes of the current model, this cursory approach to the sensitivity of the material properties is sufficient for the current model.

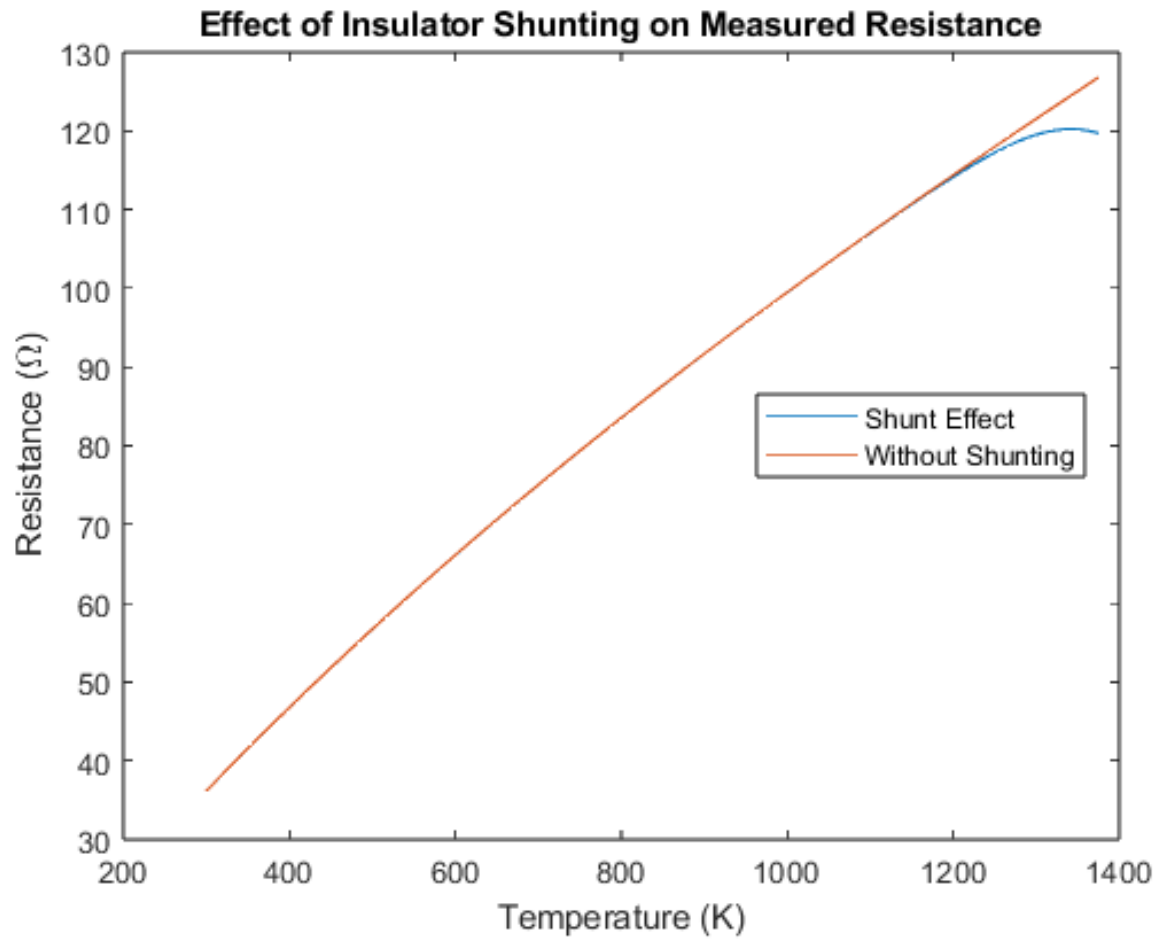


Figure 7.3: Resistance of the proposed equivalent niobium equivalent niobium sensing element with and without the effect of insulator shunting.

Table 7.1: General Geometry of RTD for Model Verification

Parameter	Design #1	Design #2
Outer Diameter	10 mm	3.15 mm
Sheath Wall Thickness	1.85 mm	0.05 mm
Insulator Thickness	2.15 mm	0.254 mm

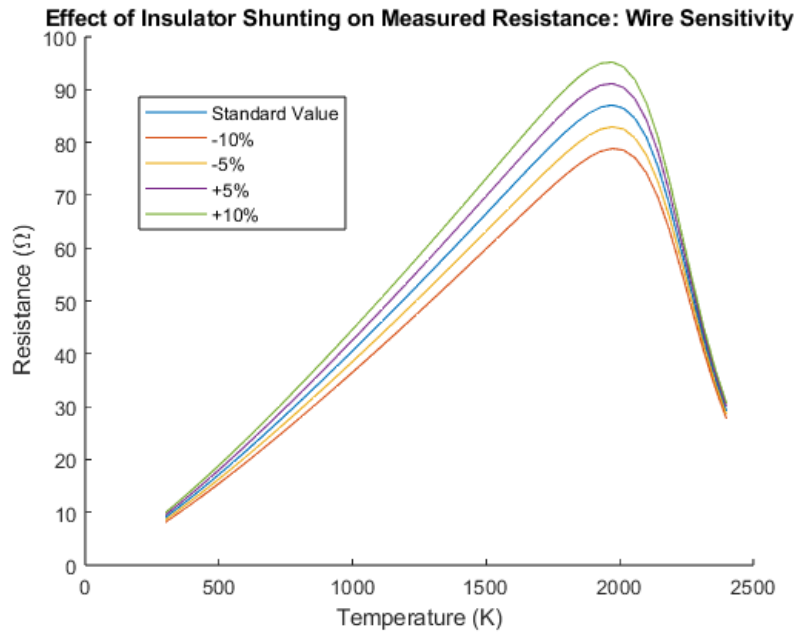


Figure 7.4: Sensitivity analysis of the wire resistivity for the electrical shunting model.

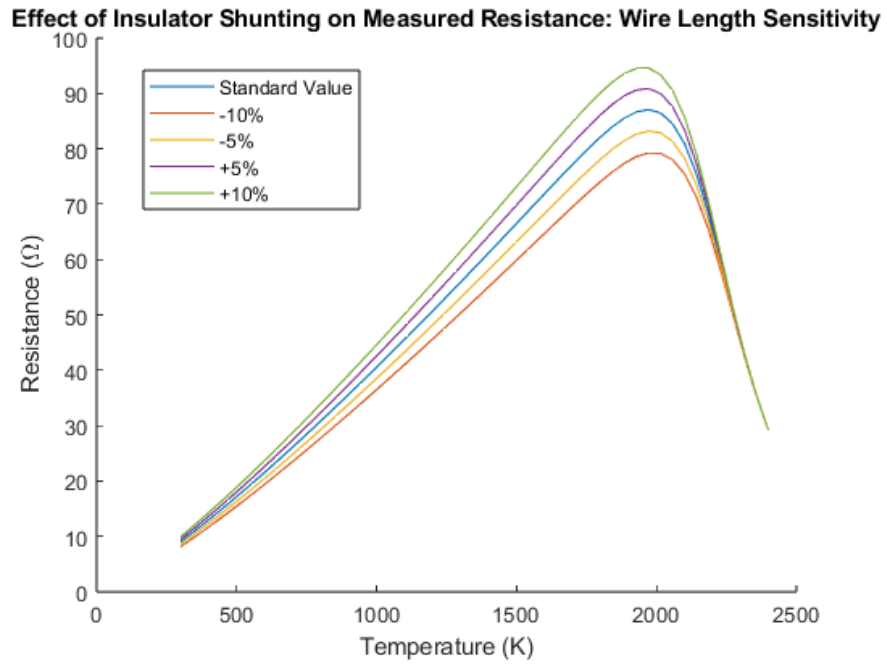


Figure 7.5: Sensitivity analysis of the wire length for the electrical shunting model.

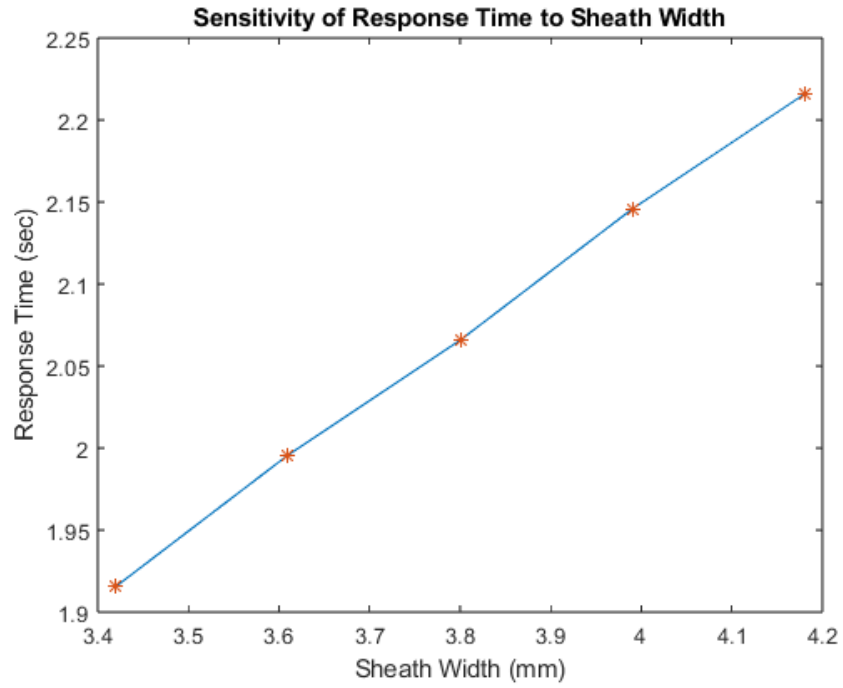


Figure 7.6: Sensitivity of the model to changes in the width of the RTD sheath.

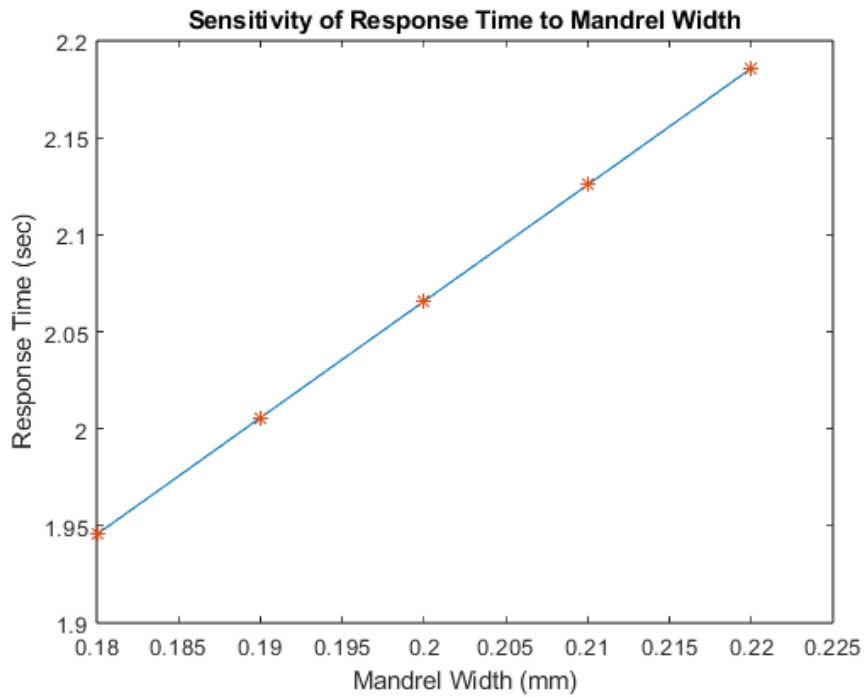


Figure 7.7: Sensitivity of the model to changes in the width of the RTD mandrel.

Chapter 8: Experimental Design

8.1 Overview of Needs

The validity of the conceptual instrument design requires further investigation in the form of numerous experiments. Completing these experiments will allow for the accuracy of the model and the performance estimation to be verified. Due to the various components evaluated in the model, experimental validation is required over a wide range of material interactions. This includes the various interactions between the resistive element, radiation, reactions with the insulator, and electrical shunting that may occur. As such, the main focus of the experimental work will be regarding the resistance-temperature relationship of a constructed resistor. This requires several resistors to be constructed for use in non-nuclear (out-of-pile) and nuclear (in-pile) tests. Figure 8.1 provides a simple visual representation of the phases needed to validate the conceptual instrument design.

8.2 Out-of-Pile Testing

The non-nuclear testing can be separated into several phases to streamline the process. Each phase is critical to the overall development of the instrument and can be used to improve the design of the instrument if needed. The first phase of out-of-pile testing can be labeled as bare resistor testing.

Bare resistor testing focuses on verifying the relationship between electrical resistivity and temperature for tungsten, the repeatability, and stability of the base resistor geometry. Verifying the temperature relationship will provide a rudimentary calibration curve that can be compared to the electrical resistance calculated from tabulated values of resistivity. Additionally, the tabulated experimental data is for extremely high purity tungsten and the wire used in the conceptual design is only 99.95% tungsten. The tungsten under test is type 1 A in compliance with ASTM F288. The main impurity present in the tungsten is potassium to strengthen the material. As such, the shift in electrical resistivity relationship is likely to have a constant bias that shifts the relationship to a higher position while maintaining the curves shape. Benchtop testing of this material will allow for a basis for a calibration curve for the instrument.

Due to the oxidation potential of oxygen, the bare resistors need to be tested within a vacuum or inert environment. This will allow for the resistance change to be measured without oxidizing the wire and causes significant changes to the composition of the material. As the purpose of the instrument is to survive extreme temperatures, the resistors should be tested up to 2000°C. However, this can be broken into additional phases and steps like that shown in Figure 8.1. An idealized temperature trajectory for testing can be seen in Figure 8.2. Figure 8.2 covers the operating temperature range of an NTRE from room temperature, ~300K, to the full power operating temperature. Covering this temperature would need to be completed several times to verify the measurement and evaluate the repeatability of the resistance measurement. Additionally, measurements taken from the maximum operating temperature to the idle point are needed to determine any differences that may occur.

Once the performance of the bare resistors has been verified, the next test phase can be initiated. This phase focuses on the usage of an electrical insulator and sheath material. A similar test plan as seen in Figure 8.2 is necessary to be conducted to verify the performance of the instrument. The greatest concern for the full instrument is the shunting of the insulator. As such, a significant portion of testing is needed to be done at temperatures from 2000 K to the melting point of the insulator. In addition to characterizing the effect of insulator shunting, melting the insulator allows for the effect of it freezing to be investigated as the temperature is decreased. Finally, this also allows for oxidation of tungsten from the sublimation of the insulator to be properly investigated. This will allow for sublimation rates, reaction rates, and the effect of tungsten trioxide production to be characterized.

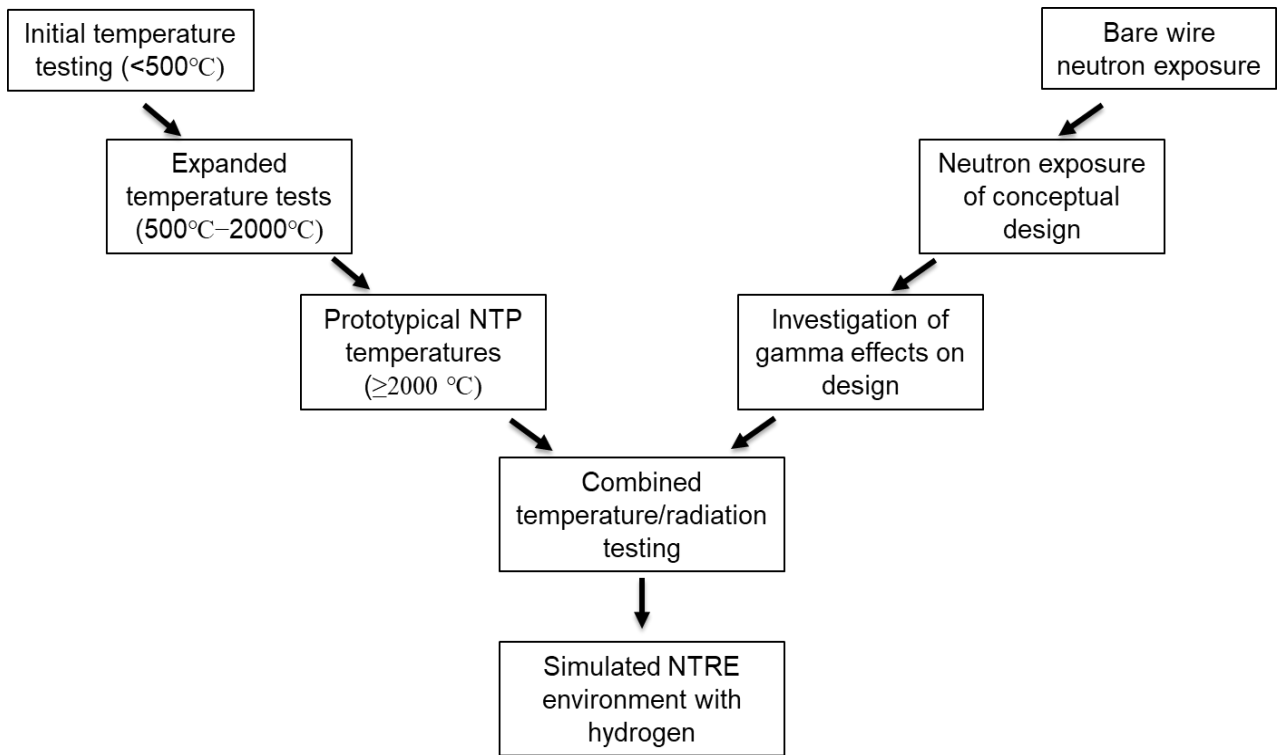


Figure 8.1: Visual representation of experimental phases.

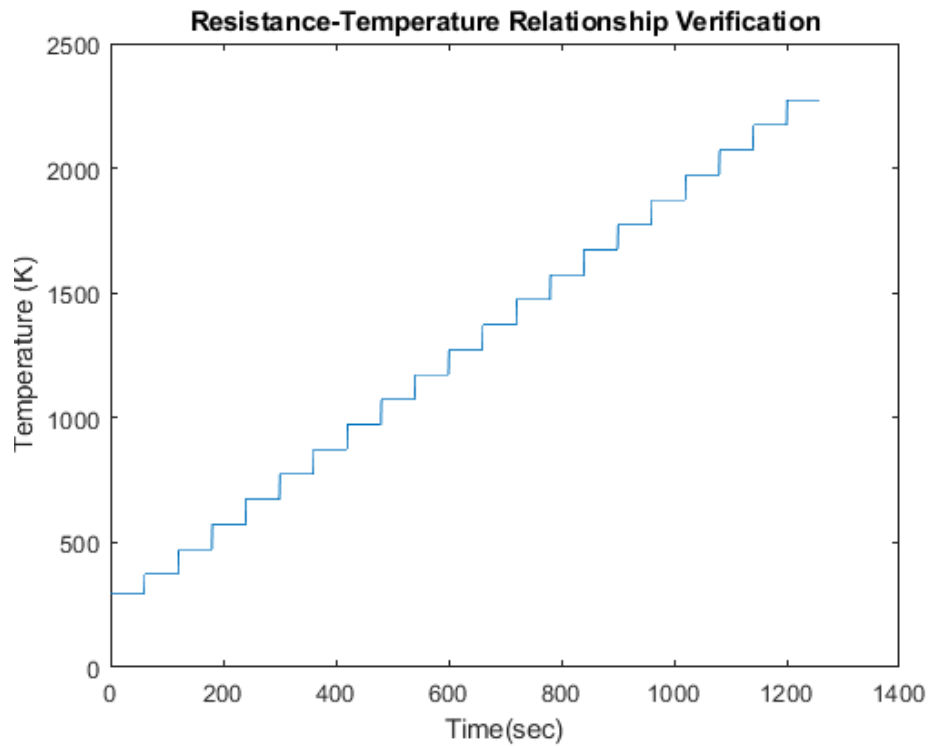


Figure 8.2: Desired test plan to determine calibration of the resistor.

Additionally, significant long-term tests need to be conducted as well as thermally cyclical tests. Long-term testing at high temperatures will provide the long-term stability of the instrument at these temperatures. As the instrument is designed for use in a NTRE and is unavailable for maintenance activities, the stability of the measurement is critical. Thermally cycling the instrument is necessary to ensure that the sensing element does not experience a mechanical failure during operation. Initial cycling tests should provide severe changes in temperature that are similar to the temperature transitions in NTREs, 300 K to 2400 K in ~30 seconds.

Finally, the conceptual instrument needs to be tested in a prototypical NTRE environment. However, this does not require the presence of radiation. A prototypical NTRE environment benchtop test requires the usage of high temperatures, flowing hydrogen, and replicating the operating pressure of the system. In addition to this, the periods where the system is at low temperatures when the reactor is not operating need to be evaluated. As materials have different recovery stages with some occurring at extremely low temperatures, the effect the low temperature will have on the sensing element. While the previous tests are necessary to validate the general performance and capabilities of the instrument, this stage ensures that the instrument is adequate for a NTRE system.

8.3 In-Pile Testing

The focus of the in-pile testing phase is to investigate the performance of the resistor and how it degrades when exposed to a neutron flux. Similar to the out-of-pile phase, the in-pile test plan can be separated into several phases. The first of these is a bare wire investigation of resistance changes that occur when a tungsten resistor is irradiated.

While there is some historical data regarding the resistivity change of tungsten due to irradiation, it appears that none of these historical experiments were conducted using continuous, in-situ measurements of the parameter of interest. Additionally, the available information is not sufficient to fully evaluate the irradiation effects. This is especially true when considering the irradiation temperature in a NTRE is ~2400 K. In comparison, the report that provides the most usable data conducted irradiations at ambient reactor conditions. As such, an irradiation of various tungsten resistor samples is needed to verify and improve the available data regarding the changes in its electrical properties.

Initial irradiations can be completed at ambient reactor temperatures to ensure that only the effects of radiation are recorded. With this data recorded, a combined effects test of high temperature and radiation can be conducted. As the first phase of the benchtop testing is focused on characterizing and heating the tungsten resistor, it provides a strong basis to evaluate the effects that could occur in when the resistor is exposed to both temperature and radiation as the effects were initially evaluated separately.

The neutron flux requirements of historical NTRE provides a noticeable challenge for the facilities that are currently available for extreme temperature irradiations. The Ohio State Research Reactor (OSURR) has the facilities to allow for the usage of a specially designed heater known as INSET [102]. However, the flux of the dry tube that allows for the usage of INSET does not receive a prototypical neutron flux. A NTRE is expected to provide a 10-hour thermal and fast fluence of $1.32 * 10^{17} \frac{n}{cm^2}$ and $1.71 * 10^{20} \frac{n}{cm^2}$, while the OSURR irradiation facility is only capable of a 10-hour thermal fluence of $3.96 * 10^{16} \frac{n}{cm^2}$. A facility like the High Flux Isotope Reactor (HFIR) provides a much higher flux that could be used to achieve a prototypical neutron fluence, but it currently does not have the capabilities to allow for the use for the INSET heating system. Similar things can be said regarding other neutron irradiation facilities such as the Advanced Test Reactor (ATR) and the Massachusetts Institute of Technology Reactor (MITR). Because of this, there is a significant potential to irradiate the bare wires at

several facilities at ambient reactor temperatures. This will allow for a series of resistors to be exposed to a variety of neutron fluence values.

Taking the resistor to the operating temperature of a NTRE requires the usage of a furnace, but this then precludes the ability of the test to replicate the neutron fluence conditions of an NTRE. While this is a notable concern, it cannot be completed without the construction of an adequate irradiation facility. As such, it is pertinent to use the OSURR to implement combined effects testing. With the data from the combined effects testing and the swathe of information from the separate effects testing, informed decisions and statements can be made regarding the performance of the material in a nuclear environment. Furthermore, this should allow for the verification of the historical data that is available for tungsten irradiations. With this data verified, a higher level of confidence can be placed on the information and allows for improved informed decision making.

Once the bare wire resistors have been irradiated, the conceptual design can be constructed to then investigate the effect the electrical insulator and the sheath will have on the measurements of the instrument. This allows for the determination of irradiation effects on the insulator and how that may alter the known properties of the material. Additionally, it will evaluate the sheath material for neutron embrittlement which could cause the instrument to experience a mechanical failure with extended use. The actual testing should be the same as that described for benchtop testing with the addition of neutrons and gamma radiation being the main factors separating the tests.

Finally, the conceptual instrument design needs to be evaluated for the desired environment. This is likely to provide the greatest challenge as there is not currently a facility capable of providing flowing hydrogen, temperatures up to and greater than 2000°C, and neutron irradiation. As such, fully testing the instrument requires the construction of a NTRE test stand similar to the items produced during Project Rover and the NERVA Program. Alternatively, there are plans to modify INSET to allow for hydrogen flow and this would allow for each of the stated conditions to be implemented during a test of the instrument.

8.4 Resistor Construction and Test Plan

8.4.1: Test Element Design

Several configurations for test samples have been configured to facilitate experiments in nuclear environments. Due to the dangers associated with beryllium oxide, alternative insulators have been investigated for use in low temperature experiments.

The main insulators available for use are hafnia, alumina, and magnesia. While hafnia would be preferable due to temperature capabilities, reactor staff indicated that use of alumina would be more desirable than hafnia due to criticality concerns. Because of its prevalent use and availability, alumina was chosen to use in the initial development of the test elements. As an aside, the use of magnesia viable for these tests as well. However, both magnesia and alumina are unsuitable for high temperature tests. This is due to the melting point of alumina being ~2345°K, which is lower than the operating temperature of a nuclear rocket. Magnesia is unsuitable due to its small resistivity at high temperatures (1 Ω-cm) that will cause excessive shunting. For comparison, a pure sample of beryllia is projected to have a resistivity of 1000 Ω-cm and hafnia would provide 10 Ω-cm at ~2345°K [3].

Initially, each test element was to be constructed by wrapping a tungsten wire around an alumina mandrel. Two methods were proposed to ensure the wire did not move along the mandrel during tests. These consisted of the potential usage of an epoxy that was compatible in a nuclear environment or

boring holes at the top of the alumina mandrel to allow for a pass through for the wire. A general view of this configuration can be seen in Figure 8.3.

While the use of the epoxy would guarantee the wire would not move during irradiation, it was not possible to determine if it would be acceptable to use during the irradiation. As such, this method was abandoned in favor of the mechanical pass throughs. To generate the holes, the equipment in the machine shop at the University of Tennessee, Knoxville was used. However, it appears that the equipment is not sufficient for a novice to bore holes through the hard material. After several attempts, additional information regarding the requirements to machine ceramics indicated the equipment was not sufficient to continue upon this pathway.

Due to the significant issues encountered with limited equipment and materials, the final mandrel for the low temperature test element is composed of halogen free G10, a fiberglass resin material used in previous tests. The material is capable of withstanding the low temperature irradiation conditions as well as function as an insulator. To create the mandrel, a sheet of G10 is cut into an appropriately sized amount and then scored along each side. The wire can then be placed at each of these scores to hold the wire in place. An example of this implementing stainless steel wire can be found in Figure 8.4.

The resistance of a portion of wire can be computed by using its length, cross-sectional area, and the resistivity of the material it is composed of. Because of this, tungsten wire with a 0.02 mm diameter was purchased to work on the development of the simple test item. This would allow for a 100 Ω resistor to be constructed from a small length of wire. However, this proved to be too difficult to work with using the facilities currently available. This led to additional amounts of tungsten wire being purchased to determine the best diameter to use in the construction of the test elements. Currently, this work is expected to continue via incoming graduate students in support of an awarded rapid turnaround experiment (RTE).

8.4.2: Irradiation Basket

The test elements have to be lowered into the reactor via the usage of an irradiation basket that must be fabricated by the experimenter. The current RTE makes use of the Ohio State University Research Reactor, specifically the auxiliary irradiation facility. This requires the basket to have a maximum diameter of 2.4 inches. To meet the requirements of the facility and the experiment, a relatively simple basket has been constructed.

The main component of the basket is a hollow cylinder of G10. One end of the cylinder is closed via the usage of a machined piece of G10 and appropriate screws. This allows for the test elements to be placed in the tube during the irradiation period. The irradiation basket has been constructed and can be seen in Figure 8.5, which includes a standard 16.9 fluid ounce water bottle for scale.

During irradiation, it is critical that the test elements do not make contact with each other. The use of epoxy would prevent electrical contact, the inability to use epoxy requires the usage of a mechanical means of separating the test elements. To accomplish this, a cross-shaped piece of G10 has been fashioned from several sheets of the material. This allows for a total of 4 resistors to be irradiated simultaneously without concern for inadvertent electrical contact occurring. Figure 8.6 and 8.7 shows the constructed G10 cross-shaped structure as well as a cutaway diagram of the constructed system.

Due to the nature of the experiment and the irradiation facility, the basket for the test elements has a simple design. Additionally, the materials are low cost and easy to acquire. This allows for several baskets to be made at a low overall cost without requiring access to materials beyond simple power tools.

Tungsten Resistor Geometry

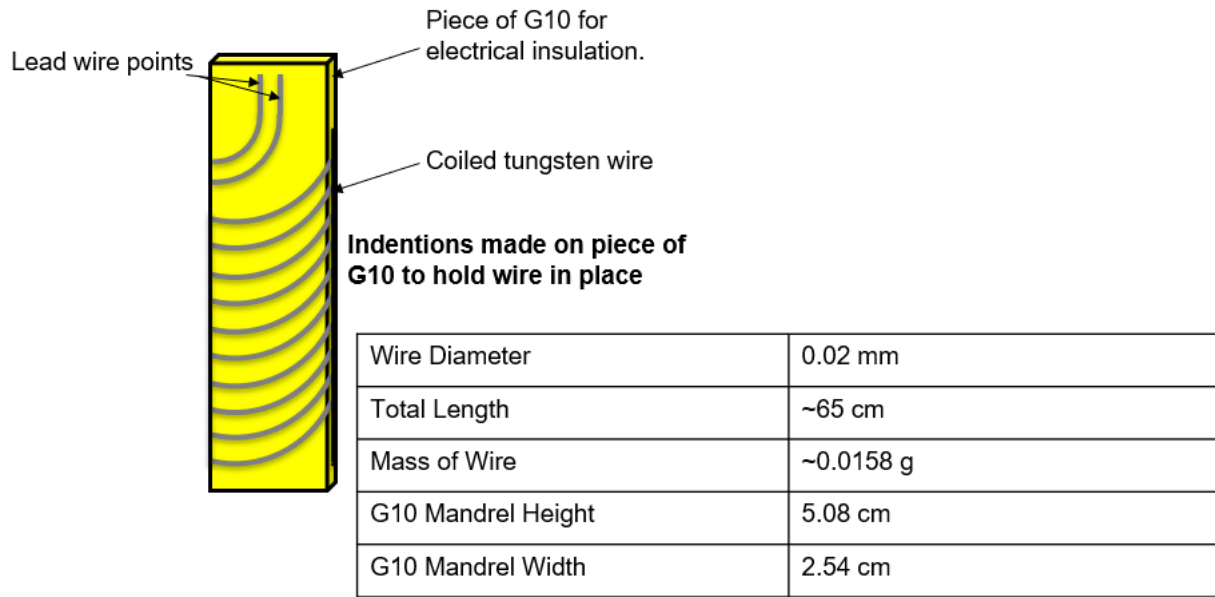


Figure 8.3: Schematic of tungsten resistor test element as well as pertinent dimensions.



Figure 8.4: Example of test element holder implementing large gauge stainless steel wire for visual clarity.

8.3.3: Non-radiation Environment Testing

Testing the samples in a non-radiation environment is necessary to ensure that the measurements made during irradiation have an accurate comparison point. The electrical connection between the test samples and the lead wires can be completed via the use of solder or through a mechanical connection. The use of solder requires the application of a welding box to provide a low oxygen environment to prevent the oxidation of the test samples during soldering. Some amount of tungsten oxide forms at room temperature but does not produce a visually noticeable change until 300°C, which is necessary to provide a clean solder joint for the wire [51]. Alternatively, making the connection through a mechanical means does not require a glove box and may provide a more suitable means of joining the test samples and lead wires.

Each sample requires 4 wires to be connected to facilitate a 4-wire measurement of resistance. An example of this can be found in Figure 8.8, which shows the use of separate lead wires to provide a current to the resistor and measure the voltage drop along its length. The outer wires labelled 1 and 4 provide current to the resistor, while wires 2 and 3 are connected to a DAQ to measure the voltage across the test sample. With the resistance of the labelled wires being equivalent, the effect of the wire resistance due to the current carrying source wires is not measured by the associated voltmeter. Difference in lead wire resistance is minimal due to the use of a single 4 conductor wire that ensures the length of each wire is the same. The constant current can then be provided to the system via the use of a standard transconductance circuit. Figure 8.9 provides an overview of the proposed measurement system using a transconductance circuit, a bridge measurement of voltage, and instrumentation differential amplifier; however, the differential amplifier is not critical to the measurement of the test sample voltage for this application.

Once these steps are completed, the measurement of the test sample resistance can be completed in an equivalent environment to the proposed ambient temperature irradiation. The temperature of the test samples due to gamma heating is not expected to exceed 100°C and should be around 70°C during test. The validity of this is being validated through the use of a finite element model of the test sample and a gamma heating rate determined via simulation in MCNP. To replicate these changes in resistance due to temperature, the test samples require exposure to temperatures up to 100°C. To achieve these temperatures, an equivalent self-heating rate can be determined to replicate the gamma heating rate seen in MCNP simulations. These tests can then be conducted in an inert environment, such as helium or argon, as well as in air to replicate the expected conditions of the tungsten RTD during irradiation. This will allow for the effects of oxidation to be evaluated, as well as the effects of irradiation. While only 4 test samples are to be irradiated, each of these tests will be repeated using several different samples. Bench-top testing of the samples that are to be irradiated can only take place in an inert environment to prevent formation of oxides that will further complicate data analysis.



Figure 8.5: Constructed irradiation basket with 16 fl. oz. water bottle for scale.

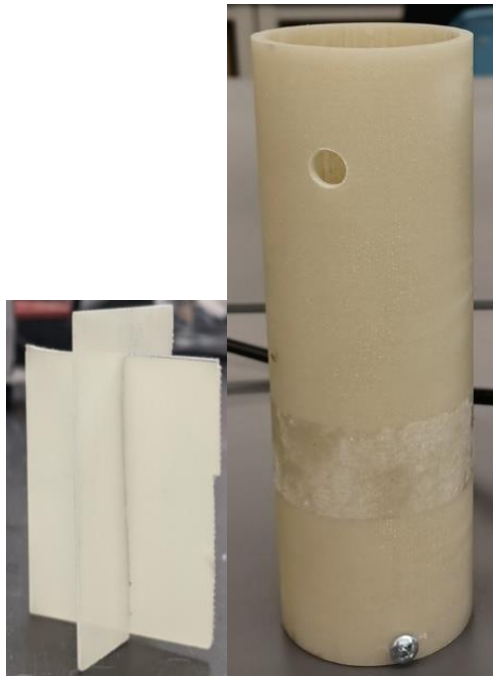


Figure 8.6: View of the physical separator composed of G10 with water bottle for approximate scale.

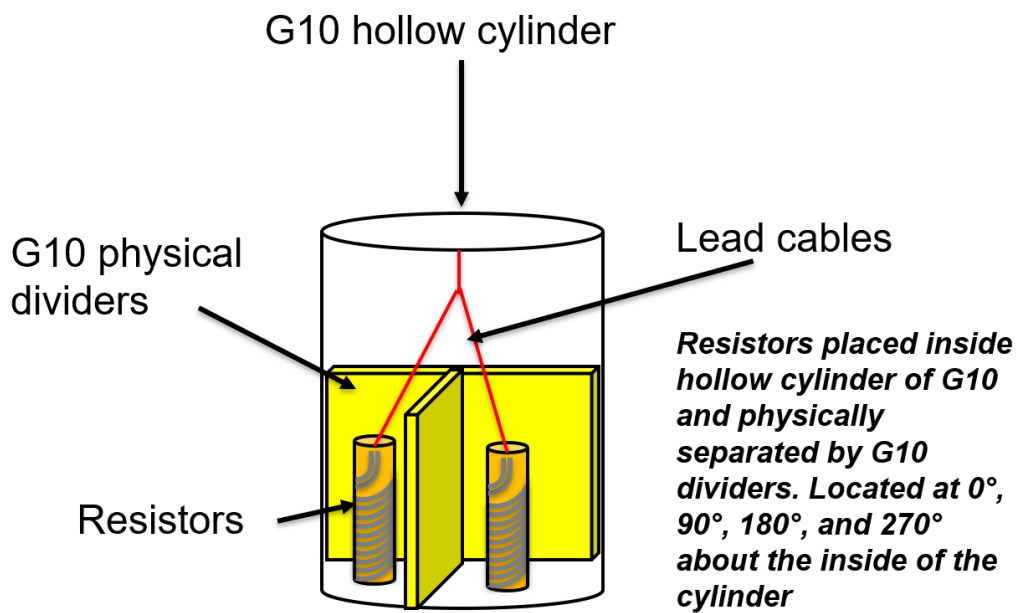


Figure 8.7: Cutaway diagram of irradiation basket.

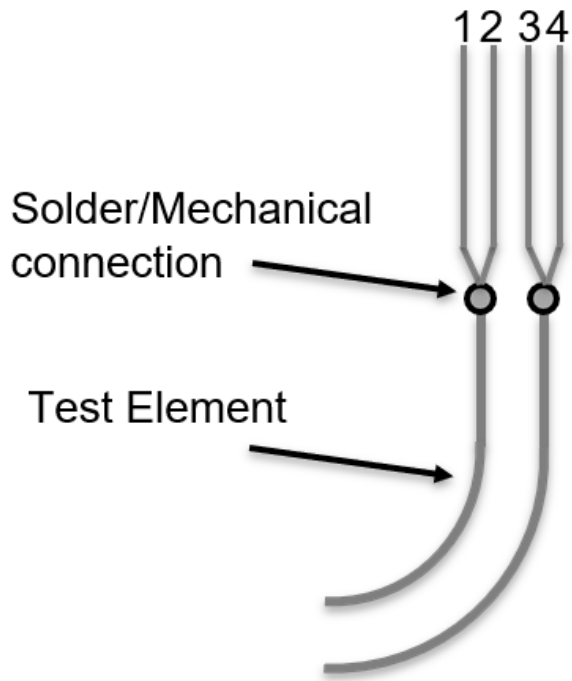


Figure 8.8: 4-wire configuration for test sample resistance measurement.

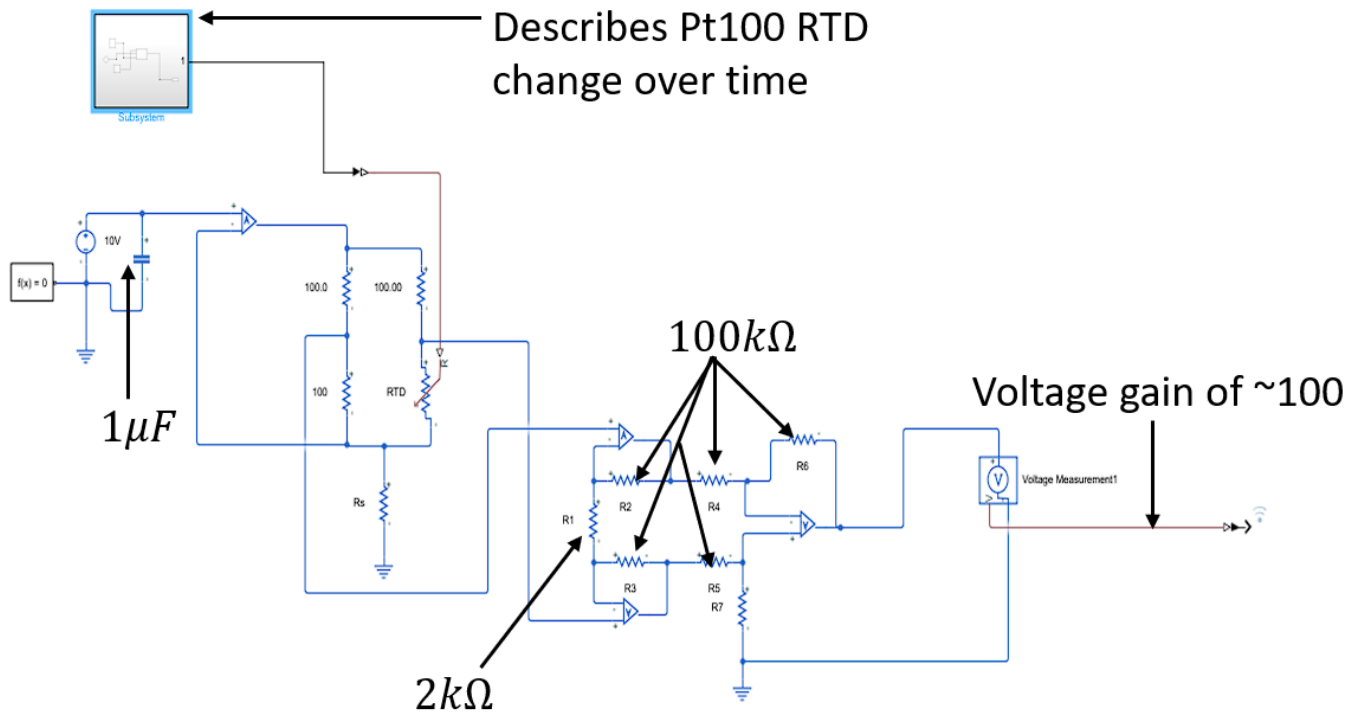


Figure 8.9: General circuit for measurement of test sample resistance.

Chapter 9: Conclusions

9.1 Summary

The extreme environmental conditions that are present in a NTRE limit the instrumentation options for temperature measurement, a critical control parameter in NERVA and the Project Rover based designs. As such, this work was motivated by the desire to expand the potential options due to the various limitations that are associated with currently available temperature measurement technology. To do this, a conceptual RTD has been proposed to address the current gaps in the temperature measurement technology and aid in the facilitation of an extreme temperature noise thermometry system. The development of an RTD that is capable of withstanding a NTRE environments provides benefits beyond application in space reactor technology as it provides an additional methodology for temperature measurement for other processes that produce extreme environments.

To accomplish this goal, first a literature survey of NTRE was conducted with a focus on U.S. programs such as Project Rover and the NERVA program. This was followed by an extensive investigation of suitable measurement technologies, identifying technological gaps, and determining the measurement technology that would be most adequate for a critical space mission. These literature surveys provided a well-founded basis for development and investigation of the conceptual design as well as the limitations that would need to be overcome to provide functionality. Due to the extensive use of modeling and simulation, a secondary goal of providing the base functions for a software-based evaluation tool was formulated.

With the construction of the various models, several aspects have been investigated to evaluate the credibility of the results as well as the suggestions regarding improvement in the conceptual design. The electrical shunting model, heat transfer model, and chemical reaction model have been evaluated based on historical data of similar components. In addition, the heat transfer model and electrical shunting have undergone sensitivity analysis to ensure that suggestions for design improvement are valid based on the model. To fully validate the conceptual design, an experimental test plan has been formulated for both nuclear and non-nuclear environments. Additionally, the design of the test elements for an upcoming irradiation campaign has been provided. The accomplishments of this work have been summarized in the following sections that contain the critical findings of the evaluation of the conceptual design and the future work that is needed for the real-world development of the conceptual instrument design.

9.2 Findings

From the analysis of the thermal, electrical, chemical, and nuclear effects that are pertinent to a temperature instrument in a NTRE, it can be seen that there are several shortcomings to the conceptual design.

Thermal analysis indicates a desirable heat transfer, but the differences in the CTE of the sensing element and the electrical insulator can cause catastrophic thermal stresses in the wire. This shows that the initially proposed design of winding the sensing element around a cylindrical insulator is not feasible. The thermal stress will need to be minimized by the usage of a sensing element with a CTE closer to that of beryllia and/or through the usage of the insulator in a different form. For example, niobium has a room temperature CTE of $7.3 * 10^{-6} \frac{m}{mK}$ which differs from beryllia by $0.7 * 10^{-6} \frac{m}{mK}$ in comparison to the $3.5 * 10^{-6} \frac{m}{mK}$ difference with tungsten. It could also be replaced with an alloy of tungsten that similar thermal, electrical, and nuclear properties that has more favorable strength properties. Additionally, designing a mandrel similar to what is shown in Figure 6.1 can limit the strain on the wire. The powdered

insulator allows the wire to contract and expand without the CTE mismatch with the insulator causes excessive damage.

Even though beryllia was chosen due to its relatively high resistivity at the operating temperature of a NTRE. However, the use of an impure beryllia sample causes significant insulator shunting and a decrease in the overall resistance of the RTD. Even using a pure sample with a resistivity that is two orders of magnitude larger than an impure sample, the resistance still sees a significant decrease. While increasing the size of the RTD will slightly improve the measured resistance, the best way to limit the effect of insulator shunting is by decreasing the nominal resistance of the RTD. Since the insulator is in parallel with the sensing element, decreasing the nominal resistance further limits the effect of insulator shunting. Because of this, using an RTD with a low nominal resistance appears to be more desirable than using the more standard 100 Ω . However, this reduces the sensitivity of the RTD due to smaller changes in resistance with temperature. For example, a 10 K increase in temperature causes a 4.5 Ω change in resistance for a 100 Ω RTD but only a 1.2 Ω change for a 25 Ω RTD. Even though the sensitivity is significantly smaller, this is still larger than the sensitivity of comparable type C thermocouples.

Based on the chemical analysis, it appears that the dissociation of the beryllia will consume an excessive amount of the tungsten wire. Based on historical tests of tungsten alloy thermocouples using beryllia, it is likely that this is a significant overestimation due to the assumptions made to determine the value of the reaction rate constant. Additionally, this assumes that the sensing element is in a vacuum environment. In reality, this is not likely to occur and the RTD will likely be back filled with an inert gas up to 1 atm. This will induce a hoop stress in the RTD sheath, but it is estimated to be an order of magnitude lower than the yield strength of tungsten at the operating conditions of an NTRE. As such, the chemical analysis needs extensive verification.

Overall, the proposed conceptual design suffers from several drawbacks that can be corrected for through design iteration and experimental testing. A full study regarding the benefits of using a different material for the sensing element as well as the costs and benefits of insulator shunting, nominal resistance, and sensitivity needs to be conducted. While there are several points that design iteration is needed, it appears that the RTD has the potential to function at the desired temperatures. The use of the RTD in a noise thermometry system will greatly improve the instrument and aid in reducing insulator shunting. Additionally, the programs written to complete this work provide the basis for the development of instrument evaluation tool but requires significantly more work to ensure accuracy and performance as well expanding the functions to be applicable to instruments other than RTDs.

9.3 Future Work

The future work of this project can be separated into three main categories: (1) improvement of the conceptual design, (2) model and simulation improvements, and (3) validation of modeled instruments.

One of the main goals of this work was to development a high temperature RTD that could be implemented in a NTRE either as a stand-alone instrument or as part of a Johnson Noise Thermometry system. The current model and simulations indicated significant changes would be required to provide a functional system. Implementing a wire-wound RTD design is not feasible due to the excessive strain that will be generated by the mismatched CTE of the insulator and the sensing element, unless the configuration shown in Figure 6.1 is implemented. As such, a coiled-element design that is more commonly implemented in industrial processes will likely improve the stress issues of the material. The usage of the insulator in a powdered form will aid in several aspects of the RTD as the loosely packed powder will cause lower stress and can positively affect the electrical properties of the insulator. Another potential solution could be to replicate the “strain free” design that is used in for the National Institute for

Standards and Technology in the development of temperature scales. However, this brings forth the potential for issues with system vibrations that need to be investigated in laboratory tests. The design may also benefit from an improvement in material selection. The materials of the conceptual design were based on the currently available literature, but this does not mean that a material may have been missed. For example, tungsten-rhenium alloys may provide may prove more feasible due to their improved strength over pure tungsten. However, this requires an in-depth investigation of the materials with the specific goal of use in the conceptual design to be carried.

Another of the main goals of this work is to provide a software tool that can be used in the evaluation of different materials and instruments in nuclear environments. Currently, there are several aspects of the model that can be improved upon to provide better functionality. The first of this is the choice of programming language. While Matlab is an incredibly powerful tool, a language such as C++ is more suitable to generate an executable program of this magnitude. This should allow for more accessibility as well as improvements in execution time. Beyond this, the fidelity of the models needs to be improved to a greater extent. Several assumptions and simplifications are made to allow for a solution to be computed. However, the application of ab initio methods in regard to the properties of the materials and the chemical reactions will improve the estimations provided by the program. Finally, the various functions need to be truly brought together to allow for a single command to provide the desired output. Currently, a script that calls each function with the appropriate inputs is implemented. However, this is not efficient and will be addressed in future iterations of the software after a transition to a different programming language.

A large portion of future work is dedicated to validating the results of the various simulations. This will allow for potential issues in material properties, assumptions, and simplifications to be identified as well as provide a way to quantify the accuracy of the model and simulations. This is a critical step as a model is only as good as the data that is provided to it. Without the necessary experimental tests that have been provided in Chapter 8, the results of the model remain speculative and based on conservative scenarios for each aspect. Currently, the Nuclear Science User Facilities (NSUF) have funded a Rapid Turnaround Experiment (RTE) to investigate the effects of neutron irradiation on the resistance of tungsten.

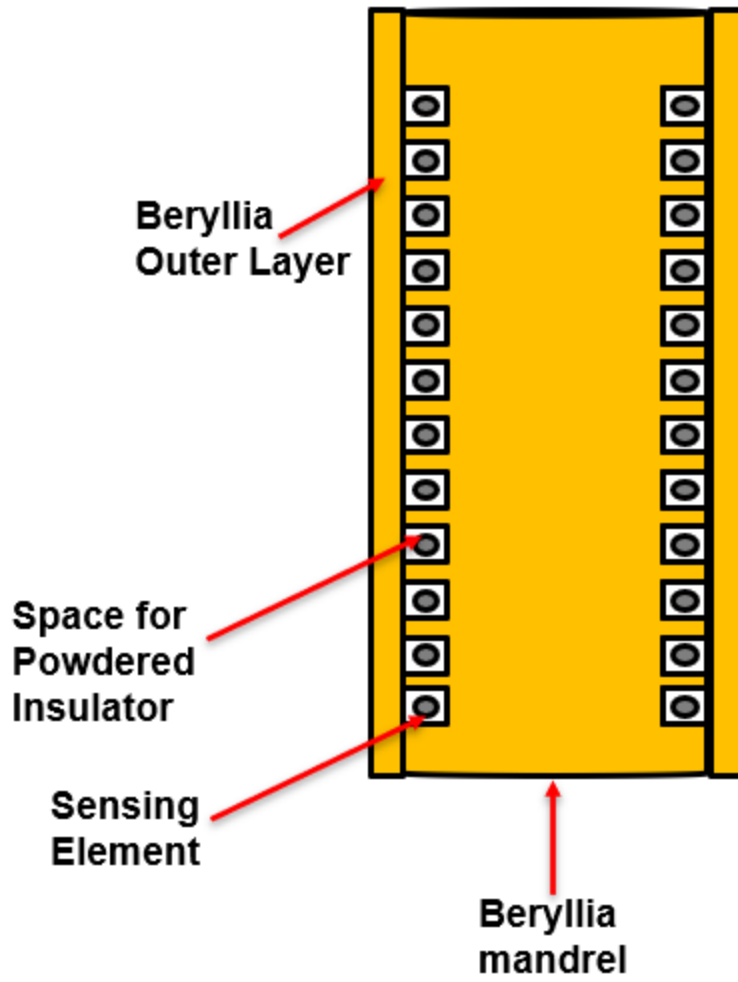


Figure 9.1: Conceptual design with accommodations made to account for potential challenges due to thermal strain.

References:

1. *XE-prime engine, final report. Volume I. Engine and facilities description.* 1969, ; Aerojet-General Corp., Sacramento, Calif. (USA). Nuclear Div. p. Medium: X; Size: Pages: 332.
2. *XE-prime engine final report. Volume II. Assembly, test, and disassembly operations.* 1970, ; Aerojet Nuclear Systems Co., Sacramento, Calif. (USA). p. Medium: X; Size: Pages: 482.
3. *Nuclear subsystem instrumentation.* 1971, ; Westinghouse Electric Corp., Pittsburgh, Pa. (USA). Astronuclear Lab. p. Medium: ED.
4. Hashemian, H.M., *Maintenance of Process Instrumentation in Nuclear Power Plants.* Power Systems. 2006: Springer-Verlag Berlin Heidelberg.
5. Koenig, D.R., *Experience Gained From the Space Nuclear Rocket Program.* Los Alamos National Laboratory. LA-10062-H (May 1986), 1986.
6. *Integrity of Reactor Pressure Vessels in Nuclear Power Plants: Assessment of Irradiation Embrittlement Effects in Reactor Pressure Vessel Steels.* 2009, Vienna: INTERNATIONAL ATOMIC ENERGY AGENCY.
7. *Pre-irradiation analysis of tungsten--rhenium thermocouples.* 1964, ; Aerojet-General Corp., Sacramento, Calif. (USA). p. Medium: ED.
8. Skaggs, S., W. RANKIN, and A. Patrick, *Decalibration of a Tungsten-Tungsten 25% Rhenium Thermocouple in a Neutron Flux.* LA-3662, Los Alamos Scientific Laboratory, 1967.
9. Fluke, G., *Tungsten--rhenium thermocouple performance in GTR-13 test.* 1964.
10. Heckelman, K.J.D. and R.P. Kozar, *Measured drift of irradiated and unirradiated W3%Re/W25%Re thermocouples at a nominal 2000 K.* Conference: Proceedings of the 5th symposium on temperature, Washington, DC, 21 Jun 1971; Other Information: Orig. Receipt Date: 30-JUN-74; Bib. Info. Source: IAA (International Aerospace Abstr.); Related Information: Symposium on temperature. Part 3. 1972: Instrument Society of America, Pittsburgh; Lewis Research Center, Cleveland. Medium: X; Size: Pages: 1935-1949.
11. Sandefur, N., J. Steibel, and R. Grenda, *Emf drift of chromel/alumel and W3%/W25% Re thermocouples measured in pile to high neutron exposures.* Trans. Amer. Nucl. Soc, 1973. **16**.
12. Vitanza, C. and T. Stien, *Assessment of fuel thermocouple decalibration during in-pile service.* Journal of Nuclear Materials, 1986. **139**(1): p. 11-18.
13. Wood, V.E., *Thermal Neutron Transmutation Effects on W/W-26Re Thermocouples.* Journal of Applied Physics, 1967. **38**(4): p. 1756-1758.
14. Ernest, O.D., *Measurement systems: Application and design.* 1990, McGraw-Hill.
15. Martin, R., *The use of thermocouples which transmute during service in nuclear reactors.* 1980, Atomic Energy of Canada Ltd.
16. Kelly, M. *Changes in EMF Characteristics of Chromel/Alumel and Platinum/Platinum-Rhodium.* in *High Temperature Thermometry Seminar: Held October 1-2, 1959, at Oak Ridge National Laboratory.* 1960. United States Atomic Energy Commission, Technical Information Service Extension.
17. Trauger, D. *LITR Experiments Relating to Rhenium/Tungsten and Platinum/Platinum-Rhodium Thermocouples.* 1959.
18. *Radiation and shielding analysis report, nuclear subsystem.* 1971: United States. p. Medium: ED.
19. *Pre-irradiation analysis of test 23/L302 tungsten/tungsten--rhenium thermocouples ground test reactor (GTR) irradiation test No. 13.* 1964: United States. p. Medium: ED.
20. Rempe, J., et al., *Thermocouples for high-temperature in-pile testing.* Nuclear Technology, 2006. **156**(3): p. 320-331.
21. Rempe, J.L., et al., *Long duration performance of high temperature irradiation resistant thermocouples.* 2007, Idaho National Laboratory (INL).

22. Skifton, R.S., et al., *Summary of High Temperature Irradiation Resistant Thermocouple Standardization Tests*. Conference: 11th Nuclear Plant Instrumentation, Control and Human-Machine Interface Technologies (NPIC&HMIT) 2019, Orlando, FL, 02/09/2019 - 02/14/2019. 2019; ; Idaho National Lab. (INL), Idaho Falls, ID (United States). Medium: ED.
23. Anheier, N.C., et al., *Technical readiness and gaps analysis of commercial optical materials and measurement systems for advanced small modular reactors*. 2013, Pacific Northwest National Lab.(PNNL), Richland, WA (United States).
24. Petrie, C.M., et al., *Reactor radiation-induced attenuation in fused silica optical fibers heated up to 1000 C*. Journal of Non-Crystalline Solids, 2015. **409**: p. 88-94.
25. Petrie, C.M., W. Windl, and T.E. Blue, *In-situ reactor radiation-induced attenuation in sapphire optical fibers*. Journal of the American Ceramic Society, 2014. **97**(12): p. 3883-3889.
26. Petrie, C.M. and T.E. Blue, *In situ reactor radiation-induced attenuation in sapphire optical fibers heated up to 1000° C*. Nuclear Instruments and Methods in Physics Research Section B: Beam Interactions with Materials and Atoms, 2015. **342**: p. 91-97.
27. Carlson, G.A. and W.H. Sullivan, *An Ultrasonic Thermometry System for Measuring Very High Temperatures in Reactor Safety Experiments*. 1979.
28. Daw, J., J. Rempe, and S. Wilkins, *Ultrasonic thermometry for in-pile temperature detection*. 2002, Idaho National Lab.(INL), Idaho Falls, ID (United States).
29. Daw, J., J. Rempe, and S. Wilkins, *Ultrasonic thermometry for in-pile temperature detection*, in *7th International Topical Meeting on Nuclear Plant Instrumentation, Control, and Human Machine Interface Technologies*, 2010.
30. Lynnworth, L. and D. Patch, *Ultrasonic measurement of core material temperature Final report*. 1937.
31. Shepard, R., et al., *Ultrasonic and Johnson noise fuel centerline thermometry*. 1974, Oak Ridge National Lab., Tenn.(USA); Tennessee Univ., Knoxville (USA). Dept
32. Arave, A., F. Panisko, and J. Christensen, *High-temperature ultrasonic thermometer in-reactor fuel rod centerline temperature test results*. ANCR-1091, Aerojet Nuclear Company, 1972.
33. Carlson, G., W.H. Sullivan, and H. Plein, *Application of ultrasonic thermometry in LMFBR safety research*. 1977, Sandia Labs., Albuquerque, N. Mex.(USA).
34. Carnevale, E. and L. Lynnworth, *Ultrasonic temperature measuring device Final report*. 1967.
35. Tasman, H. *Nuclear applications of ultrasonic thermometry*. in *Ultrasonics Symposium Proceedings*. 1979.
36. *Nuclear Technology Division annual progress report for period ending June 30, 1974*. 1975: United States. p. Medium: ED; Size: Pages: 570.
37. Tasman, H., et al., *The TRESON experiments: measurement of temperature profiles in nuclear fuels by means of ultrasonic thermometers*. High Temperatures-High Pressures, 1977. **9**(4): p. 387-406.
38. Arave, A. and J. Buchenauer, *Use of tungsten--2% thoria ultrasonic transmission line and sensor to improve the performance of high-temperature ultrasonic thermometry*. 1976, EG and G Idaho.
39. Britton Jr, C.L., et al., *Johnson noise thermometry for advanced small modular reactors*. 2012, Oak Ridge National Lab.(ORNL), Oak Ridge, TN (United States).
40. Brixy, H., *Temperature measurement in nuclear reactors by noise thermometry*. Nuclear Instruments and Methods, 1971. **97**(1): p. 75-80.
41. Brixy, H. and H. Thyssen, *Noise thermometer*. 1976.
42. Bull, N.D., *An Innovative Approach to Johnson noise thermometry by means of spectral estimation*. 2016.
43. Ezell, N.D.B., et al., *A novel technique applying spectral estimation to Johnson noise thermometry*. Nuclear Technology, 2018. **202**(2-3): p. 173-179.
44. Holcomb, D.E., R.A. Kisner, and C.L. Britton Jr. *Fundamental thermometry for long-term and hightemperature deployment in generation IV reactors*. in *Proceedings of the International Symposium on Future Instrumentation and Controls 2005*. 2006.

45. Sias, F., J. Macintyre, and A. Hansen, *A Tungsten resistance thermometer*. Transactions of the American Institute of Electrical Engineers, Part I: Communication and Electronics, 1954. **73**(1): p. 66-69.
46. Sias, F., *A resistance temperature detector for reactors*. Electrical Engineering, 1957. **76**(8): p. 692-692.
47. Sias, F.R., *A resistance-temperature detector for nuclear reactor service*. Transactions of the American Institute of Electrical Engineers, Part I: Communication and Electronics, 1957. **76**(3): p. 363-365.
48. Hashemian, H.M., *Sensor performance and reliability*. 2005: Isa.
49. Arblaster, J.W., *Selected electrical resistivity values for the platinum group of metals Part I: palladium and platinum*. Johnson Matthey Technology Review, 2015. **59**(3): p. 174-181.
50. *DOE Fundamentals Handbook: Instrumentation and Control, Volume 1*. 1992: United States. p. Medium: ED.
51. Lassner, E. and W.-D. Schubert, *Tungsten: properties, chemistry, technology of the element, alloys, and chemical compounds*. 2012: Springer Science & Business Media.
52. Wurster, S., B. Gludovatz, and R. Pippan, *High temperature fracture experiments on tungsten-rhenium alloys*. International Journal of Refractory Metals and Hard Materials, 2010. **28**(6): p. 692-697.
53. Grimvall, G., M. Thiessen, and A.F. Guillermet, *Thermodynamic properties of tungsten*. Physical Review B, 1987. **36**(15): p. 7816.
54. Riesch, J., et al., *Tensile behaviour of drawn tungsten wire used in tungsten fibre-reinforced tungsten composites*. Physica Scripta, 2017. **2017**(T170): p. 014032.
55. Škoro, G., et al., *Dynamic Young's moduli of tungsten and tantalum at high temperature and stress*. Journal of Nuclear Materials, 2011. **409**(1): p. 40-46.
56. Toliás, P. and E.M. Team, *Analytical expressions for thermophysical properties of solid and liquid tungsten relevant for fusion applications*. Nuclear Materials and Energy, 2017. **13**: p. 42-57.
57. Webb, J., S. Gollapudi, and I. Charit, *An overview of creep in tungsten and its alloys*. International Journal of Refractory Metals and Hard Materials, 2019. **82**: p. 69-80.
58. Keys, L. and J. Moteff, *Comparison of the recovery of damage in W and Mo after neutron irradiation*. Journal of Applied Physics, 1969. **40**(9): p. 3866-3868.
59. Keys, L. and J. Moteff, *Point defect recovery in neutron-irradiated tungsten at 0.31 Tm*. Physics Letters A, 1969. **29**(11): p. 706-707.
60. Keys, L. and J. Moteff, *Neutron irradiation and defect recovery of tungsten*. Journal of Nuclear Materials, 1970. **34**(3): p. 260-280.
61. Keys, L., J. Smith, and J. Moteff, *High-temperature recovery of tungsten after neutron irradiation*. Physical Review, 1968. **176**(3): p. 851.
62. Keys, L., J. Smith, and J. Moteff, *STAGE III RECOVERY IN NEUTRON-IRRADIATED TUNGSTEN*. 1967, General Electric Co., Cincinnati.
63. Kinchin, G. and M. Thompson, *Irradiation damage and recovery in molybdenum and tungsten*. Journal of Nuclear Energy (1954), 1958. **6**(4): p. 275-284.
64. Bradhurst, D. and H. De Bruin, *The electrical conductivity of BeO and BeO binaries*. Journal of Nuclear Materials, 1967. **24**(3): p. 261-269.
65. Cline, C.F. and H.W. Newkirk, *Electrical transport processes in beryllium oxide*. The Journal of Chemical Physics, 1968. **49**(8): p. 3496-3504.
66. De Bruin, H., G. Watson, and C. Blood, *Cation Self-Diffusion and Electrical Conductivity in Polycrystalline Beryllium Oxide*. Journal of Applied Physics, 1966. **37**(12): p. 4543-4549.
67. Lakel, S., F. Elhamra, and K. Almi, *Structural Phase Transition, Electronic, and Mechanical Properties of Beryllium Oxide: Temperature and Pressure-Induced Effects*. physica status solidi (b), 2018. **255**(4): p. 1700524.

68. Pryor, A., *The electrical conductivity of beryllium oxide*. Journal of Nuclear Materials, 1964. **14**: p. 258-264.
69. Popper, G.F. and A.E. Knox, *FARET IN-CORE INSTRUMENT DEVELOPMENT*. 1966, Argonne National Lab., Ill.
70. McDearman, J.R., *Digital computer simulation of high-temperature thermocouples subject to insulator shunting errors*. 1975.
71. Toropov, N.A., *High-Temperature Chemistry of Silicates and Other Oxide Systems/Vysokotemperaturnaya Khimiya Silikatnykh I Drugikh Okisnykh Sistem/Высокотемпературная Химия Силикатных И Других Окисных Систем*. 2012: Springer Science & Business Media.
72. Lukin, Y.S. and D. Poluboiaininov, *Vaporization of pure-oxide ceramics at high temperatures*. 1965, FOREIGN TECHNOLOGY DIV WRIGHT-PATTERSON AFB OH.
73. Darnell, A. and W. McCollum, *High Temperature Reactions of Thorium and Thoria and the Vapor Pressure of Thoria*. 1961: Atomics International.
74. Hsu, T.-R., *The finite element method in thermomechanics*. 2012: Springer Science & Business Media.
75. Gallet, D., et al., *Creep laws for refractory tungsten alloys between 900 and 1100 {sup o} C under low stress*. 2001.
76. Purohit, A., et al., *Development of a steady state creep behavior model of polycrystalline tungsten for bimodal space reactor application*. 1995, Argonne National Lab., IL (United States).
77. Cantor, B., *The Equations of Materials*. 2020: Oxford University Press, USA.
78. Shillady, D., *Essentials of physical chemistry*. 2011: CRC Press.
79. Vallance, C., *An Introduction to Chemical Kinetics*. 2017: Morgan & Claypool Publishers.
80. Houston, P.L., *Chemical kinetics and reaction dynamics*. 2012: Courier Corporation.
81. Chupka, W.A., J. Berkowitz, and C.F. Giese, *Vaporization of beryllium oxide and its reaction with tungsten*. The Journal of Chemical Physics, 1959. **30**(3): p. 827-834.
82. Pollock, B., A. Saul, and T. Milne, *The Vaporization of Beryllium Oxide*. 1960: Atomics International.
83. Lukin, E. and D. Poluboyarinov, *Volatilization of pure-oxide ceramics at high temperatures*. Refractories, 1964. **5**(9): p. 443-449.
84. Samsonov, G.V., *The oxide handbook*. 2013: Springer Science & Business Media.
85. Tallman, C., *Analytical model for study of thermocouple error attributed to electrical conduction in insulation*. 1965, Los Alamos Scientific Lab., Univ. of California, N. Mex.
86. Anderson, R., R. Adams, and B. Duggins, *Limitations of thermocouples in temperature measurements*. 1979, Oak Ridge National Lab., TN (USA).
87. McDearman, J., J. Googe, and R. Shepard, *A three-wire insulator-shunting model for high-temperature thermocouple errors*. IEEE Transactions on Industrial Electronics and Control Instrumentation, 1971(4): p. 137-144.
88. King, R.W.P., *Transmission-line theory: by Ronald W.P. King*. 1965.
89. Jeans, J., *Mathematical theory of electricity and magnetism*. 1925: Cambridge University Press.
90. Gorynin, I., et al., *Effects of neutron irradiation on properties of refractory metals*. Journal of nuclear materials, 1992. **191**: p. 421-425.
91. Schultz, H., *Die Erholung des elektrischen Widerstandes von kaltverformtem Wolfram*. Acta Metallurgica, 1964. **12**(5): p. 649-664.
92. Tanno, T., et al., *Effects of transmutation elements on the microstructural evolution and electrical resistivity of neutron-irradiated tungsten*. Journal of Nuclear Materials, 2009. **386**: p. 218-221.
93. Hasegawa, A., et al., *Neutron irradiation behavior of tungsten*. Materials transactions, 2013: p. MG201208.
94. Hasegawa, A., et al., *Property change mechanism in tungsten under neutron irradiation in various reactors*. Journal of nuclear materials, 2011. **417**(1-3): p. 491-494.

95. Berry, R., *Platinum resistance thermometry in the range 630–900 C*. Metrologia, 1966. **2**(2): p. 80.
96. Berry, R., *Analysis and control of electrical insulation leakage in platinum resistance thermometers up to 1064 C*. Metrologia, 1995. **32**(1): p. 11.
97. Carroll, R. and R. Shepard, *The Method of Construction of a Dual Johnson-Noise-Power and Resistance Thermometer for 1375 K (1100° C) Service in a Vacuum Environment*. 1994, Oak Ridge National Lab.(ORNL), Oak Ridge, TN (United States).
98. Shepard, R., et al., *Tuned-circuit dual-mode Johnson noise thermometers*. 1992, Oak Ridge National Lab., TN (United States).
99. Chohan, R., F. Abdullah, and L. Finkelstein, *Mathematical modelling of industrial thermometers*. Transactions of the Institute of Measurement and Control, 1985. **7**(3): p. 151-158.
100. Teilab, M., *Détermination du temps de réponse d'un capteur de température (par modèle mathématique)*. 1982.
101. Gulbransen, E., K. Andrew, and F. Brassart, *Kinetics of oxidation of pure tungsten, 1150°–1615° C*. Journal of the Electrochemical Society, 1964. **111**(1): p. 103.
102. Steiner, T.R., E.N. Hutchins, and R.H. Howard, *Steady-State In-Pile Nuclear Thermal Propulsion Experimental Testbed Initial Demonstration at The Ohio State University Research Reactor*. Nuclear Technology, 2022. **208**(1): p. 100-114.
103. Meaden, G.T., *The Theory of the Electrical Resistance of Metals*, in *Electrical Resistance of Metals*. 1965, Springer. p. 59-94.

Appendix A: Funded NSUF RTE Proposal

Technical Abstract:

Temperature measurements in excess of 2000°C are limited to a handful of applicable technologies. Nuclear systems with such temperatures are further limited by the materials that are capable of surviving the temperature and radiation of the system. Tungsten-rhenium alloy thermocouples are commonly used in such applications, but experience calibration drift due to neutron exposure. For remote, high temperature nuclear systems the use of a material that transmutes during reactor operation is undesirable. A measurement technique such as Johnson noise thermometry would account for such drift but requires a resistive element or resistance thermometer to operate. As such, a tungsten resistance thermometer is being evaluated for use in nuclear thermal rocket systems. While the usage of Johnson noise thermometry should account for radiation induced calibration drift, the effects of radiation on the electrical resistance of a tungsten resistance thermometer need to be understood. Tungsten appears to be a viable material for the desired application, but the material requires further evaluation. Additionally, understanding the effects of radiation will aid in the evaluation of the instrument's potential to operate without the use of a noise thermometry recalibration system. This will allow for the production of a new high temperature measurement device to improve diversity in measurement. During the course of the irradiation at the Ohio State University Research Reactor, 4 tungsten resistor samples will be irradiated to a thermal neutron fluence that is comparable to nuclear thermal rocket systems. The electrical resistance will be continuously monitored via a 4-wire measurement, with gamma heating accounted for via thermal simulations.

Programmatic Relevance Abstract:

This work proposes to characterize the effects of neutron irradiation on the electrical resistivity of tungsten wire that could be used in an extreme temperature resistance thermometer. Tungsten provides the highest melting point of any pure metal, a notable relationship between electrical resistance and temperature, and does not chemically react with hydrogen. Additionally, the material has been the subject of resistance thermometer research historically. As such, this indicates the material's strong potential for the evaluation and development of a high temperature resistance thermometer. However, the performance of the material in a nuclear environment requires evaluation.

The proposed work is in the aid of the development and deployment of nuclear thermal rocket systems. Historical nuclear thermal rocket designs have implemented tungsten-rhenium alloy thermocouples that are known to experience calibration drift after extended exposure to a neutron flux. The proposed resistance thermometer has the potential to replace these instruments when used in conjunction with a Johnson noise thermometry system. It also provides additional diversity in measurement to prevent reliance on a singular measurement. While the target application is nuclear rocket systems, the development of such an instrument provides more measurement options for nuclear systems, such as Very High Temperature Gas Reactors, that exceed the operating temperature of standard platinum resistance thermometers.

With the NSUF RTE funding, the goal is to characterize the effects of radiation on a tungsten resistor. This information is critical to the development of a tungsten resistance thermometer for application in nuclear environments. Understanding the change of electrical resistance will further define the suitability of the material for high temperature applications.

Characterization of Irradiation Effects on the Electrical Resistance of Tungsten

Introduction:

Nuclear thermal rocket engines (NTREs) produce harsh nuclear environments with temperatures exceeding 2000°C and provide limited options for maintenance. In-core and core outlet temperatures are necessary for reactor control and have been completed historically through the use of tungsten-rhenium alloy thermocouples [1, 2]. However, these instruments experience calibration drift when exposed to a neutron flux. As such, a measurement capable of in-situ self-recalibration such as Johnson noise thermometry (JNT) is desirable but requires a resistive element to function. This work looks to develop a high temperature tungsten-based resistance temperature detector (RTD) that can be used for extreme temperature measurements and in a JNT measurement system.

Description of Research:

The need for instrumentation that can withstand nuclear environments with minimal need for maintenance is necessary for the long-term operation of remote reactors. Extended exposure to fast and thermal neutrons induces crystallographic defects and composition changes that can alter the properties of a material. While there are several components that require consideration, the sensing element currently takes priority. For the proposed tungsten resistance thermometer, understanding the effects of irradiation on the material's electrical resistivity is critical.

The resistivity of a metal can be separated into several independent factors, generally referred to as Matthiessen's rule [103].

$$\rho_{tot} = \rho(T) + \rho_{impurity} + \rho_{defect} \quad 1$$

Equation 1 provides the general representation of Matthiessen's rule with ρ_{tot} being the total resistivity, $\rho(T)$ being the temperature dependent aspect, $\rho_{impurity}$ being the scattering effect of impurity atoms, and ρ_{defect} being the effect of structural defects. However, there are additional effects that further complicate the material's electrical resistivity. This prevents the use of transmutation codes and neutron-induced damage simulations to provide results with minimal uncertainty.

While there are historical investigations regarding this phenomenon, the data is limited and has been attained through post-irradiation evaluation (PIE). This allows for the irradiated specimens to decay and may not provide a full view of the irradiation effects. To understand the degradation of a calibrated sensing element, continuous measurements are necessary during irradiation. This will allow for any transient effects to be accounted for and will allow for any changes in the electrical resistivity as the neutron fluence increases to be measured. PIE can then be implemented to further characterize the material and indicate potential changes in electrical resistivity that may occur during the decay of the irradiated specimen. With this information, it provides necessary information regarding material selection for instrumentation in nuclear environments and data for models of the proposed tungsten resistance thermometer.

Experimental Plan:

A minimum of 4 tungsten resistors will be irradiated at the Ohio State University Research Reactor (OSURR). This is an ambient temperature irradiation that requires full power operation of the OSURR and a 7-hour long irradiation period. This experiment will make use of the Auxiliary Irradiation Facility (AIF) to provide a thermal neutron fluence $1.50 * 10^{17} \frac{\text{neutrons}}{\text{cm}^2}$, comparable to historical NTRE designs [18]. During the course of the irradiation, the resistance of the wire will be monitored continuously via a 4-wire measurement.

The resistors are composed of ASTM F288-96 type A tungsten wire and an alumina mandrel. The resistance of each resistor is to be $\sim 100 \Omega$, with any deviations accounted for during pre-irradiation evaluation. Each resistor is constructed by coiling the tungsten wire in a single or double helix around the alumina mandrel. Once coiled, the wires are coated with a radiation tolerant and electrically insulating

epoxy, such as Torr Seal, to ensure the shape is maintained throughout the irradiation. Electrical contact is then made with the lead wires and the ends of the tungsten wire using lead-based solder. To prevent the oxidation of the tungsten and to limit the adsorption of oxygen on the surface of the wire, the wires are constructed in an oxygen free environment. The general configuration described above is shown in Figure A.1 along with providing the expected mass of single tungsten sample.

The temperature effect due to gamma heating and Joule heating is being computed via thermal simulation. The temperature effect on the resistors will then be recorded via benchtop characterization. This allows for the alterations in the resistance due to the temperature increase from gamma heating to be separated from the effects induced by neutron irradiation. Furthermore, the resolution of the DAQ is $\sim 0.6 \mu\text{V}$ which will allow for changes in the electrical resistance as small as $0.6 \text{ m}\Omega$ to be measured when the provided current is 1 mA.

Approach Detail: Time at OSURR – 1 days

Task 1: Irradiate at the OSURR – 1 days

Task 2: Analyze data and publish results

Risk Mitigation:

Risk for this proposed irradiation is low. The tungsten wire and readout equipment have already been acquired and the experiment team has previously conducted multiple experiments at the OSURR. The largest risk is the failure of the airtight seal on the experiment which may induce larger error in the measurements along with the error uncertainties of gamma heating on the tungsten wire.

Qualifications:

1. Dr. Richard T. Wood will be the PI on this project. He is currently a professor in the Nuclear Engineering Department at the University of Tennessee-Knoxville. He is also a member of the IAEA, the IEC, and a Fellow of the American Nuclear Society. His background covers instrumentation and controls for nuclear systems, reactor safety, and licensing.
2. Dr. N. Dianne Bull Ezell will be a co-Pi for this work. She is currently the group leader of the Nuclear and Extreme Environment Measurement Group at Oak Ridge National Laboratory and has a background in electrical engineering and instrumentation for nuclear environments. She has overseen several irradiation projects at both the High Flux Isotope Reactor and the OSURR regarding fuel and instrumentation.
3. Dr. Brandon A. Wilson is a co-PI for this project and is currently an R&D staff member in the Nuclear and Extreme Environment Measurement Group at Oak Ridge National Laboratory. His background includes work on the effect of radiation in optical materials and the design of reactor instrumentation. He has also developed in-depth models of the OSURR in MCNP and conducted activation analysis for various irradiation campaigns.
4. Dan Caleb Floyd will be a co-PI for this project. Currently, he is a doctoral student in the Nuclear Engineering Department at the University of Tennessee-Knoxville. He has a background in nuclear and electrical engineering and is currently working on the evaluation of instrumentation for nuclear thermal rocket systems. He has been a part of two previous irradiation tests regarding the performance of instrumentation in nuclear environments.

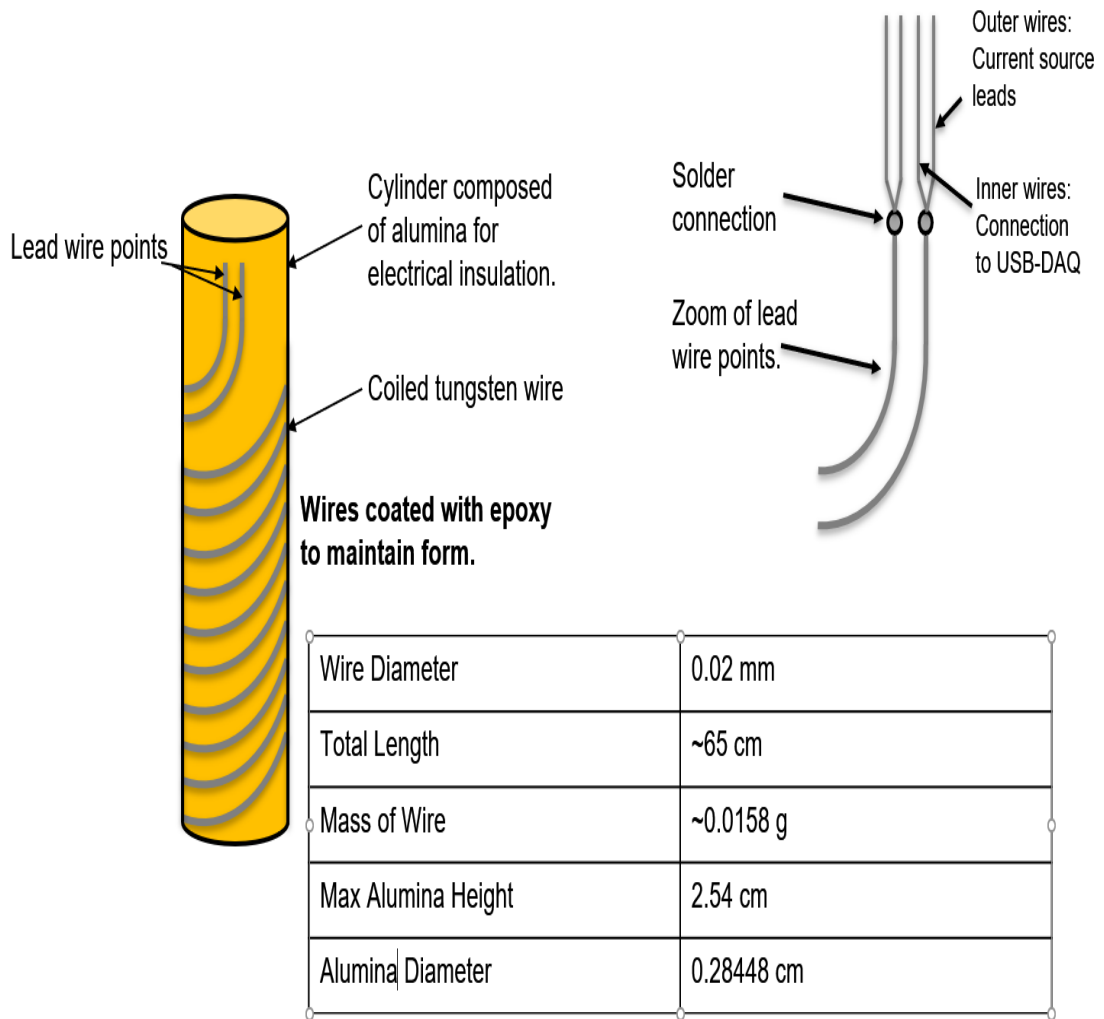


Figure A.1: Configuration of tungsten resistors for the proposed irradiation experiment.

Vita:

Dan C. Floyd was born in 1996 and had decided at a young age that he wanted to be an engineer. To accomplish this, he became a student at The University of Tennessee, Knoxville in 2014 and started his undergraduate studies in the Nuclear Engineering Department. He completed his bachelor's degree in 2018 and realized that he would likely never get a graduate degree if he took a break from school. As such, he continued his education by achieving a master's degree from the Electrical Engineering Department as well as writing his thesis for a doctorate in nuclear engineering.